Geochemical Iron Dynamics and Passive Treatment of Acid Mine Drainage with High Dissolved Iron Concentration for Sustainable Green Mining

A dissertation submitted in partial fulfillment of the requirements for the degree of Doctor of Philosophy in Engineering

By

Sereyroith TUM

Division of Sustainable Resources Engineering
Graduate School of Engineering, Hokkaido University, Japan

March 2022

Abstract

Acid mine drainage generated from dissolved metals sulfide is one of the world's environmental risks once it exposes to the environment. Typical toxic elements such as As, Ni, Cu, Se, Pb, Cd, and Fe release from AMD highly impact human health and aquatic lives. Some AMD cases are naturally attenuated without human interventions. Unfortunately, human assistant for water treatment is essential if natural attenuation is inadequate. Passive treatment is the sustainable method for AMD treatment, but it is dependent on site-specifics. Passive treatment is applicable only if a detailed study of natural remediation in AMD contamination sites. Ferric iron minerals such as schwertmannite, commonly found in an acidic environment, have potential roles in natural attenuation for heavy metal scavenges. Regardless of the significant roles of schwertmannite in natural attenuation, the gaps of the schwertmannite formation based on the iron dynamics study applied to natural environments remain uncertain. Therefore, the two case studies of AMD contamination are selected to investigate in this research to cover the broad scope of the relationship of iron dynamics and natural attenuations in the implication for passive treatment.

Chapter 1 introduces the research introduction, background, and problem statements. The overall objective of this research is to elucidate the effects of natural attenuation occurrences for various sources of iron species in acid mine drainage in different climate conditions and its implication for passive treatment methods. The implementation to reach these goals, the aspects that mainly focus on are: (1) the characterization of the various AMDs' geochemical behaviors in different climate conditions that possibly control the natural attenuation mechanisms, (2) elucidating the impacts of iron species and its dynamics that may well influence to AMD attenuations, and (3) the advantage of natural attenuation mechanisms to apply to AMD passive treatment methods by using geochemical modellings.

Chapter 2 reviews the existing literature to deliver this research's background knowledge. The appraisals include the roles of ferric iron minerals to remove toxic elements from AMD, the relationship of Fe dynamics, the formation of schwertmannite in the mine site, and the overview of AMD treatment methods.

Chapter 3 discusses the case study of Mondulkiri mine site, where the sources of AMD come from the discharge of tailing and AMD generation from the excavated area.

Fe^{2+} is the major iron species released from AMD. The toxic elements which are more than the WHO regulation limit are As, Ni. Se, and Cu. Iron oxidizing bacteria in the tributary is one of the factors controlling the natural attenuation process. The rapid oxidation of Fe^{2+} to Fe^{3+} occurred under the biotic condition in the tributary. When pH increases in the rainy season, Fe^{3+} starts to precipitate in the tributary as schwertmannite, enabling As adsorption in the rainy season. Yet, Ni, Se, and Cu concentrations were diluted by rainwater. The natural attenuation successfully remediated the target contaminants to less than the WHO regulation limit in the rainy season. The tributary's pH decreases in the dry season led to the dissolution of schwertmannite, where As was also released back to the river. The seasonal dynamics in the study area caught great attention of the role of rainwater or dilution in natural attenuation. In the rainy season, rainwater elevates the pH in the tributary from 2.7 to 3.4 and dilutes the contaminant concentrations. The dilution is insufficient to dilute As concentration to less than the environmental regulation limit, but the rising pH in the tributary facilitates schwertmannite precipitation. Thus, As adsorption onto schwertmannite occurs.

Chapter 4 is the case study of Shojin mine, the abandoned mine site in a temperate climate zone in northern Japan. The sources of the river contaminant are different from the Mondulkiri mine. The drainage seepage from the waste dams leaks to the nearby natural rivers rich in Fe, As, Cd and Pb. At the monitoring point, the contaminants of the Shojin river decreased to below the standard environmental level. In contrast, Cd and Pb concentrations in Amemasu river remain slightly higher than the standard environmental level, even though the two rivers have the same contamination sources. The Fe^{3+} is the dominant species released from drainage water, which is different from the Mondulkiri mine. After AMD had mixed with the Shojin river's pH decreased from 6.9 to 3.1. The formation of schwertmannite can be found just after mixing, and all the contaminant targets are less than WHO guidelines. Arsenic concentration decreases due to its adsorption onto the schwertmannite surface. Nevertheless, the concentrations of Pb and Cd were decreased by dilution of the natural water in the river. In contrast, Amemasu river's pH dropped from 7.1 to 2.8 after mixing with the drainage water. There was no significant effect of the natural attenuation in Amemasu river as it is in Shojin river.

Chapter 5 provides a detailed study of the iron dynamics in the study areas. The dominant ferric iron mineral found in both study areas is schwertmannite, has a

significant role in natural attenuation. Iron dynamics in AMD control the rate-limiting of schwertmannite formation. Fe^{2+} is commonly found as the rate-limiting species in AMD treatment, yet in the case of Mondulkiri mine is different. Fe^{2+} is not the rate-limiting parameter. The presence of iron-oxidizing bacteria boosts the oxidation rate of Fe^{2+} to Fe^{3+}. Fe^{3+} precipitation rate constant of the study areas was obtained from the experimental data is relatively quick in acidic conditions at pH 3 to 3.5.

Chapter 6 and 7 describe each case study of toxic elements removal methods. The Acid neutralization by dilution and the utilization of limestone in AMD by the geochemical model was conducted to compare the efficiency of passive treatment implications. The Mixing models of the study areas were implemented to understand the role of dilutions in AMD contamination. The model shows the dilution could elevate the pH in rivers water and dilute the concentrations of the toxic elements. In addition, the drainage water reaction with the limestone model could also indicate the required limestone that is necessary for acid neutralization. Both methods provided significant results to the study area; however, the dilution of neutral water is limited to Amemasu river.

Chapter 8 concludes the natural attenuations mechanisms in each case studies and its future implications for passive treatment. This study shows some essential parameters that should be considered for passive treatment design, including iron species, iron concentration, dilution sources, flowrate, and etc. Moreover, this study validated the existed geochemical models and databases from previous studies to the measurement data from the natural environment. These findings are essential for the AMD contaminated area for future treatment implications.

Acknowledgements

Foremost, I would like to express my deep gratitude to my research supervisor Prof. Tsutomu SATO, Professor of Laboratory of Environmental Geology, Sustainable Resources Engineering division, Faculty of Engineering, Hokkaido University, for giving me the opportunity to do the research and providing valuable guidance throughout this Ph.D research. He has patiently taught me the research methodology to implement the research and to produce the research works as clearly as possible. His great visions and activities have inspired me to work harder for own passion. It was a great honor to work under his supervisions. I would not be able to describe all his kindness and patience toward me, yet I am extremely thankful for everything he has offered me.

Besides my supervisor, I would like to extent my appreciation to Dr. Tsubasa OTAKE, associate professor of Laboratory of Environmental Geology, Dr. Yoko OHTOMO, and Dr. Ryosuke KIKUCHI, assistant professors of Laboratory of Environmental Geology, for their kindness, great support, and the guidance during my research. I would also like to thank all the committee members of my doctoral thesis for their constructive comments, encouragement, and the good recommendations.

I would never forget to give my gratefulness to my research team, Frances CHIKANDA and Tatsuya MATSUI, for their hard work, and good collaboration. I am grateful to have them as teammates. I also want to thank to my fellow lab mates for all the kindness and unlimited support. Particularly, I am thankful my seniors Kanako TODA and Ryohei KAWAKITA for their guidance and teaching me to use various equipment in the laboratory. I want to give my gratitude to Yoshie HOSHI and Yuka ISHIOKA, secretary of Laboratory of Environmental Geology for their kind support and caring in all of my activities.

I would like to thank my colleges at Institute of Technology of Cambodia, and all my friends in Japan and Cambodia, especially, Muoy Yi HENG for their fully support, especially during the COVID-19 pandemic. I also thank the Ministry of Mine and Energy, Cambodia for giving me permission to use the study area in Cambodia. I would like to thank Dr. Sitha KONG, Panha MEAS, Unsovath EAR, and Ratha PIL for the fieldwork guidance and all the support.

I would like to extent my gratitude to Geological Survey of Hokkaido, and Mr. Susumu NOROTA for giving me the opportunity use the study area in Hakodate. I would also like to thank JICA for granting me Scholarship under KIZUNA program, which supported all the activities in the PhD program.

I am extremely grateful to my family for their love, prayers, caring, sacrifices, patience and continues to support me until I successfully finished my research. Their presents are the great motivation for me to pursue my own dream. In addition, I would like to dedicate my work to my mother, who looks from the heaven. I hope you would be proud of me.

Finally, my appreciation to everyone who directly or indirectly supported me to complete this research.

Sereyroith TUM

Table of Content

List of tables

List of Figures

List of abbreviation

ALD	Anoxic Limestone Drains
BET	Brunauer-Emmett-Teller
CB	Charge Balance
CD	Charge Distribution
DNA	Deoxyribonucleic Acid
DO	Dissolve Oxygen
DV	Diversion Wells
EC	Electric Conductivities
ETLM	Extended Triple-Layer Model
Fe^{2+}	Ferrous iron
Fe^{3+}	Ferric iron
GDL	Generalized Double-Layer
GSH	Geological Survey of Hokkaido
GSS	Geochemist's Spreadsheet
GWB	Geochemist's Workbench
ICP-AES	Inductively Coupled Plasma–Atomic Emission Spectroscopy
ICP-MS	Inductively Coupled Plasma–Mass Spectrometry
IRGS	Intrusive Gold-Related System
JOGMEC	Japan Oil, Gas and Metals National Corporation
LDH	Layer Double Hydroxide
LOI	Loss On Ignition
LST	Limestone Sand Treatment
NA	Natural Attenuation
NTU	Nephelometric Turbidity Units
OLC	Open Lime Channel
ORP	Reduction Potential
QGIS	Quantum Geographic Information System
SAPS	Alkaline Producing Systems
SEM-EDS	Scanning Electron Microscopy-Energy and Dispersive X-Ray Spectroscopy
SRB	Bioreactors Or Sulfate-Reducing Bioreactors
SSA	Specific Surface Area
SSLB	Steel Slag Leach Beds
TDS	Total Dissolve Solid

TE	Tris and Ethylenediaminetetraacetic Acid
TLM	Triple-Layer Model
USGS	United States Geological Survey
VFW	Vertical Flow Wetlands
WHO	World Health Organization
XRD	X-Ray Diffraction
XRF	X-Ray Fluorescence

I. General introduction

1.1. Acid mine drainage and natural attenuation

Acid mine drainage (AMD) contaminations are the worldwide environmental challenges, where 19,300 km of river and 72,000 ha of lakes and reservoirs reported seriously affected form mining activities since 1989 (Johnson, 2009; Sarmiento et al., 2018). In the past decades, some of mining activities were closed, but AMD remains generate. Once, AMD leaks to the environment, it severely affects to soil, aquatic ecology, as well as human health (Kefeni et al., 2017). AMD is generated by oxidation of metal sulfides dissolved oxygen and water release from mining activities including active mines, abandoned mines, dumping site, and mine tailing (Berger et al., 2000; Fukushi and Sato, 2005; Kefeni et al., 2017). The reaction of pyrite, a common mineral among of metal sulfides, responsible for AMD generation (Kefeni et al., 2017). Dissolved ferrous iron and sulfuric acid are generated during their reaction, which lead to decreasing pH of natural water and promote hazardous elements dissolution from ore and waste rock to environment. The trace metals cations associate with metals sulfides such as; Cu, Cd, Pb, Ni, and Zn and metalloids AsO_4^{3-}, CrO^{4-} , $Sb(OH)^{6-}$, and SeO_3^{2-} , were also reported as the toxic elements release from AMD which concern to human health (Baleeiro et al., 2018; Chikanda et al., 2021; McNeal and Balistrieri, 1989; Regenspurg and Peiffer, 2005; Zhou et al., 2018). The environmental pollution measurement depends on chemistry of AMD and pH which are wisely different according to geological setting, hydrological, and geochemical setting (Kefeni et al., 2017). For instant, Tito river basin in Spain was contaminated by AMD had an average pH 2.38, total Fe (3,954 mg/ L), Ni (0.887 mg/L) and SO_4 (15,164 mg/L) (Nieto et al., 2013). An acid pond in northern Manitoba, Canada contains maximum 10,900 mg/L Fe, 21,400 mg/L SO_4, 50.5 mg/L Zn, 252 mg/L Al, 15.8 mg/L Cu, and 0.972 mg/L Pb with pH 2.33 (Moncur et al., 2006). In Sao Domingos mine waste leachates had pH 2.6 and the average concentration; 4,210 mg/L Fe, 1,480 mg/L Al, 2448,070 mg/L Zn, 30 mg/L Pb, 6.2 mg/L As, and 7,700 mg/L SO_4 (Abreu et al., 2008). In Dabaoshan mine, in south China, supplied a pH 2.8, SO_4 19940 mg/L, Mn 60 mg/L, Pb 0.60 mg/L and Mg 130 mg/L (Chen et al., 2015). An abandoned mine in Nishinomaki in South West Gumma, Japan has pH 3.08, Fe 13.5 mg/L, SO_4 374 mg/l, Co; 0.012 mg/L, As 0.255 mg/L (Fukushi et al., 2003a). The most extreme AMD is at the underground of Iron

Mountain, California, where the lowest pH had ever recorded in the literature was -3.6 with the total concentration of metals as high as 200,000 mg/L and sulfate concentration 760,000 mg/L (Nordstrom et al., 2000).

AMD can be naturally remediated while flowing into natural river due to natural attenuation (NA) mechanisms (Fig. I-1) known as the act without human intervention to reduce the mass, toxicity, mobility, volume, or concentration of contaminants by volatilization, incorporation as biomass, degradation, and stabilization such as sedimentation, precipitation, and phytostabilization (Favas et al., 2019). Dilution of background river is one of the physical mechanisms of natural attenuation to neutralize AMD in the stabilization process, and diluting the contaminants from the drainage (Ito et al., 2017). Previous studies reported some AMD cases naturally remediated to less than environmental regulation limit without human assistant. For examples; Fukushi et al. 2006 found an abandoned mine self-remediated after leaching to environment when there was formation of schwertmannite. Schwertmannite successfully removed As from the drainage to less than WHO guideline. Similarly, at Ilwang mine, Korea, As coprecipitates and adsorbs by schwertmannite in acidic conditions (Park et al., 2016). Ito et al. (2017) reported several natural attenuation mechanisms the river contaminated by AMD including mineral precipitation of Th, and U adsorption onto ferrihydrite at near neutral pH ~5.5. At circumneutral pH at an abandoned mine Anai, Japan, As, and Zn were removed ferrihydrite and Zn-Fe-LDH from the mine drainage (Chikanda et al., 2021). Favas et al. (2019) shows phytostabilization potentially uptake U from water contamination by roots or rhizomes. The AMD from Pecos mine in New Mexico leaked from the mine site mix with a tributary and reacted with limestone of the local bedrock resulted increasing the pH to greater than 7. This phenomenon allows Al, Cu, Fe and Pb precipitation while other minerals like Zn, Mg, Mn, and SO_4 decreased by dilution (Berger et al., 2000).

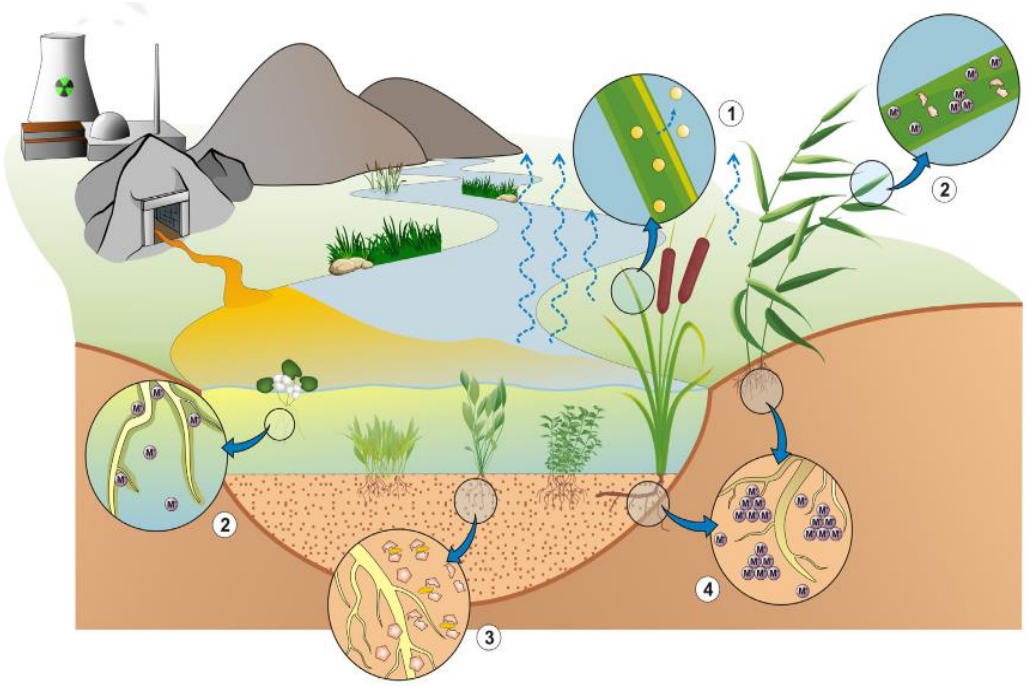

Fig. I-1. Schematic of AMD natural attenuation 1) Volatilization (2) incorporation as biomass (3) degradation and (4) stabilization (precipitation, sedimentation, phytostabilization). (Favas et al., 2019)

1.2. Problem statements

The artisanal or unofficial mines are extremely concerned to environment due to lack of control by the local authorities, particularly in least developed countries. The artisanal mining impacts are separated into parts; (1) the impact of mining operation by chemical and biological contamination, and (2) the socio-political and economic issues (Tarras-Wahlberg, 2002). The tailing and AMD generation from artisanal mines during the operation and after operation are not well treated before releasing to natural environment.

In addition to artisanal mines, the abandoned mine is also the challenges. The numbers of abandoned mine sites are not well determined but it is estimated around several millions abandoned mine worldwide. At least 50,000 abandoned mines are known in Australia, while in the USA, it is more than 550,000 have been discovered, and more than 10,000 are identified in Canada (Hufty, n.d.). River catchments about 12 000 km^2 in northern England was directly affected by historical metals mines (Great Britain and Environment Agency, 2008). More than 5000 abandoned mines in Japan, while about 450 mine sites reported having mine and water pollution (Tomiyama et al., 2019). Since 1973, Japan Oil, Gas and Metals National Cooperation (JOGMEC) have been responsible for mine pollution control under the fund support from Ministry of

Economy, Trade, and Industry. JOGMEC spend ¥17 billion (Japanese yen) to support 45 wastewater treatment projects at the abandoned mine sites since 1973 to 2019 ("JOGMEC," n.d.). In the active mine sites, the mining companies are responsible for AMD treatments due to the governmental restriction of each country. The mining companies could cover all the expenses during their activities. Yet, once the mining activities close, the mining company may no longer be responsible for the treatment. There is no specific person responsible for water treatment artisanal and abandoned mines.

The artisanal mines and the abandoned mines without proper treatment are highly depending on the natural attenuations. Unfortunately, not all natural attenuation occurrences can secure the water quality at the contaminated areas. Thus, AMD treatment is mandatory to ensure the water quality and the environmental risks. The AMD treatment methods are commonly used include active and passive treatment. Active treatment methods are the simple approaches, involve chemical reagents to neutralize acids, however it produces the huge amount of sludge, requires regularly maintenances, and quite costly (Naidu et al., 2019). In contrast to active treatment, passive treatment is highly depend on natural processes such as; biological, geochemical, and physical processes to treat AMD (Skousen and Ziemkiewicz, 2005). Therefore, passive treatment is more sustainable and cost-effective than active treatment is recommended. However, passive treatment is practical only if there is enough understanding of natural attenuation mechanisms. Ferric iron minerals, the ubiquity minerals in the AMD environment, has the capacity to remove toxic element due to surface complexation, structural incorporation, and surface precipitation (Shi et al., 2021). Ferric iron minerals have the essential roles in natural attenuation as well as passive treatment (Florence et al., 2016; Fukushi et al., 2003a). Despite the critical roles of ferric iron in passive treatment, it is remains uncertain how it forms in natural environments. It is necessary to clarify the dynamics of irons species of AMD in various hydrological conditions as the essential indication for passive treatment.

1.3. Objectives

The objectives of this doctoral research are to elucidate the effects of natural attenuation occurrences for various sources of iron species in acid mine drainage in

different climate conditions and its implication for passive treatment methods. The implementations to reach these goals, the aspects that particularly focus on:

- Climate conditions are the main factors controlling hydrological condition of the water body included river flowrate, rain falls, water input, water discharge and many other parameters. In case of the river catchment that contaminated by AMD, the river water input might affect to the pH and water chemistry in the rivers. Thus, one aspect of this research is to characterize the differences of various AMDs' geochemical behaviors in different climate conditions that possibly control the natural attenuation mechanisms.
- Ferric iron mineral formations can be found in different conditions including the acidic environment. Since it is simply forms in various conditions, so, these minerals can facilitate the natural attention processes. Ferric iron minerals require dissolved ferric iron as the formation source. On the other hand, the dominant iron species from AMD is typically ferrous iron. Therefore, another aspect of this study is to elucidate the impacts of iron species and its dynamics that may well influence to AMD attenuations.
- Besides understanding the different aspects of natural attentions impacts and mechanisms, it is necessary to understand in what manners that the natural attenuation mechanisms may be feasible to apply in AMD passive treatment. Hence, the last aspect of the research is to ascertain the advantage of natural attenuation mechanisms to apply to AMD passive treatment methods by using geochemical modellings.

1.4. Approach and methodology

To cover a wide-ranging investigation of AMD characteristics, two different locations of AMD contamination sites were selected for this study. One location is Mondulkiri mine site situates in Mondulkiri province, Cambodia. Mondulkiri mine site is an active artisanal gold mine, where tailing and AMD waste discharged randomly without appropriate treatment. Another study area is Shojin mine in Shikabe town, Hokkaido, Japan. Shojin mine is an abandoned mine, where the mining activities was closed a few decades ago. The implementation of this study was separated into three different approaches as listed in Table I-1. Firstly, filed investigations were conducted

in each study areas base on the measurement targets included field data measurement, water sampling, sediments, and rock sampling. Later, the data analysis of the water, sediments, and rock samples were analyzed at Hokkaido University. The last approach of this study is the data interpretation and geochemical modelling to facilitate the study.

Table I-1. The approach and methodology of that were used to for this research.

Field investigation	Data analysis	Geochemical modelling
- On site measurement for water parameters (temperature, pH, ORP, DO, EC, Alkalinity) -Water sampling (preserve for anion, cations) -Sediment and ore sampling (Sediment along the stream bank, and waste and ore from the mine site)	-Water chemistry analysis (IC/ICP-AES, ICP-MS) -Sediment and ore's minerals identification (XRD, SEM, Petrography) -Sediment and ore's chemical composition identification (XRF, acid digestion, selective extraction)	-Determine the mineral formation -Obtained the adsorption behaviors of toxic elements -Determine the process of natural attenuation -Devise the passive treatment methods (Geochemist's Workbench and Phreeqc)

1.5. Thesis outline

This thesis contains of eight chapters (I-VIII), which describes all the aspects regarding the natural attenuation, iron dynamics, and passive treatment implications from introduction to conclusion. Firstly, Chapter 1 introduced the general introduction, problem statements, and objectives of the research.

Chapter 2 aims to describe the detail literature reviews of the import roles of iron in AMD to remove hazardous elements from contaminated water, the impact of AMD in the mining sites, the treatment methods for AMD, and the passive treatment methods.

Chapter 3 provides the detailed case study of an artisanal gold mine in Cambodia. This chapter shows the effect of the seasonal dynamics that effect to natural attenuation of contaminated tributary. The accomplishments of the investigations are the determination of natural attenuation mechanisms in the study areas. Dilution of neutral

water and rainwater play the major role to raise the pH and diluted toxic elements in the tributary. While the pH of tributary increase to above 3, schwertmannite started to form and act as the absorbent materials for As.

Chapter 4 describes the case study of an abandoned mine site in the northern Japan. The field investigation was conducted on two rivers where they were negative impacted by AMD from the same sources. This investigation successfully determined the important role of dilution of the background river to the drainage water. In this case study, rainwater is not effectively influence to the seasonal changes of the natural attenuation mechanisms as it was in Chapter 3. Schwertmannite found in the rivers has similar roles to the schwertmannite found in Chapter 3. Schwertmannite adsorbed As from the contaminated rivers.

Chapter 5 shown the significant roles of iron species and dynamics in the study area. This chapter highlights the important factors including iron kinetics, and adsorption that can be taken into consideration while designing the passive treatment methods. The Fe^{2+} oxidation rate and rate constant were obtained from the field data. In addition, schwertmannite precipitation rate and rate constant were determined using the drainage water experiments. The drainage with Fe^{2+} dominant, iron oxidizing bacteria is necessary for Fe^{2+} oxidation rate. On the other hand, in the mine drainage where Fe^{3+} is dominant, Fe^{2+} oxidation rate can be neglected. Yet, determining the precipitation rate and the optimum pH for schwertmannite formation are important. The chapter also described the surface complexation model of As, Cd, Pb, and Ni on schwertmannite using generalize double layers model.

Chapter 6 and Chapter 7: intends to investigate the geochemical signatures of each case study by using geochemical modelling. The process models of the represent the study area were conducted and validated by measurement data. Geochemical models are applicable to use for geochemical behaviors characterization that can represent the field investigation. This finding could be used to predict the geochemical behaviors while applying for passive treatment or devise the passive treatment methods for AMD.

Chapter 8 describes the general conclusion of this thesis and its implications of the research. This chapter points out the finding of this study and delivers the implication that can be also utilized for various case studies.

II. Literature review

The literature review's objective is to deliver the background knowledge regarding the AMD generations, the role of iron in natural attenuation of AMD and its relationship to passive treatment methods.

2.1. Roles of Fe minerals in toxic elements scavenges from AMD

Ferric iron minerals found in the mine drainage can be identified such as; ferrihydrite, lepidocrocite, goethite, jarosite, and schwertmannite and so on (Shi et al., 2021; Wang et al., 2006). It is able to incorporate metals and metalloids by surface complexation, surface precipitation, structural incorporation (Acero et al., 2006; Meng et al., 2020; Paikaray, 2020). The metals and metalloids retention on iron (oxyhydr)oxides and/or oxyhydroxysulfates mechanisms are minerals species dependent to surface sites and morphological structures (Fukushi and Sato, 2005). Metals ions species properties such as ironic radius, hydration energy, solubility, electronegativity, and geometry or coordination numbers are also significantly control their interactions with iron (oxyhydr)oxides and/or oxyhydroxysulfates as well (Shi et al., 2021). Highly toxics elements that mostly found in acid mine drainage such as As, Se, Cu, Cd, Pb, and Ni reported having bad impact to human health in case of overdose of usage. The environmental regulation limit for drinking water set by World Health Organization (WHO) for those elements are 2 mg/L (Cu), 0.003 mg/L (Cd), 0.010 mg/L (Pb), 0.07mg/L (Ni), 0.010 mg/L (As) and 0.040 mg/L (Se).

In most of geological environments, ferric iron minerals have isoelectric points of 8.6 with a net positive charge, having high sorption affinities for As species. The adsorption capacity of As^{3+} onto Fe hydroxide occurs at pH between 7 and 10, while As^{5+} adsorption has strong adsorption capacity at between pH 4 to 7 (Wang and Mulligan, 2006). Park et al. (2016) reported that As co-precipitates with Ferrihydrite is greater than adsorption, yet these mechanisms is no significant different on schwertmannite. Selenium species present in several oxidation state in environment but the species concern to human health and ecosystem are selenite (Se^{4+}) or selenate (Se^{6+}) (Das et al., 2013). In acidic condition Se^{4+} and Se^{6+} can be co-exists in the oxidation state. The binding the mechanisms of Se^{4+} and Se^{6+} to the ferric (oxyhydr)oxide minerals contrast to each other. Se^{4+} has the affinity to form outer-spere surface

complexes on goethite while Se^{6+} tends to attach to an inner-sphere bidentate surface complex on ferrihydrite and lepidocrocite (Marouane et al., 2021; Rovira et al., 2008). Se^{4+} and Se^{6+} behave similarly while binding to schwertmannite by mainly bounding to inner-sphere corner-sharing and partially to outer-spere complexes with Fe^{3+} surface sites. Yet, Se^{4+} has higher affinity to sorb onto schwertmannite (Marouane et al., 2021). Cations present in acidic condition such as Cu^{2+}, Cd^{2+}, Pb^{2+}, and Ni^{2+} bond to iron (oxydyr)oxide and the adsorption mechanisms are depended to miner species, pH, and surface loading, and metal ion concentration (Benjamin and Leckie, 1981; Moon and Peacock, 2012; Saeki and Kunito, 2012; Shi et al., 2021). The adsorption of Cd^{2+} occurs at the higher pH (> 7), yet having a weaker biding affinity on iron (oxyhydr)oxides than Cu, Pb or Ni (Buerge-Weirich et al., 2002; Liang et al., 2018; Shi et al., 2021).

2.2. Fe^{2+} and Fe^{3+} dynamics in mine drainage

Iron, one of the major elements, predominant in AMD due to the dissolution of pyrite (Fe_2S), Arsenopyrite (FeAsS), and chalcopyrite ($CuFeS_2$). In aqueous solution, iron species exist as ferrous iron (Fe^{2+}) and ferric iron (Fe^{3+}). In acid mine drainage, the reaction and transformation of iron from one to another species are quite complex. The dissolution of pyrite in (Reaction II-1) releases in Fe^{2+}, while Fe^{3+} liberates from Fe^{2+} by the oxidation process under abiotic or biotic condition (Reaction II-2). Dissolved Fe^{3+} can also exist as complexes such as $FeOH^{2+}$, $Fe(OH)_2^{+}$, $Fe(OH)_3^{0}$, or $FeSO_4^{+}$ (Table II-1) (Grundl and Delwiche, 1993) in aqueous solution. Hydrolysis of Fe^{3+} resulted the precipitation of amorphous phase such as ferric oxyhydroxides and/or oxyhydroxysulfates (4) (Grundl and Delwiche, 1993; Paikaray, 2020) according to various conditions as shown the iron mineral stability diagram in Fig. II-1. The stability diagram of ferric iron minerals (Blanc et al., 2012; Sánchez-España et al., 2011). Iron (oxyhydr)oxides and/or oxyhydroxysulfates exist in natural environment, contaminated land environment, or mine contamination environment, yet having significant roles to remove metal(loid)s in solution (Schoepfer and Burton, 2021; Shi et al., 2021).

$$FeS_2 + 7/2O_2 + H_2O \rightarrow Fe^{2+}_{(aq)} + 2SO_4^{2-} + 2H^{+} \quad \text{(II-1)}$$

$$Fe^{2+}_{(aq)} + ¼\ O_2 \rightarrow Fe^{3+}_{(aq)} + ½\ H_2O \quad \text{(II-2)}$$

$$Fe^{3+}_{(aq)} + H_2O \rightarrow Fe^{3+}_{(ppt)} \quad \text{(II-3)}$$

$$Fe^{3+}_{(ppt)} \rightarrow \text{amorphous crystallite} \quad \text{(II-4)}$$

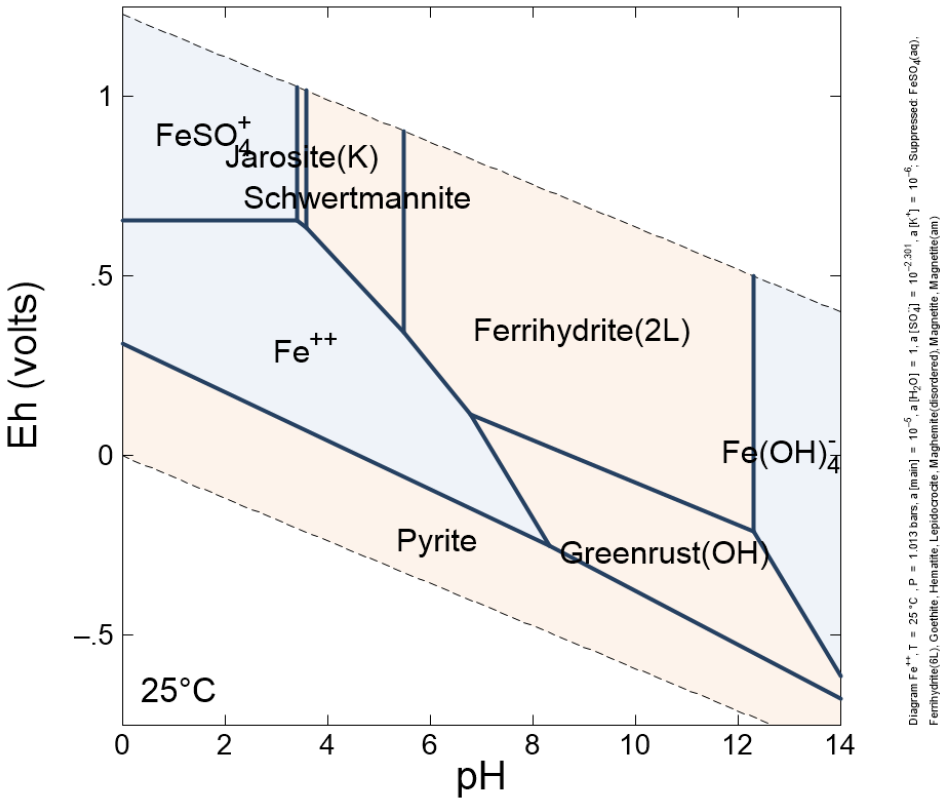

Fig. II-1. The stability diagram of ferric iron minerals obtained by using React module of Geochemist's workbench

Table II-1. Iron species in queues solution and ferric iron minerals

Species	**Formation reaction**
$FeOH^{2+}$	$Fe^{3+} + H_2O \rightarrow FeOH^{2+} + H^+$
$Fe(OH)_2^+$	$Fe^{3+} + 2H_2O \rightarrow Fe(OH)_2^+ + 2H^+$
$Fe(OH)_3^0$	$Fe^{3+} + 2H_2O \rightarrow Fe(OH)_3^0 + 3H^+$
$FeSO_4^+$	$Fe^{3+} + SO_4^{2+} \rightarrow FeSO_4^+$
Ferrihydrite	$Fe^{3+} + 3H_2O \rightarrow Fe(OH)_3 + 3H^+$
Goethite	$Fe^{3+} + 2H_2O \rightarrow FeO(OH) + 3H^+$
Schwertmannite	$8Fe^{3+}_{(aq)} + ySO_4^{2-}{}_{(aq)} + (24\text{-}2y+x)/2H_2O \rightarrow Fe_8O_8(OH)_x(SO4)_{y(s)} + (24\text{-}2y)H^+_{(aq)}$
Jarosite	$3Fe_2(SO_4)_3 + K_2SO_4 + 12H_2O \rightarrow Fe_3(SO_4)_2(OH)_6) + 6H_2SO_4$

The reaction rate from Fe^{2+} to Fe^{3+} is commonly a rate limiting process of ferric iron mineral formation. Kinetics of reaction (II-2) is dependent to pH, temperature,

concentration of dissolve oxygen, and catalysts (Stumm and Lee, 1961) given in equation (1). Metals ions and microbial in acid mine drainage are the significant catalyzers in Fe^{2+} oxidation process, yet the microbial activities have a greater catalyzer capacity than metals ions (Pesic et al., 1989; Stumm and Lee, 1961). In acidic condition pH below 4.5 of abiotic condition, the kinetic of ferrous oxidation dependence of the oxygenation rate and hydrogen ion concentration as written in Equation 1 (Stumm and Lee, 1961). Under pH 4.5, the initial 0.001M ferrous iron concentration, the oxidation of 50% of ferrous iron to ferric iron would take 286 days with the oxidation rate constant; k= 8×10^{13} L^2/mol^2 at 25 ^oC. On the other hand, under the biotic condition the oxidation of ferrous iron would take on 31 minute to oxidize 50% of 0.001M of Fe^{2+} (Pesic et al., 1989).

Iron bacteria is recognized carrying geological process known as iron oxidation catalyzer since the 1830s (Emerson et al., 2010). In the extreme environment as it is in mining environment, microbial community are not well characterized, yet, it was reported that 1-10% of the microbial community can be cultured and isolated for the study of living organisms (Cardenas and Tiedje, 2008). In the sulfate rich mining environment, acidophilic bacteria such as *Acidithiobacillus ferrooxidans*, *Leptospirillum ferrooxidans* and other iron oxidizing bacteria act as the catalyzer to oxidize ferrous sulfate to ferric sulfate (Auld et al., 2013). Pesic et al. (1989) conducted the study of the role of iron oxidizing bacteria in ferrous oxidation rate using *Thiobacillus ferrooxidans*; belong to *Acidiphilum* genus (Rawlings and Kusano, 1994). In acidic condition, at pH 2.2 to 3.5 under atmospheric condition (25 ^oC), the rate expression can be written as Equation II-2; where C_{bact} is the concentration of bacteria, R; universal gas constant, kJK^{-1} , T; absolute temperature, K. P_{O2} is oxygen partial pressure.

$$\frac{-dFe^{2+}}{dt} = \frac{k[Fe^{2+}]}{[H^+]^{1/4}}(P_{O_2}) \qquad \text{Equation II- 1 (abiotic condition)}$$

$$-\frac{d[Fe^{2+}]}{dt} = k[Fe^{2+}] = 1.62\times10^{11}C_{bact}\,[H^+][Fe^{2+}]P_{O_2}e^{-(\frac{58.77}{RT})} \qquad \text{Equation II- 2 (biotic condition)}$$

The ferrous oxidation rate constant (k) in biotic condition is:

$$k = k'C_{bact}\,[H^+]P_{O_2};\ k' = 1.62\times10^{11} \qquad \text{Equation II- 3}$$

The present of iron oxidizing bacteria is one of the driven pathway controls formation of ferric minerals natures, morphology, and phase transformations (Feng et al., 2021). For example, the various *A. ferrooxidans* strains in the same AMD environment promote various minerals precipitation such as tooeleite, schwertmannite, and jarosite (Egal et al., 2009). Schwertmannite and jarosite are commonly found as the products of iron-oxyhydroxysulfate materials in the mining environment due to the involvement of the *A. ferrooxidans* strains (Zhu et al., 2013). Schwertmannite is the primary solid phase mineral (Egal et al., 2009; Feng et al., 2021), while jarosite requires the monovalent (Na^+, Ag^+, NH_4^+, H_3O^+, K^+) compounds (Dutrizac, 2008) during formation.

2.3. Schwertmannite in mine drainage environment

Occurrences: The schwertmannite is commonly found deposit in the pyrite rich mine environment such as coal mines, metalliferous mines, and acid sulfate soils (Childs et al., 1998; Fitzpatrick et al., 2017; Nieto et al., 2013). Schwertmannite color range from yellow to brown consists of Fe^{3+} coordinates with SO_4^{2-} and OH^- ions under the influence of drainage contaminant with an ideal chemical formula of $Fe_8O_8(OH)SO_4$ (Regenspurg et al., 2004; Schwertmann et al., 1995), form under acidic condition (pH: 2.5-4.5) according to reaction II-5. In natural condition, schwertmannite formation is most likely under the effect of microbial activities that spurs up the newly from Fe^{2+} oxidation (Reaction 2) (Baker and Banfield, 2003).

$$8Fe^{3+} + SO_4^{2-} + 14H_2O \rightarrow Fe_8O_8(OH)_6(SO_4) + 22H^+ \qquad \text{(II-5)}$$

Morphology: Schwertmannite has two morphological structures; smooth and rough surface, particle sizes range from nano scale to microscale (Fernandez-Martinez et al., 2010; Zhang et al., 2018). Fig.II-2 show schwertmannite particles aggregated from various synthesis methods. The particle sizes in model (i) given the smooth rounded surface due the quick supply rate of H_2O_2. Model (ii) and (iii) provided the rough surface, where it aggregated as hedge-hog-like or sea urchin-like structures due to higher synthetic temperature (> 60 ^oC) or a slow addition rate for H_2O_2. pH value set as environment factor determining the precipitation efficiency of Fe in oxidative reaction or hydrolysis (Feng et al., 2021). Schwertmannite surface structures have a great impact on metal(loid)s surface complexation. The more the roughness surface structure, the

larger the specific surface area (SSA), and the better for metal(loid)s adsorption (Dzombak and Morel, 1990a).

Stability and transformation: Schwertmannite is a meta stable mineral that form directly after Fe^{2+} oxidation process, can be transform or aging to jarosite or goethite base on various condition (Kim and Kim, 2020; Knorr and Blodau, 2007; Wang et al., 2006). Schwertmannite stability directly link to pH condition. At pH 3 to 4, schwertmannite is at the most stable phase and might takes several years to transform to other phases (Regenspurg et al., 2004). Schwertmannite tents to transform to jarosite if there is the adequate present of monovalent cations like K^+, NH_4^+, or Na^+ at low pH condition (pH<3) (Acero et al., 2006). At pH from 4 to 7, schwertmannite is more likely to age as goethite since the transformation rate increases to double (Schwertmann and Carlson, 2005).

Environmental implications: The ubiquity formation of schwertmannite in the mine areas has the important roles in natural attenuation processes (Fukushi et al., 2003a; Park et al., 2016; Webster et al., 1993). The ability of schwertmannite to form in acidic condition facilitates the toxic metals retention. Its formation successful uptakes As, Cr, Cu, and many more elements greater than 90% from mine drainage water (Khamphila et al., 2017; Webster et al., 1993) . Its implications are used for AMD treatment (Florence et al., 2016; Paikaray, 2020) for both passive and active treatment methods.

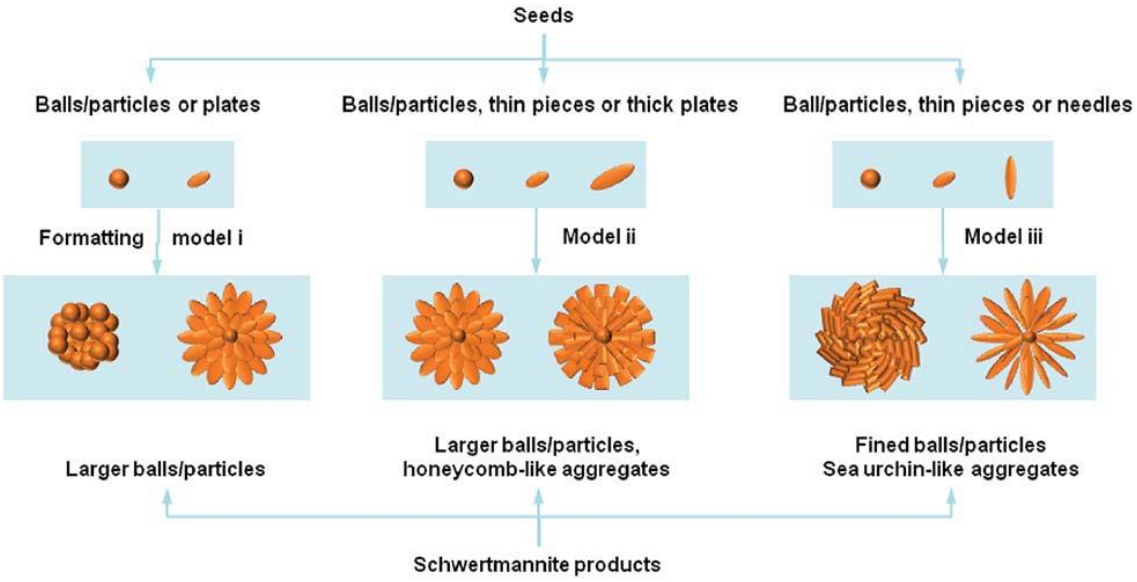

Fig. II-2. Schematic illustration of the formation process from seeds to schwertmannite products(Zhang et al., 2018)

2.4. Acid mine drainages treatment

Numerous of rivers catchments are reported negatively impact by AMD that is not consumable. The increasing of water consumption triggers the need of safety drinking water level. Various remediation methods have been research and implemented worldwide on physical and chemical, electrochemical, and biological process in order to secure the water quality and quantity of portable water as well as the natural water resources (Speight, 2020). The mechanisms that are used in AMD treatment are listed in Table II-2. Treatment technologies to attain those mechanisms are separated to two methods: active and passive treatment methods. The most common mechanisms are pH control and oxidation by alkalinity generation by additive alkaline material or biological mediation by bacteria metabolism by organic matters as below.

- Alkalinity generation by limestone dissolution equation:

$$CaCO_3 + H^+ \rightarrow Ca^{2+} + HCO_3^- \text{ (II-6)}$$

- Oxidation and hydrolysis (metals precipitation) in aerobic system

$$4Fe^{2+}_{(aq)} + 4O_2 + 10H_2O \rightarrow 4Fe(OH)_{3\downarrow} + 8H^+ \text{ (II-7)}$$

- Sulfate reducing bacteria metabolism for alkalinity generation:

$$2CH_2O + SO_4^{2-} \rightarrow H_2S + 2HCO^{3-} \text{ (II-8)}$$

Table II-2. The AMD treatment by chemical, physical, and biological mechanisms (Taylor et al., 2005)

pH control	oxidation/ reduction	Chelation
Adsorption	Electrochemical	Biological mediation
Adsorption	Sedimentation	Ion exchange
Complexation	Flocculation-filtration-settling	Crystallization

The selection of active or passive treatment base on several factors, but the essential variable are acid, acidity, acidity load, and flow rate (Taylor et al., 2005; Trumm, 2010) as shown in Fig. II-3. Besides, other parameters should be considered are location of the mine site, topography, and climate conditions (rainfall pattern) (Trumm, 2010). Acid and acidity sound similar but they are different in definition. “Acids” are the compounds or ions that can promote protons, basically, it is the measure of H^+ or pH

(Puchtler et al., 1985; Taylor et al., 2005). "Acidity" is the measurement of both H^+ and mineral or latent, which is the potential concentration of H^+ generated by the precipitation of metals hydroxides in solution at a given pH (Taylor et al., 2005). "Acidity load" is the product of "Acidity" and flow rate, which is crucial for ideal treatment requirement (Taylor et al., 2005). Acidity and acidity load are calculated as the equations below for instant AMD contain Fe, Al, and Mn at a given pH.

- Acidity (mg/L $CaCO_3$) = $50 \times \{3\times[Fe^{3+}+ Fe^{2+}]/56 +3\times [Al^{3+}]/27+ 2\times[Mn^{2+}]/55 +1000\times10^{-(pH)}\}$ (Equation II-4)
- Acidity load (tonnes $CaCO_3$/day) = 10^{-9} × 86400 (conversion factor) × flow rate (L/s) × acidity (mg/L $CaCO_3$) (Equation II-5)

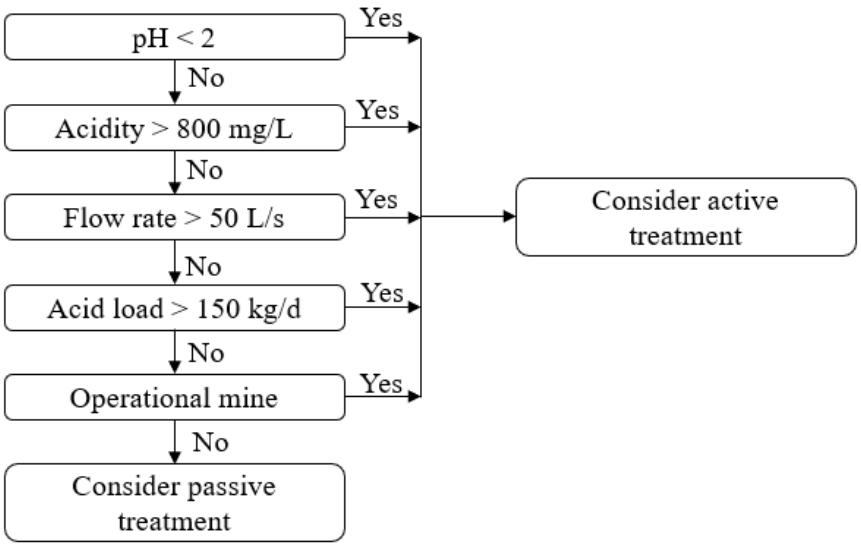

Fig. II-3. Active or passive treatment decision making flow chart (Trumm, 2010)

2.4.1. Overview active treatment methods

Active treatment is the conventional mechanical mechanism to ameliorate the contaminated water by adding alkaline chemicals to raise the pH, counteract acidity, and precipitate the metals (Seervi. et al., 2017). The active treatment technology involving; cost of equipment and machines, chemicals reagent, and manpower, which is quite costly and regularly need maintenance (Eppink et al., 2020). The active predominant methods using in AMD treatment methods include chemical precipitation, in-line aeration, oxidation, electrochemical, dosing with alkali, reverse osmosis, iron exchange, and sedimentation (Seervi. et al., 2017; Trumm, 2010). These methods produce a significant amount of sludge which required proper place to dispose. This

chapter will not discuss in detail for active treatment, however, the design or suggestion of active treatment of AMD can be determined by using computer software AMDTreat (Cravotta et al., 2015).

2.4.2. Passive treatment

Passive treatment is an AMD treatment method rely on natural process of AMD systems such as physical, geochemical, and biological processes. It takes the advantage of the natural systems to improve the water quality with the minimal operation and maintenances (Gazea et al., 1996). The design of passive treatment required the detail study of site characteristics, water chemistry, bioavailability, local topography, flow rate (Skousen et al., 2017) as shown in Fig II-4. The system easily fail to operate if it is not well designed (Trumm, 2010). Passive treatment systems divided into main type, biological and geochemical passive treatment. The passive metals retention mechanisms are: (1) metal oxidation and hydrolysis (facilitate by oxidizing bacteria), hydroxide floc formation, precipitation, co-precipitation of trace metals with Fe hydroxide, Al hydroxide or Mn oxide; (2) reduction of metals and formation of metals sulfides in organic matters; (3) surface complexation, sorption to organic matters and uptake by plans; (4) alkaline materials addition (Gazea et al., 1996; Seervi. et al., 2017).

Biological process of passive treatment

Biological treatment process is the treatment methods base on the biogeochemical dynamics reaction with AMD by using a constructed wetlands to mimic the natural ecosystem. When AMD is in contact with the artificial shallow pond systems fill with limestone, gravel, soil, or organic matter enables the redox, acid neutralization, and minerals precipitation functions the wetland plans (Skousen et al., 2017).

Aerobic wetlands (AeWs) are the system to treat net alkaline waters with the main contamination targets are Fe or Mn. The roles of aerobic wetland is allow the oxidation of ferrous iron by aerated water to ferric iron and precipitation as hydroxide, oxyhydroxide and oxides floc (Gazea et al., 1996) . The bottom layer of the channel commonly impermeable layer to prevent the contamination infiltrate to groundwater. The additive suitable medium should be added in the AeWs channels (depth: 10 cm to 50 cm) included soil, and vegetations (Typha) to promote the slow flowrate and

attachment sites for floc. In addition, limestone should be add to maintain the net alkaline water conditions in the systems (Skousen et al., 2017).

Anaerobic wetlands (AnWs) or bioreactors relatively deep channels (depth > 30 cm) filled with permeable substrates consist of soil mixed with peat moss, mushroom compost, saw dust hay bales, and organic matters. Limestone is added to improv alkalinity generation. Commonly, Typha and other wetland vegetation are grown in the systems (Skousen et al., 2017). The water flow pass through the permeable substrates promotes bacterial sulfate reduction due to lack of oxygen, thus enable insoluble metals precipitation. Alkalinity is produced by microbial sulfate reduction allow metal precipitation hydroxides. The metals can removal by organic matter is also reported in the AnWs, but it limited to the different types of organic matter, however metals removal by hydroxide precipitation is the dominant mechanisms (Skousen et al., 2019).

Vertical flow wetlands (VFWs) or alkaline producing systems (SAPS) is the combination of AnWs and anoxic limestone drains as it includes the organic matters and limestone beds, however the water flow downward from the top of the system throw the drainpipes. The mechanisms control the VFWs are: (1) organic matter reduce the oxidized water and removes Fe and Al by ions exchange or filtering; (2) and later the water under reducing conditions with less heavy metals flow toward limestone produces more alkalinity (Demchak et al., 2001). The method is able to raise the drainage pH and avoid the armored limestone in the system.

Bioreactors or sulfate-reducing bioreactors (SRB) is similar to SARS methods, however limestone and organic matter mixes together in the system (Skousen et al., 2017). The suitable organic carbon sources in anaerobes system introduce sulfate-reducing bacteria to reduce sulfate to sulfide by bioenergetic metabolism (Neculita et al., 2007). The organic carbon sources for SRB system can be found in the degradable organic carbon sources from food or agricultural waste such as chicken manure, dairy manure, sawdust, hay, and wood chips (Neculita et al., 2007; Zhang and Wang, 2014).

Geochemical Systems

Anoxic limestone drains (ALDs) are sealed trenches filled crushed limestone or carbonate rocks (Watzlaf et al., 2000). The drain water flows throw the buried limestone by gravity produce alkalinity under anoxic condition. The bicarbonate buffering increases the pH to about 6.5. The system can avoid the mineral precipitation in

trenched due to low dissolved oxygen. Yet, the minerals precipitation and metals removal perform at the exits of the drain by the direct oxidation with oxygen at the natural environment (Genty et al., 2012). Thus, the settling pond is constructed at the effluent drain.

Open limestone channels (OLCs) are the open trenches filled with dimension limestone or gravel limestone with steep slopes to allow AMD flow about the channels. The systems are designed to add alkalinity in the drainage water to promote the ferric and aluminum hydroxide precipitation (McCauley et al., 2008; Trumm, 2010). OLCs method is suggested to designed for the steep slope (>12%) to reduce the metals hydroxide clog in the limestone pores (Ziemkiewicz et al., 1997), however it is limited to AMD with Fe and Al concentration.

Lime leach beds (LLBs) is a basin filled with gravel limestone sizes from 2 to 10 cm diameter. It is constructed to add alkalinity in the treatment system with a resident time of 30 min. This methods is suitable for AMD (pH < 3) pre-treated or acidic metals free water (Black et al., 1999). It can be used at the upstream end of OLCs or stand-alone systems by incorporated with self-flushing systems for more effective floc removal (Skousen et al., 2017)

Steel slag leach beds (SSLBs) is the use of by-product; slag from steel-making process contains that calcium compounds complexes such as aluminum, silica, phosphorus and other impurities in iron (Simmons et al., 2002). Sleep slag is considered as waste, yet it can be used in acid neutralization due to calcite leaching from the slags. It is effectively restored the acidic water to circumneutral pH, but it is necessary to understand the leaching capacity of its by-product (Kruse et al., 2019; Simmons et al., 2002).

Limestone sand treatment (LST) is the alkalinity added method using the sand-size limestone, ditch in the contaminated streams or creeks. Streamflow distributes the limestone sand toward downstream (Skousen et al., 2017). The sand-size limestone mixes with background sediment dissolves in the stream neutralize the acidic water enable mineral precipitation. Hydroxide minerals coated sand-size limestone does not decrease the efficiently of the acid neutralization (Menendez et al., 2000).

Low-pH Fe oxidation channels is recent innovation method uses to treat the AMD with Fe concentration. Limestone and sandstone are used to enhance Fe oxidation

promoting co-precipitation and adsorption in a shallow channel at low pH < 4.5 (Skousen et al., 2017). Hydraulic resident time of the system between 5 h to 10 h is able to oxidize > 95% of influent Fe2+ and remove 70% of total Fe when there is present iron oxidizing bacteria (DeSa et al., 2010).

Diversion wells (DVs) is a cylinder of metals or concrete with diameter of 1.5 to 1.8 m and deep 2 to 2.4 m filled with sand to gravel size limestone. The drainage water is feet up the cylinder by a large vertical pipe (20-30 cm in diameter) at the center of limestone bed (Arnold, 1991). The acidic water dissolves the limestone and produces alkalinity which elevates the mineral precipitation. The metals suspended floc settle at the settling pond at the downstream (Skousen et al., 2017).

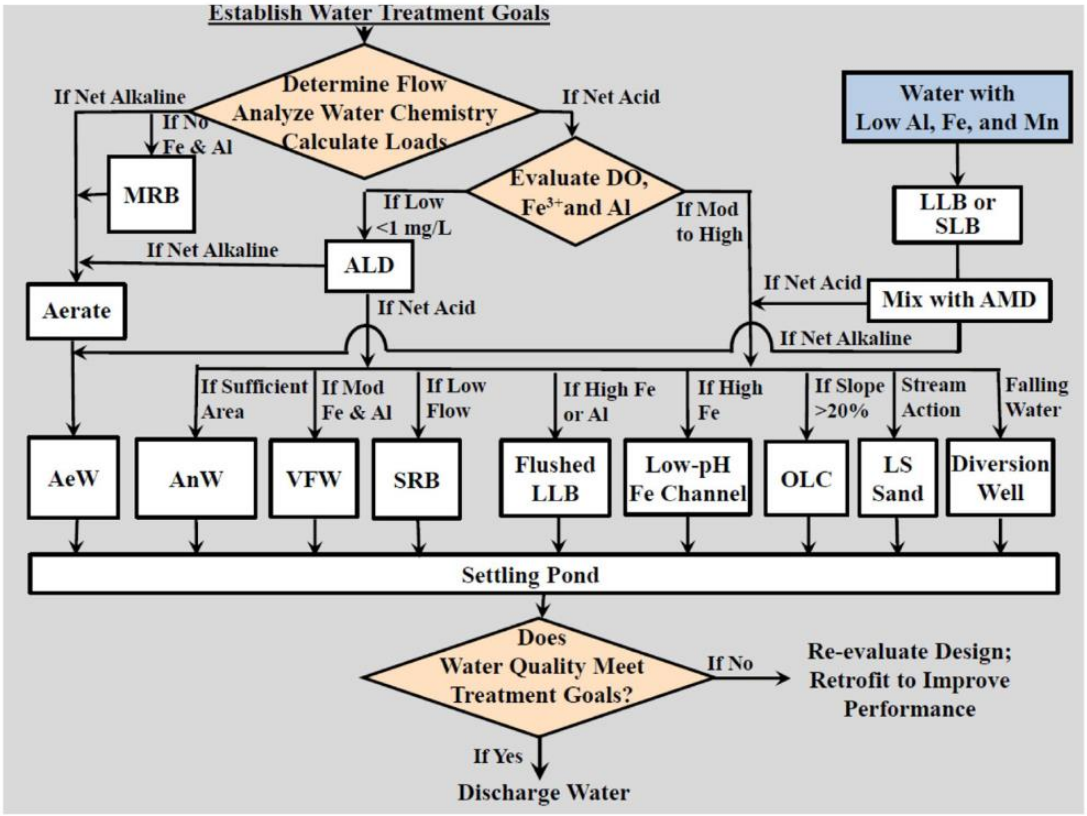

Fig. II-4. The flow chart of passive treatment selections base on water chemistry and flowrate (Skousen et al., 2017); AeW: aerobic wetlands; AnW: anaerobic wetlands; VFW: vertical flow wetlands; SRB: bioreactors or sulfate bioreactors; Flushed LLB: flush limestone leach bed; OLC: open limestone channel; LS sand: limestone sand

III. Seasonal effects of natural attenuation on drainage contaminants from an artisanal gold mining in Cambodia

3.1. Introduction

Artisanal mining is one of the major environmental risks due to inefficient and non-existent pollution management of waste from mineral extraction and processing (Ncube-Phiri et al., 2015). The technical knowledge limitation and environmental impacts of ignorance of artisanal miners resulted in severe problems such as tailings discharge and acid mine drainage (AMD) generation (Appleton et al., 2000; Tarras-Wahlberg, 2002). Tailings are the fine-particle residue after mineral extraction from ores, including crushed rocks, water, trace metals, and additive materials used in processing (Yannopoulos, 1991). In addition, AMD is generated by the oxidative dissolution of metal sulfides and dissolved oxygen in the water from active and abandoned mines and the dumping site of mine tailings (Fukushi et al., 2003a). To simplify the two mechanisms of artisanal mine contamination, AMD was used to represent tailing discharge and acid mine drainage generation in this study. AMD with high concentrations of hazardous metals and metalloids potentially affects the water quality in the surrounding environment (Berger et al., 2000). The impact of trace metals and metalloids in AMD on the surrounding environment depends on AMD chemistry, based on hydrological, geological, and geochemical settings (Webster et al., 1993). Some AMD is treated naturally to meet environmental standards. For example, acid neutralization by host rock with a high buffering capacity or dilution by background water is the primary means of natural AMD attenuation (Adriano et al., 2004; Wang and Mulligan, 2006). The increase in pH causes precipitation of oxide and hydroxide minerals, which effectively adsorb metals and metalloids in AMD (Chikanda et al., 2021; Ito et al., 2017). However, when the NA process is insufficient, human intervention is required to treat AMD by active or passive treatment methods to avoid surface or groundwater contamination. Passive treatment should be implemented at the mine site for sustainability purposes; however, it is essential to understand the geochemical process onsite and learn from NA before the implementation.

Iron commonly precipitates as hydroxides or hydrosulfates such as schwertmannite under acidic and oxidative conditions in AMD, which may be facilitated by biological processes (Laroche et al., 2018; Webster et al., 1998; Yan et al., 2017). Iron minerals

are effective adsorbents for the adsorption of toxic elements such as As, Sb, Se, Cr, Cu, and Zn (Francisco et al., 2018; Khamphila et al., 2017; Zhou et al., 2018). However, these mechanisms are controlled by the concentration of ferric iron and hydrological conditions. Climate is one of the major factors affecting hydrological conditions. It may vary from a temperate climate to a tropical monsoon. Several studies have been conducted on NA in AMD; however, limited studies have followed the seasonal variation in NA processes. The seasonal variation between spring and summer changed in the hydrogeochemistry of AMD and secondary precipitated mineralogy (Kumpulainen et al., 2007). The temperature changes in winter and summer significantly affect the attenuation rates of iron and As (Chen and Jiang, 2012). Although these studies were conducted in temperate climates, they cannot be applied to a tropical monsoon climate with only rainy and dry seasons with year-round warm temperatures. AMD in the tropical monsoon is expected to differ significantly between the rainy and dry seasons. Thus, an artisanal gold mine in Mondulkiri Province, Cambodia, was selected to study the mechanisms controlling the NA processes in the rainy and dry seasons and its implications for geochemical passive treatment. This study aims to (1) determine the chemistry and behavior of toxic elements within the tributary system in different seasons; (2) elucidate the seasonal dynamics of the natural attenuation of metals and metalloids in the tributary.

3.2. Sampling and methods

3.2.1. Site description

Active artisanal gold miners in Mondulkiri Province, eastern Cambodia, discharge tailings and wastewater into a small tributary of the Prek Te River (Fig. III-1a). Miners excavate gold ore randomly from quartz veins that appear on the surface and process ore in situ (Fig. III-1b). The gold ore was ground and treated with sulfuric acid. The tailings and wastewater from the processing (Fig. III-1c) are dumped at the mine site, flowing into the tributary system. The excavated area and the waste rocks are exposed to the surface without any cover by an impermeable layer from rainwater. The I1 sampling point was a pond resulting from mining excavation in the study area.

The regional geology of this area is characterized by Pleistocene basalt, Triassic sandstone interbedded with mudstone, and micro-breccias with some intrusion of

granodiorite surrounded by hornfels (BRGM, 1973). There have been no previous studies regarding the ore deposit type or ore characteristics; however, an exploration project indicates an intrusive gold-related system (IRGS) present across the Prek Te River, ~20 km from the artisanal mine site ("Okvau Gold Project," 2015). Metal zonation in the study area was created by the intrusion of granodiorite, which altered the sedimentary rocks to hornfels. Gold ore occurs mainly in the quartz vein on the surface, developed by a plutonic thermal aureole.

Rainfall plays a major role in controlling hydrological conditions in the study area. Monsoon cycles separate the Cambodian climate into two major seasons: rainy (June–October) and dry (November–May) seasons. The average inland precipitation in the rainy and dry seasons was 877 mm and 137 mm, respectively (Tsujimoto et al., 2018), with significant geochemical and physical effects affecting the waterbody in both seasons.

3.2.2. Sampling and on-site measurements

Preliminary field sampling was conducted in February 2019. Ore and waste rock samples were collected from processing plants. Water samples were collected from the tailings and contaminated tributary. Water samples were also collected from the Prek Te River. Detailed sampling took place in the rainy season of October 2019 (Fig. III-1d), with sampling points as shown in Fig. III-1a. Sampling points are named as follows: T1 to T8 in the tributary, from upstream to downstream of the mine site, R1 upstream in the Prek Te River, and R2 downstream (after mixing with contaminated tributary water). I1 and I2 are the extra water input sources to the tributary. Precipitate sediments with a color of 2.5Y7/6 following the Munsell color chart at the bottom of the tributary (Fig. III-1f) were collected at T2 and T4 after mixing with I1 and I2.

At the same sampling points in the rainy season, the sampling was conducted again in the dry season (February 2020; Fig. III-1), although some (T1 and I2) were dry (orange color in III-1a). T3 and T4 were regarded as a single sampling point, as there was no flow from I2. The 2.5Y7/6 precipitate sediment could not be collected in the tributary, except after the R2 mixing point. Sediments with a color of GLEY18/5GY were collected along the tributary bank (III-1g). The precipitate sediment at R2 was

also sampled for DNA extraction to investigate the microbial community in the tributary.

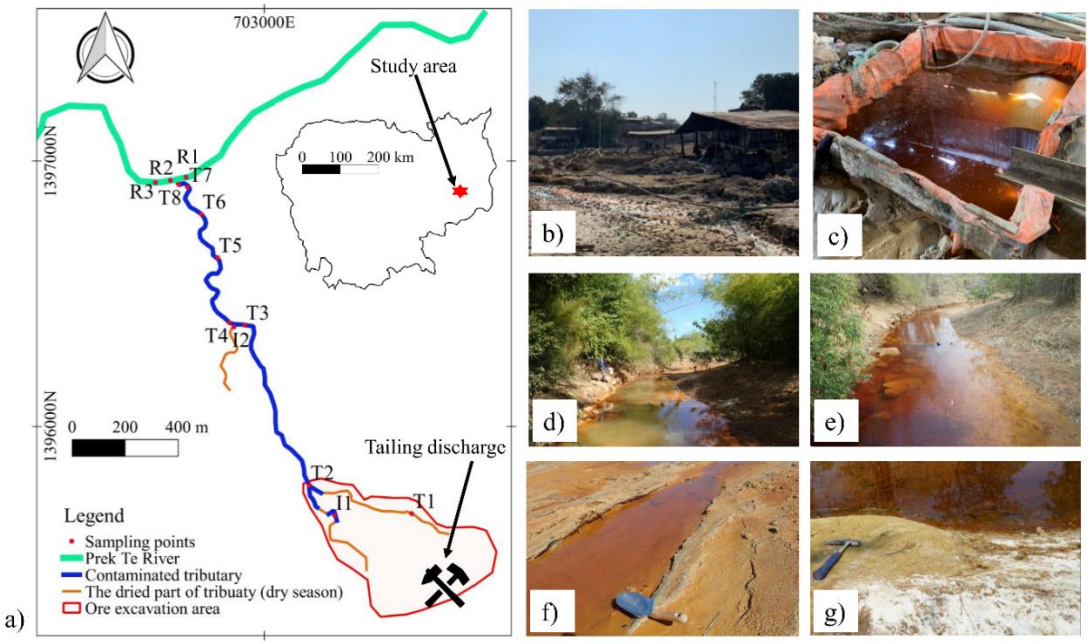

Fig. III-1. (a). Map showing the study area in relation to the inset map of Cambodia and Mondulkiri Province and the locations of sampling points. (b–g) Photographs of the sites. (b) The artisanal mine site. (c). Wastewater from gold-ore processing. (d) Drainage water in rainy season. (e) Drainage water in dry season. (f) Yellow-brown precipitated sediment in rainy season. (g) Greenish sediment along the drainage bank in dry season.

On-site measurements were undertaken at all sampling points, including pH, electrical conductivity, redox potential, temperature, turbidity, and alkalinity. Alkalinity was obtained by the titration of 0.16 N HNO_3 to 50 ml of water samples, filtered with 0.45 µm membrane filters. Alkalinity measurements were conducted at the sampling points where the pH was greater than 3.5. Alkalinity as HCO_3^- was determined from Grant-function plots (Rounds and Wilde, 2012). Flow rate, initial inflow, and outflow were obtained from the on-site measurement of the float method after Dobriyal et al. (2017). The distance from each sampling point was obtained from the QGIS Desktop 2.18.24.

Water samples were filtered through 0.20 µm membrane filters and stored in two 50 mL acid-washed polyethylene bottles. One bottle was acidified with a 1% (v/v) ultrapure nitric acid preservative for cation analysis. The other was used for anion analysis and was not acidified. Fe^{2+} concentrations were measured on-site (avoiding the oxidation of Fe^{2+} to Fe^{3+} during transport) using an ion-selective pack test color

comparison method: 0-Phenanthroline reagent (Kyoritsu Chemical Check Lab., Corp; Kanagawa, Japan).

3.2.3. Analytical methods

Aqueous solutions were analyzed by inductively coupled plasma–atomic emission spectroscopy (ICP–AES; ICPE-9000, Shimadzu, Tokyo, Japan) for major cations such as Na, Ca, Mg, K, Fe, Mn, and Al, using a multi-element standard solution IV Certipur (Merck, Germany). All trace elements such as As, Se, Cu, and Ni contained in the multi-element standard solution XSTC-331 (SPEX CertiPrep, USA) were analyzed by inductively coupled plasma–mass spectrometry (ICP–MS; iCap Qc, Thermo Scientific, Massachusetts, USA). The Fe^{2+} concentration was subtracted from the total Fe content to determine the Fe^{3+} concentration. Ion chromatography (IC; IC861, Metrohm, Herisau, Switzerland) was used to analyze anions, using Anion Mixture Standard Solution1, including Br, F, NO_2, NO_3, PO_4, Cl, and SO_4 (Wako, lot number KCG3845).

Sediments, waste rock, and ore mineralogy were characterized by optical and scanning electron microscopy (SEM-EDS; JSM-6510LA, JEOL, Tokyo, Japan) and X-ray diffraction (XRD-Multiflex, Rigaku; Tokyo, Japan) analysis. The SEM working voltage was 10–15 kV. The XRD powder diffractometer was equipped with a Cu Kα X-ray source and a working voltage of 40 kV at 30 mA with a scanning speed of 6.5° min^{-1} ranging from 5° to 70°. The major chemical compositions of waste rock and ore were obtained by X-ray fluorescence using glass bead samples and a synthetic calibration standard after Ichikawa et al. (2016). Ore samples were digested in 6 M HCl, 4 M HNO_3, 30 M HF, and 7 M $HClO_4$, following the method of Chikanda et al. (2019) for trace metal composition.

Selective extraction of iron amorphous minerals from the sediment samples with the color 2.5Y7/6 (T2, T4, and R2) was extracted with 0.2 M ammonium oxalate at pH 3 for 15 minutes without exposure to UV light. The total dissolution of the same samples was later aimed at 5 M HCl for 2 h. The extracted solutions were immediately filtered with 0.20 µm membrane filters for ICP-AES, ICP-MS, and IC analyses, as described for tributary water. The specific surface areas of the 2.5Y7/6 sediment samples were determined by N_2 adsorption using the Brunauer-Emmett-Teller method (BET; NOVAtouchTM; Florida, USA). Samples were pretreated by heating for 30 min

at 110°C (Regenspurg and Peiffer, 2005) in 6-mm diameter glass tubes to remove moisture.

Bacterial DNA was extracted from sediments at the mixing point (R2) during the dry season following the ISOIL soil DNA extraction kit (Nippon Gene, Toyama, Japan). Sediment samples (5 g) were placed in 50 mL centrifuge tubes; lysis solutions HE (9.5 mL) and 20S (0.5 mL) were added, mixed well, incubated at 65°C for 1 h, and centrifuged. A supernatant sample (6 mL) was mixed with 4 mL of DNA purification solution and 6 mL of chloroform and centrifuged. The aqueous layer (8 mL) was mixed with 8 mL of the precipitation solution and centrifuged. The residue was washed with 10 mL of 'Wash Solution' and centrifuged; 10 mL of 70% ethanol and 10 µl of ethachinmate were mixed with the residue and centrifuged. The final residue was air-dried and dissolved in 0.5 mL Tris and ethylenediaminetetraacetic acid (TE) solution (pH 8.0) for microbial community characterization by Repertoire Genesis Co. (Osaka, Japan).

3.2.4. Modelling

Geochemical modeling involved the 'Geochemist's Workbench' (GWB) professional package. Chemical species activities, water-type classifications, and total dissolved solid (TDS) concentrations were calculated using the GWB geochemist's spreadsheet (GSS) module. Determination of elemental speciation and stability of iron minerals in the GWB Act2 module. Surface complexation modeling was undertaken to predict the adsorption behaviors of target toxic elements using the generalized double-layer surface complexation model by Dzombak and Morel. (1990) for the GWB act module.

3.3. Results

3.3.1. Ore Mineralogy

The ore thin section reported in Fig. III-2 shows the presence of sulfides such as arsenopyrite (FeAsS), chalcopyrite ($CuFeS_2$), pyrite (FeS_2), and oxide minerals such as biotite ($K(Mg,Fe)_3(AlSi_3O_{10})(OH)_2$), and pyrolusite ($MnO_2$). The chemical composition of the ore contains significant amounts of As and Se, whereas the Ni concentration was found to be an impurity of sulfide minerals and in the waste rock

(Supplementary data, Table.III-3 and Table.III-3). Ni and Se are commonly found in sulfide minerals such as arsenopyrite, chalcopyrite, and pyrite as Cu–Fe–Ni–S mineral assemblages (Economou-Eliopoulos and Eliopoulos, 1998; Kitakaze et al., 2016; McNeal and Balistrieri, 1989).

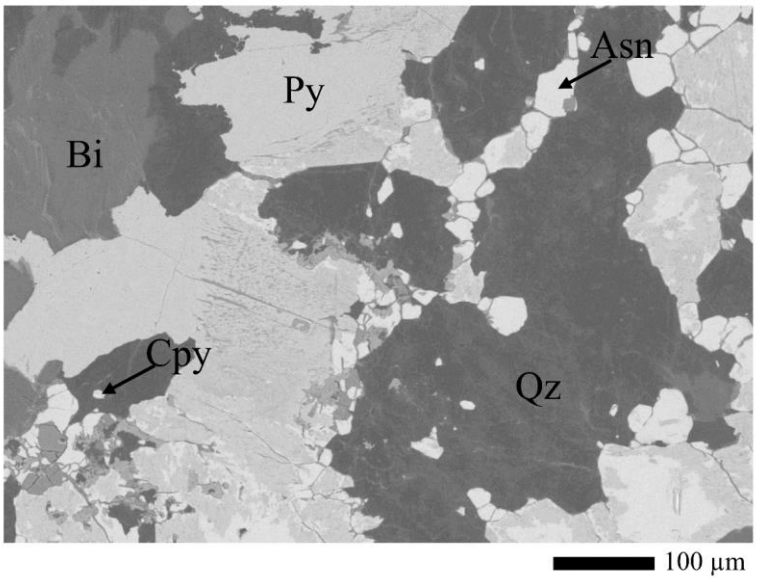

Fig. III-2. SEM image on polished thin section of the ore sample. Cpy, chalcopyrite; Asn, arsenopyrite; Py, pyrite; Bi, biotite; Qz, quartz

3.3.2. Chemistry of water samples

The on-site measurement and detailed water data results that could be detected using analytical methods are listed in Table 3 of the Supplementary data. Wastewater collected from the waste tank at the processing plant had a pH of 2.7 and a sulfate concentration of ~10.5 g/L due to the dissolution of metal sulfides from the ore and the addition of sulfuric acid during ore processing. The Ca concentration in the wastewater was ~550 mg/L, which was relatively higher than that of Mg and Na. The wastewater was also rich in dissolved Fe, As, Ni, Cu, and Se due to the dissolution of ore minerals. The Fe^{2+} concentration was ~700 mg/L, with As (17.6 mg/L), Ni (0.27 mg/L), Se (0.1 mg/L), and Cu (4 mg/L), above the WHO regulation limits of 0.01, 0.07, 0.04, and 2 mg/L, respectively (World Health Organization, 2018), with these elements being of concern to the aquatic environment and human health.

The water-type classification of the tributary in the rainy and dry season is Ca-SO_4 due to high concentrations of Ca and SO_4. The main sources of contamination of the tributary from the most upstream (T1) are the discharge of tailings from ore processing

and the oxidative dissolution of metal sulfides from waste rock in the study area. In the rainy season, HCO_3^- of the tributary could be determined from some sampling points (T4, T5, T6, and T8) with an average concentration of 13.6 mg/L. SO_4 concentration was about 4.7 g/L at T1, decreased toward downstream to T8 (175 mg/L). The Ca concentration ranged from 324 mg/L to 85.56 mg/L, whereas the Mg concentration was between 34 mg/L and 13 mg/L.

In the rainy season, there is NA process of As, Ni, Se, and Cu in tributary at T8 to below WHO guideline levels, with concentrations of 0.01 mg/L, 0.01 mg/L, below the detection limit, and 0.01 mg/L, respectively. The tributary pH at T1 was 2.9, slightly higher than that of the wastewater, increasing downstream to 3.4 at T2 due to neutral water input from I1 (pH 6.7) (Fig. III-3a). From T2 to T7, the stream pH was in the range of 3.2–4.0. The pH at the mixing point T8 was 6.3, due to the rise in the water level from the Prek Te River. After the mixing point, R2, the pH was 7.1, slightly below that of the main river (7.2; R1). The pH significantly changed, whereas the Fe, As, Ni, Se, and Cu concentrations decreased from T1 to T2 (Fig. III-3a). The Fe^{2+} concentration in T1 was 370 mg/L. At T2, the total Fe concentration was ~70 mg/L, with an Fe^{2+} concentration of ~50 mg/L. From T1 to T2 (Fig. III-3a), the Fe^{2+} concentration decreased rapidly from 370 mg/L to 50 mg/L; thus, Fe^{2+} and pH were negatively correlated. Beyond T2, the total Fe concentration in the tributary decreased downstream until mixing with the Prek Te River. The concentration of As dropped from 15.3 mg/L at T1 to 1.2 mg/L at T2, decreasing downstream with a similar trend to that of Fe in the tributary. Ni, Cu, and Se concentrations decreased by four times, from 0.11, 1.11, and 0.04 mg/L at T1 to 0.03, 0.2, and 0.01 mg/L at T2, respectively and remains constant from T2 to T7, behaving differently to As which decreased about 10 times from T1 to T2 and keep decreasing toward downstream from T2 to T7 (Fig. III-3c).

In the dry season, the tributary water had a net acidity; thus, HCO_3^- could not be determined. The Ca concentration was as high as 560 mg/L on average (T2 to T8), whereas the Mg concentration increased to 153 mg/L. SO_4 was nearly steady from T2 to T8 with an average of 5.7 g/L. As, Ni, Se, and Cu concentrations did not decrease along the stream tributary during the dry season. The pH in the tributary was sustained at 2.7–2.8, (Fig. III-3c) from T2 to T8, as there was no inflow of neutral water. Without rainwater, I1 also became an acidic pond with a pH of 2.8. Fe, As, Ni, Se, and Cu concentrations were relatively constant from upstream to downstream. The average

total Fe concentration in the tributary was 140 mg/L for each sampling point, where Fe comprised Fe^{3+} and Fe^{2+} with an average of 110 mg/L and 26 mg/L average, respectively (Fig. III-3b). The As concentration was approximately 10 times greater than that in the rainy season, whereas Ni, Se, and Cu concentrations were approximately four times higher than those in the rainy season (Fig. III.d). At the mixing point (R2), the pH was 6.7 in the dry season than in R1 (7.6). The increase in pH and the decrease in toxic elements at R2 were due to the dilution of the large water body of the Prek Te river.

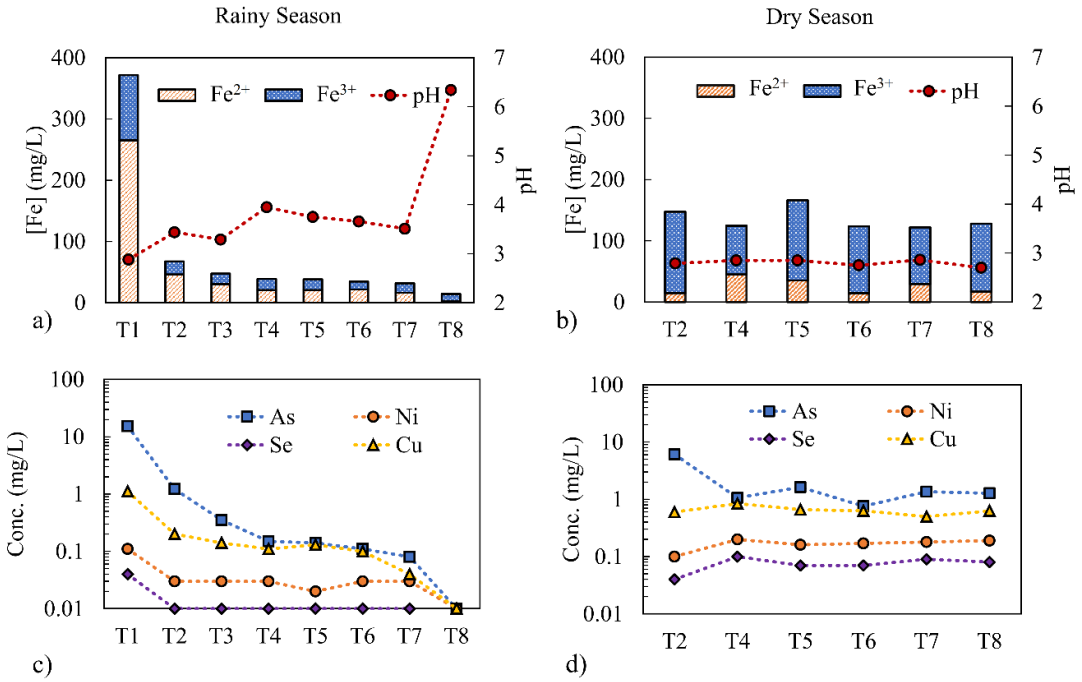

Fig. III-3. (a). Fe^{2+}, Fe^{3+}, and pH trends across sampling points in the rainy season; (b). Fe^{2+}, Fe^{3+}, and pH trends across sampling points in the dry season; (c) Ni, Cu, As, and Se trends across sampling points in the rainy season; (d) Ni, Cu, As, and Se trends across sampling points in dry season. The x axes of (c) and (d) are in logarithmic scale.

3.3.3. Precipitation mineralogy

The XRD pattern of the 2.5Y7/6 sediment during the rainy season is shown in Fig. 3. The peaks assigned to schwertmannite in Fig.3 are consistent with previous studies (Bigham et al., 1990). The sediment samples were also a mixture of goethite, jarosite, biotite, and kaolinite. In the dry season, GLEY18/5GY sediment color crystals were observed on the sediment bank at the stream tributary. The XRD pattern reported in Fig. III-5 of the crystals indicates that the crystals are composed of sulfate salts such as rozenite ($FeSO_4 \cdot 4H_2O$) and gypsum ($CaSO_4 \cdot 2H_2O$).

Schwertmannite can be completely dissolved by ammonium oxalate at pH 3 (Fukushi et al., 2003a) whereas jarosite and goethite cannot; therefore, the Fe concentration released in selective extraction is correlated with the schwertmannite content of the tributary. The 2.5Y7/6 sediment samples at T2, T4, and R2 contained schwertmannite at 63%, 57%, and 91%, respectively (Supplementary data Table III-2&3). The specific surface areas of 2.5Y7/6 precipitated sediments were 60, 122, and 137 $m^2\ g^{-1}$, respectively, which is slightly less than that found by Bigham et al. (1990) of 175–225 $m^2\ g^{-1}$, but within the range of 3.5–325 $m^2\ g^{-1}$ reported by Zhang et al. (2018). The specific surface area is different because of its morphological variation from smooth-rounded to rough surfaces and its variable precipitation rate (Zhang et al., 2018). The large specific surface area of schwertmannite enables many chemical species to sorb onto its surface (Dzombak and Morel, 1990; Song et al., 2015). Schwertmannite in the study area aggregated as fibrous needle-like structures with rough surfaces, as shown in Fig. III-4b. The morphological and structural similarity of schwertmannite to that found in previous studies and its large specific surface area implies that it potentially serves as an adsorbent in the tributary during the rainy season.

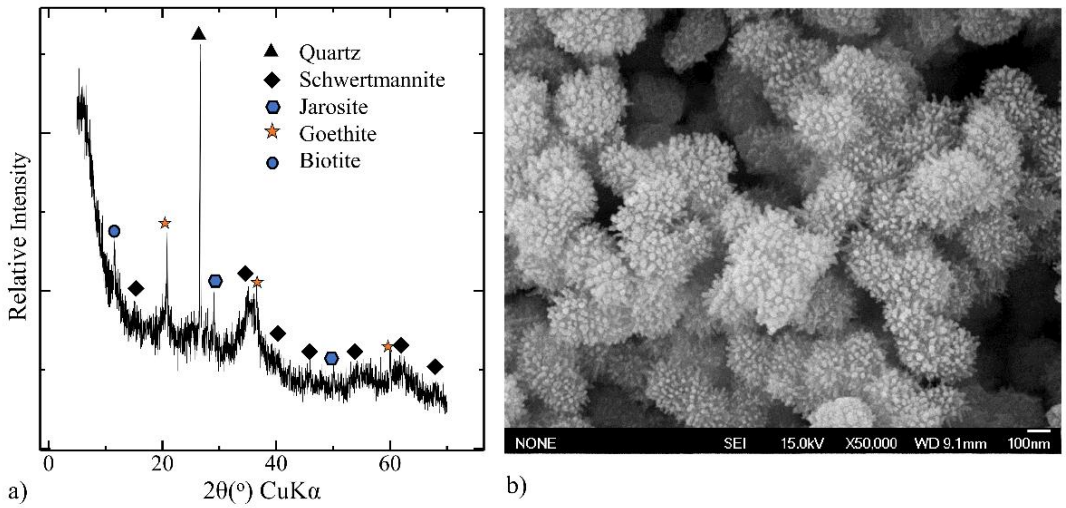

Fig. III-4. a) The XRD pattern of 2.5Y7/6 precipitated mineral in the tributary in the rainy season. b) The SEM image of the 2.5Y7/6 precipitated sediment.

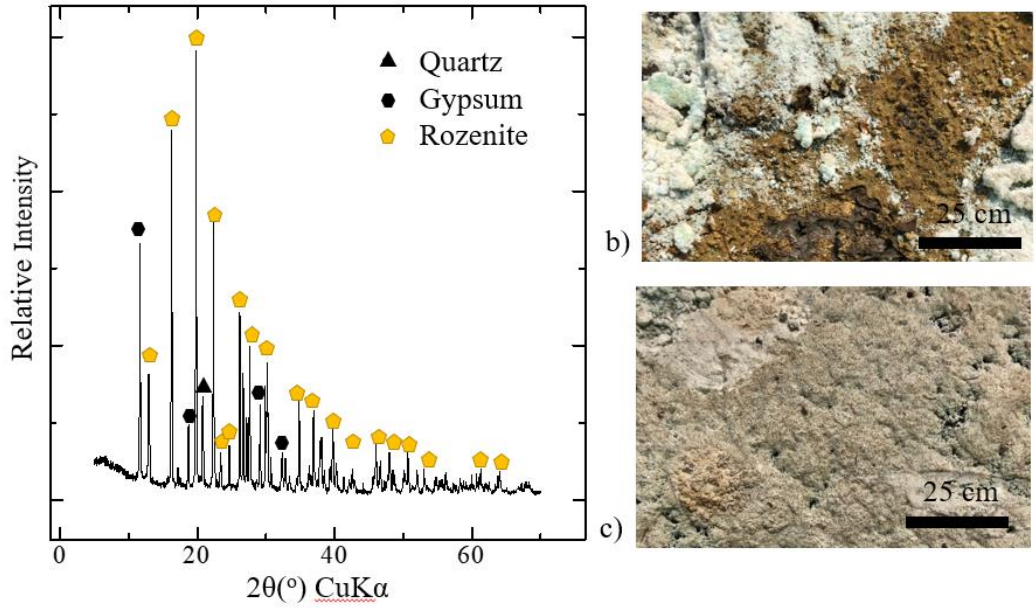

Fig. III-5. The XRD pattern of greenish sediment along the drainage bank in the dry season. (b) and (c) the field images of the greenish sediment.

3.3.4. Microbial community

Up to 48% of the bacterial cells could be identified from library databases. Proteobacteria were the dominant phylum, constituting 65% of identifiable species, followed by actinobacteria (15%) and acidobacteria (7%). Iron-oxidizing bacteria species are normally found in proteobacteria phylum. The iron-oxidizing acidithiobacillus bacterium constituted <1% of the proteobacteria phylum. The thiomonas genus, an As-oxidizing bacterium (Garcia-Rios et al., 2020), was also found from the proteobacteria phylum.

3.4. Discussion

3.4.1. Natural attenuation of contamination

Schwertmannite in the tributary forms during the rainy season can scavenge As by adsorption and coprecipitation. Under acidic conditions, schwertmannite has a positive surface charge (Khamphila et al., 2017; Park et al., 2021) which enables the adsorption of As. The schwertmannite at the study area had Ni, Se, and Cu concentrations of < 0.1 mg/g; however, the As concentration exceeded 14.6 mg/g at T2, 3.5 mg/g at T4, and 6.9 mg/g at R2. During the selective extraction, only As was the dominant element

released from schwertmannite over Ni, Se, and Cu. Tributary conditions during the rainy season are highly suitable for As adsorption, as found in previous studies (Paikaray et al., 2012); however, the pH range in that season is too low for the removal of Ni, Se, and Cu as the schwertmannite surface remains positively charged, as with Ni and Cu in solution at low pH. Ni (>90%) can be adsorbed on iron hydroxide at pH > 7 (Flynn and Catalano, 2017). Cu adsorption (>80%) on the inner structure of schwertmannite occurs at pH > 5.5 (Otero Fariña et al., 2015). Selenium exists in aqueous solutions as selenite or selenate metalloids. Selenite tends to be adsorbed on amorphous iron hydroxide (McNeal and Balistrieri, 1989), whereas selenate is adsorbed on the outer sphere of the schwertmannite structure, similar to sulfate (Khamphila et al., 2017). Selenate was found to incorporate schwertmannite by substitution into the sulfate structure (Bigham et al., 1994). During As adsorption onto schwertmannite, sulfate is released from the schwertmannite structure, approximately half of the adsorbed As (Fukushi et al., 2003b; Khamphila et al., 2017). This mechanism may also be applied to selenate. In this study, selenium likely exists as selenate, as it displays trends similar to those of sulfate. These trends indicate that selenate does not adsorb onto schwertmannite. Thus, schwertmannite is responsible for removing As from the tributary during the rainy season (by coprecipitation and adsorption); however, it does not account for the adsorption of Ni, Se, or Cu.

To determine the effect of rainwater dilution and the input water from (I1) to the tributary in the rainy season, As, Ni, Se, and Cu concentrations were plotted against Cl concentration (Supplementary data Fig-III-7), a conservative tracer element. Most As concentration fell below the mixing line. This result indicates that As coprecipitated and adsorbed by schwertmannite during the rainy season. Ni, Se, and Cu concentrations follow along the mixing line, indicating that dilution controls the reduction of Cu from the tributary. Therefore, the decrease in Se, Cu, and Ni concentrations beyond the mixing point T2 was diluted by neutral water from I1. Natural attenuation mechanisms in the rainy season thus include removal of As due to adsorption onto schwertmannite and reducing Ni, Se, and Cu concentrations by dilution with neutral water.

3.4.2. Formation of schwertmannite in the rainy season

Schwertmannite, the predominant mineral precipitated in the tributary during the rainy season, plays a major role in As removal. It exists as a metastable ferric iron

mineral formed under biotic or abiotic conditions in a pH range of 2.5–4.5 (Bigham et al., 1990). Its formation requires Fe^{3+} as a source of Fe; however, Fe^{2+} predominates in wastewater flowing to T1. The occurrence of schwertmannite and the decreasing Fe^{2+} concentration from T1 to T2 indicate the rapid oxidation of Fe^{2+} to Fe^{3+} in the drainage. This oxidation may be catalyzed by the iron-oxidizing bacteria *acidithiobacillus* found in the drainage (Section 3.3.4). The oxidation rate of Fe^{2+} to Fe^{3+} thus controls the formation of schwertmannite in the study area.

To explain the solubility field of schwertmannite in the study area could be obtained by using geochemical modelling. The solubility fields of schwertmannite and dissolved Fe^{3+} were separated by the varying slopes between -2.56 to -2.75, depending on the schwertmannite formula: $Fe_8O_8(OH)_x(SO4)_y$, (where y=8-2x, and $1 \leq x \leq 1.75$), pH, and activity of SO_4^{2-} (Bigham et al., 1996; Sánchez-España et al., 2011). The slope explains the unavailability of schwertmannite formation even if the pH is between 2.5 and 4.5 (Fig. III-6). Previous studies in Table III-1 show various equilibrium constants for the dissolution of schwertmannite (K_{sch}). The thermodynamic data of Kawano and Tomita (2000) and Yu et al. (1999) yielded solubility for schwertmannite than that described by Sánchez-España et al. (2011) and Bigham et al. (1999; Fig. 7). The activity of Fe^{3+} obtained from the GSS module was plotted on the solubility field diagram of schwertmannite (Fig. 5) to determine the most suitable thermodynamic data for the study area. In the dry season, the activity of Fe^{3+} falls into the schwertmannite solubility field of Kawano and Tomita. (2000), and Yu et al. (1999). The $logK_{sch}$ values for Kawano and Tomita. (2000), and Yu et al. (1999) do not apply to the study area because the solubility field of schwertmannite in these studies does not represent the tributary data. The solubility fields of Sánchez-España et al. (2011) and Bigham et al. (1996) $logK_{sch}$ are similar and thus represent the field dissolution and precipitation of schwertmannite. However, the $logK_{sch}$ of Sánchez-España et al. (2011) 18.8 is used to determine the optimum pH in the tributary that enables schwertmannite to precipitate based on the Fe^{3+} source.

In the dry season, Fe^{3+} activity is greater than that in the rainy season. However, the pH in the dry season was not high enough for schwertmannite precipitation. Therefore, to maintain the formation of schwertmannite in the dry season, the pH in the tributary is necessary to meet the schwertmannite solubility. The optimum pH for schwertmannite precipitation in the dry season of 3.1 with a $logK_{sch}$ value of 18.8 if the

activities of Fe^{3+} are extended (dash-dotted-dotted line) to the schwertmannite solubility field (Fig. 5).

Table III-1. Schwertmannite dissolution and log(equilibrium constant) values. 1, (Bigham et al., 1996); 2, (Yu et al., 1999); 3, (Kawano and Tomita, 2001); 4, (Sánchez-España et al., 2011).

Reaction	**log K_{sch}**	**Ref.**
$Fe_8O_8(OH)_{4.8}(SO_4)_{1.6} + 20.8H^+ = 8Fe^{3+} + 1.6SO_4^{2-} + 12.8H_2O$	18.0 ± 2.5	(1)
$Fe_8O_8(OH)_{4.4}(SO4)_{1.8} + 20.4H^+ = 8Fe^{3+} + 1.8SO_4^{2-} + 12.4H_2O$	10.5 ± 2.5	(2)
$Fe_8O_8(OH)_{5.9}(SO4)_{1.05} + 21.9H^+ = 8Fe^{3+} + 1.05SO_4^{2-} + 13.9H_2O$	7.06 ± 0.1	(3)
$Fe_8O_8(OH)_{5.2}(SO_4)_{1.4} + 21.2H^+ = 8Fe^{3+} + 1.4SO_4^{2-} + 13.2H_2O$	18.8 ± 3.5	(4)

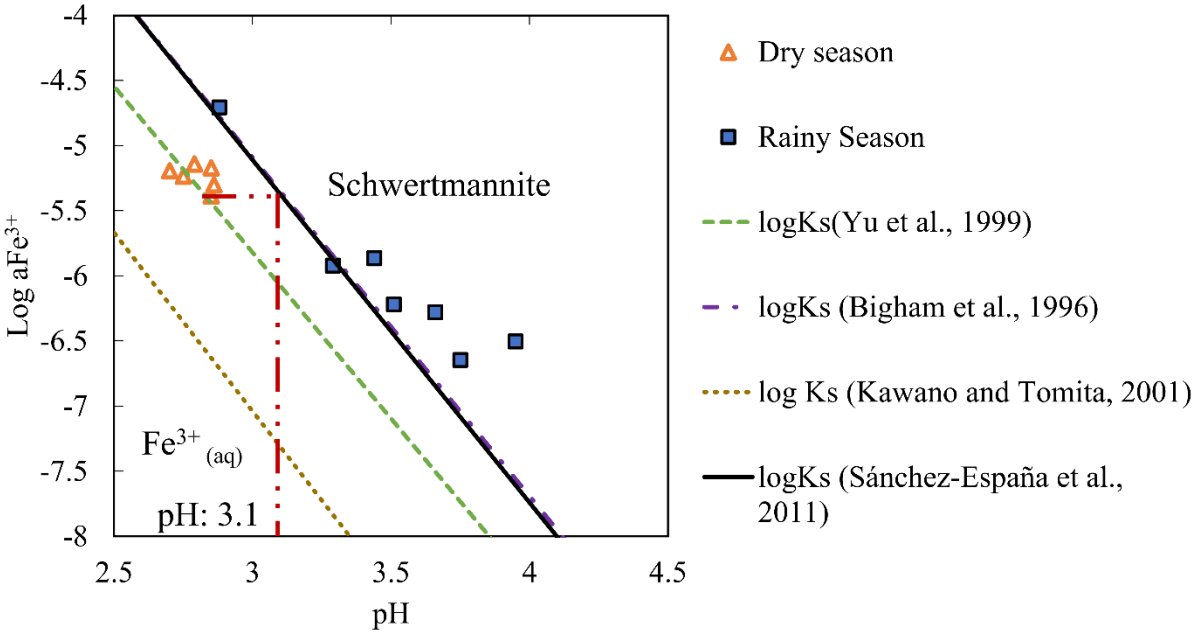

Fig. III-6. The stability of schwertmannite with different log (equilibrium constant) values with log aSO42- = 10-2.3 and field data from the rainy and dry seasons. Reference data are from and Bigham et al. (1996) (dash-dotted-line), Yu et al. (1999) (dash line), Kawano and Tomita (2001) (dot line) and Sánchez-España et al. (2011) (solid line). The dash-dot-dotted line is the extended aFe3+ to meet schwertmannite solubility field to determine the optimum pH that enables schwertmannite to precipitate by using the logKsch 18.8 form Sánchez-España et al. (2011).

3.4.3. Dissolution of schwertmannite in the dry season

In the dry season, there was no formation of schwertmannite evidence at pH 2.8, as the Fe^{3+} concentration in the tributary remained almost constant from each sampling point (Fig.II-1b). The tributary water was quite transparent (turbidity; 0.84 NTU), indicating that the metals were dissolved. Schwertmannite primarily forms in acidic

conditions depending on the activities of Fe^{3+} and pH, although it might recrystallize or transform into jarosite or goethite (Acero et al., 2006; Wang et al., 2006). At pH less than 3, protons promote the dissolution of exited schwertmannite, yet recrystallize to jarosite if there is a sufficient amount of monovalent cations such as Na^+, K^+, or NH_4^+ (Regenspurg et al., 2004). Between pH 3 and 5, schwertmannite is in the most stable condition, and will age to goethite in several years (Acero et al., 2006; Regenspurg et al., 2004). Jarosite and gothite coexist in the tributary sediment, most likely resulting from schwertmannite dissolution, recrystallization, and transformation. The Fe^{3+} concentration in the tributary was partially due to dissolution processes, as the Fe^{3+} concentration in the dry season was greater than that in the rainy season. Fe^{2+} oxidation contributed to Fe^{3+} in the dry season tributary; however, most Fe^{2+} was precipitated as rozenite (Fig. 1g). Along the tributary bank, the water rapidly dried out; thus, the time for ferrous iron oxidation to ferric iron was insufficient compared to water evaporation in the dry season. As a result, Fe^{2+} precipitated as a sulfate salt at a lower pH.

During schwertmannite dissolution in the tributary, As incorporated with schwertmannite, was subsequently released into the tributary at ~100 times the WHO guideline concentration. The decreasing the concentration of As at T2 to T4 from 6.1 mg/L to 1.1 mg/L did not show the evident As removal by schwertmannite. In contrast, it indicated that the dissolution of schwertmannite due to As concentration incorporated with schwertmannite at T2 in the rainy season was higher than at other sampling points. In addition, there was no significant decreasing trend from T4 to T8. There was no dilution by neutral water, thus Ni, Se, and Cu concentrations increased (Section 3.4.2). As a result of this cycle, natural attenuation does not occur in either the tributary in the dry season or the study area. Therefore, affordable and sustainable passive treatment methods are required to ensure the health of villagers who live near the tributary.

3.5. Summary

The Mondulkiri mine site has the typical issues compare to other artisanal mine sites. Yet, signature difference the seasonal dynamics that have significant affect the natural attenuation of AMD, particularly in tropical climate zones. Rainwater controls the seasonal variation of AMD chemistry and favors the precipitation of secondary minerals in the rainy season (except in the dry season). Natural attenuation faces some

challenges; therefore, greater attention is needed to maintaining attenuation conditions in the dry season to match that in the rainy season.

In this study, during the rainy season, the As, Ni, Se, and Cu tributary concentrations decreased to less than the WHO guideline levels without human intervention due to coprecipitation and adsorption by schwertmannite and dilution by neutral water. In the dry season, the tributary is highly contaminated because of the dissolution of precipitated schwertmannite and without dilution.

In the rainy season, Fe^{2+} is oxidized to Fe^{3+} under biotic conditions, allowing Fe^{3+} to precipitate as schwertmannite. Arsenic is naturally remediated by adsorption and coprecipitation with schwertmannite. Concentrations of other elements such as Ni, Se, and Cu were reduced only by dilution.

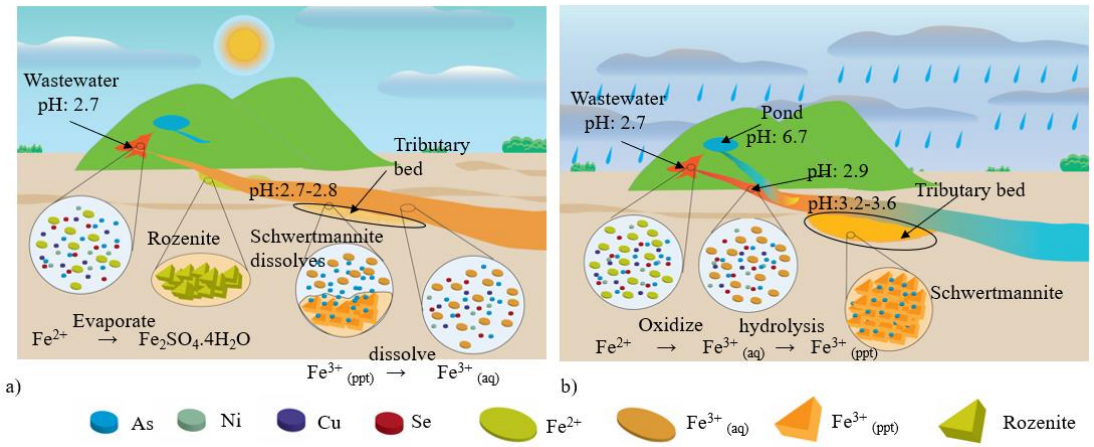

Fig. III-7. Graphical summery of Mondulkiri mine site. a) The mine site in the dry season (June-October). b) The mine site in the rainy season (November-May).

3.6. Supplementary data

Table III-2. Chemical composition of ore and waste rock obtained from XRF

	Ore	Waste Rock
Major elements (%)		
SiO_2	69.2	47.3
TiO_2	0.21	1.51
Al_2O_3	5.74	5.71
Fe_2O_3	20.1	38.5
MnO	0.02	0.08
MgO	1.17	0.93
CaO	0.17	0.96
Na_2O	0.22	0.35
K_2O	1.49	1.01
P_2O_5	0.06	0.16
LOI	5.03	8.35
Trace elements (ppm)		
V	47.8	203.8
Sc	-	1.11
Cr	23.8	205.6
Co	102.2	75.1
Ni	-	93.4
Cu	400.8	3819
Zn	8.38	66.5

Table III-3. Chemical composition of trace element of ore sample obtained from acid digestion

	As (mg/g)	Se (mg/g)
Ore	6306	0.95

Table III-4. The result of onsite measurement and water chemistry of drainage; n.d, not detected

Site	pH	ORP	EC	TDS	Turb.	HCO_3	Na	Mg	Ca	K	Fe(total)	Fe^{2+}	Fe^{3+}	Mn	Al	Ni	Cu	As	Se	SO_4	Cl
		mv	ms/m	g/L	NTU										mg/L						
		Rainy Season																			
T1	2.88	389	338.3	5.71	134	n.d	115.3	33.65	324	8.91	371.6	265	106.4	13.17	32.3	**0.11**	1.11	**15.3**	**0.04**	4763	24.1
T2	3.44	337	149.3	1.96	32.5	n.d	58.48	23.62	173.4	2.87	67.37	46	21.21	7.3	11.1	0.03	0.2	1.22	0.01	1601	9.59
T3	3.29	359	140.4	1.72	26.8	n.d	55.13	22.65	167.1	2.87	47.47	30	17.13	8.04	9.48	0.03	0.14	0.35	0.01	1394	8.98
T4	3.95	321	12.21	1.22	22.6	12.2	52.26	23.22	158.4	2.74	38.88	20	18.51	7.42	8.52	0.03	0.11	0.15	0.01	915	8.66
T5	4.02	316	118.2	1.19	10.6	12.2	51.03	22.98	155.6	2.79	38.02	20	17.65	7.49	8.61	0.02	0.13	0.14	0.01	879	8.63
T6	3.66	368	121.47	1.24	13.5	20.14	50.63	22.68	153.4	2.71	34.56	20	14.56	8.5	7.89	0.03	0.1	0.11	0.01	930	7.98
T7	3.51	398	119.27	1.22	29.7	n.d	49.86	23.11	150.7	2.75	31.48	16	15.14	11.15	7.48	0.03	0.04	0.08	0.01	919	6.8
T8	6.34	-12	41.3	0.35	19.9	8.54	19.32	12.80	85.6	2.44	14.2	2	12.40	3.56	6.27	0.01	0.01	0.01	n.d	175	3.5
R1	7.29	216	4.83	0.11	13.3	36.61	0.9	2.95	8.5	0.7	n.d	n.d	n.d	0.09	6.28	n.d	n.d	n.d	n.d	n.d	n.d
R2	7.05	-26.7	15.88	0.10	16.6	31.73	0.92	5.5	14.04	1.4	4.11	0.1	4.01	0.83	5.88	n.d	0.01	0.01	n.d	38.3	n.d
I1	6.67	-44.7	87.03	0.56	32	67.12	41.69	20.70	132.4	1.86	0.39	n.d	0.39	3.47	6.37	0.01	0.01	0.04	n.d	406	6.49
I2	7.14	-109	48.83	0.31	5.6	337.7	27.95	26.18	85.58	0.92	0.51	n.d	n.d	1.53	6.31	n.d	n.d	n.d	n.d	n.d	7.08
		Dry season																			
T2	2.79	522	428	8.10	31.7	n.d	50.01	151.4	616.5	18.11	147.7	15	132.8	26.24	22.7	0.10	0.60	6.10	0.04	5810	34.51
T4	2.85	473	416	5.96	14.0	n.d	43.94	162.2	573.5	17.75	124.7	45	79.69	47.34	22.2	0.20	0.84	1.06	0.10	5880	27.58
T5	2.85	495	388.7	5.92	8.24	n.d	41.57	147.7	523.2	18.25	166.5	35	131.2	34.75	23.3	0.16	0.66	1.63	0.07	5874	33.51
T6	2.75	513	401.7	5.81	0.99	n.d	41.34	151.1	541.7	17.12	123.7	15	109.6	33.71	25.8	0.17	0.63	0.76	0.07	5771	34.89
T7	2.86	473	417.5	5.71	13.6	n.d	41.47	154.1	547.8	17.66	122.1	30	32.57	36.43	25.6	0.18	0.50	1.36	0.09	5597	33.77
T8	2.70	516	401.7	5.55	0.84	n.d	41.91	153.4	542.8	18.60	127.9	17	111	34.77	25.9	**0.19**	0.63	**1.27**	**0.08**	5459	27.91
R1	7.63	307	6.92	0.13	0.53	45.8	1.34	1.65	2.02	2.21	n.d	n.d	n.d	n.d	n.d	n.d	n.d	n.d	n.d	3.66	1.63
R2	6.71	140	14.31	0.15	7.29	36.9	2.21	3.67	11.5	1.49	n.d	n.d	n.d	n.d	n.d	0.00	0.00	0.01	0.01	44.21	1.91
R3	7.21	223	7.87	0.09	3.19	42.7	1.4	1.42	1.39	1.67	n.d	n.d	n.d	n.d	n.d	0.00	0.00	0.01	0.01	9.73	1.75
I1	2.76	552	396	5.42	2.20	n.d	45.09	133.1	546.9	18.03	89.83	n.d	89.83	23.27	19.92	0.11	0.41	0.74	0.04	5477	34.10
		Wastewater																			
W	2.7	336	453		27.78	n.d	60.19	60.19	554.1	7.33	681.26	681	n.d	45.68	57.65	**0.27**	**3.59**	**17.62**	**0.10**	10544	24.09

Table III-5. The result of yellow brown precipitated sediment in the drainage collected in rainy season that was dissolved by 5 M of HCl.

Site	Fe	As	Se	Ni	Cu
	mg/g	mg/g	µg/g	µg/g	µg/g
T2	372	28.8	15.9	15.1	140.2
T4	326	13.9	10.2	6.87	61.26
T9	387	6.93	8.73	5.79	62.49

Table III-6. The result of yellow brown precipitated sediment in the drainage collected in rainy season that was dissolved by 0.2 M of ammonium oxalate at pH 3.

Site	Fe	As	Se	Ni	Cu
	mg/g	mg/g	µg/g	µg/g	µg/g
T2	235	14.6	8.37	5.45	72.6
T4	186	13.5	9.41	1.62	10.4
T9	353	6.93	5.08	1.98	26.2

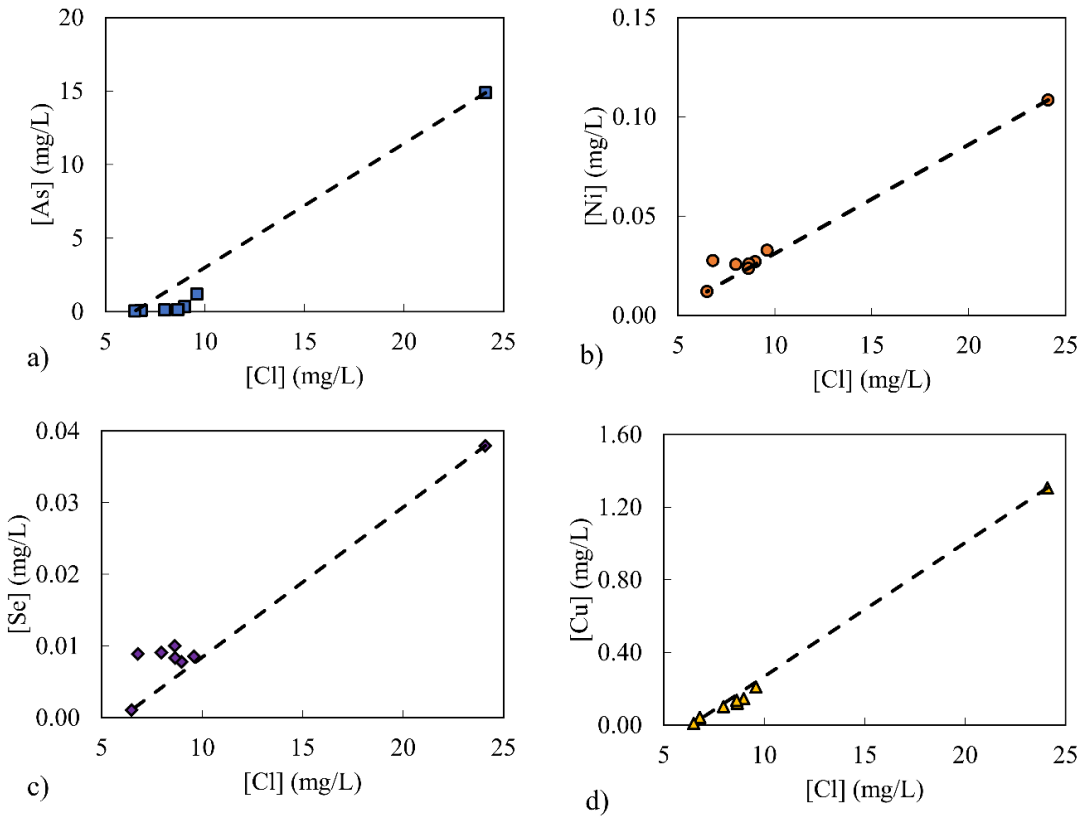

Fig. III-8. The concentration of the toxic elements in rainy season were plotted against Cl concentration in rainy season (a) As concentration against Cl, (b) Ni concentration against Cl, (c) Se concentration against Cl, and (d) Cu concentration against Cl. The dashed line represents concentration that would result from the mixing of drainage water (T1) and neutral water from I1. Concentration below the dash line indicates the removal of the element from the solution by other factors (precipitation or adsorption). Concentration above the dash line indicates the adding of the element to the solution by other sources. The concentration along the mixing line represent dilution.

IV. Geochemical characterization of rivers contaminated from an abandoned mine in Northern Japan

4.1. Introduction

Artisanal mines and abandoned mines are significant sources of environmental contamination, but AMD generation and contamination deliver different impacts. AMD generation from the abandoned mines is due to oxygen-rich groundwater flooding the abandoned mine site, promoting the reaction of pyrite and other metals sulfides with dissolved oxygen, producing acidity, and sulfate, releasing other co-occurring trace metals (Schaider et al., 2014). AMD emerges to surface water throw seepages over time, contaminating natural rivers water that surrounded the abandoned mines (Schaider et al., 2014). Thousands of kilometer untreated AMD from abandoned or closed mines seriously impact aquatic and neighboring terrestrial environments (Hengen et al., 2014; Rezaie and Anderson, 2020). The AMD remediation of the abandoned mine has been a challenge due to AMD's various physical and geochemical characteristics and the long-term AMD generation (Thisani et al., 2021).

The rainfall pattern is separated between the rainy and dry seasons in the tropical monsoon. This factor controls the various water quality of drainage water between rainy and dry seasons, as described in Chapter 3. However, in a temperate climate, rainfall, snowfall, and snow melting may affect the contamination river's hydrological condition (Kumpulainen et al., 2007). Thus, Shojin mine, located in a temperate climate, was chosen for this study. The AMD leaks contaminate the Shojin and Amemasu river adjacent rivers from waste dams. Those two rivers are about 6.5 Km long, flowing downstream and joint together, and flow to Oorito river. The monitoring point of river water quality is at Oorito river.

Shojin river and Amemasu river are under the Geological Survey of Hokkaido (GSH) administration. GSH reported that Shojin river is naturally remediated to less than WHO guidelines without any treatment before reaching the monitoring point, yet it does not occur at Amemasu river. Shojin river and Amemasu river are in the same geological setting. It is covered by alluvial sediment, andesitic lava, and tuffaceous breccia in the late Neogene Tertiary to Quaternary periods (Igarashi, 1976). The factors that control the natural attenuation mechanisms in the rivers are unidentified. Therefore,

the objectives of this chapter are (1) to determine the characteristic geochemical differences of toxic elements in Shojin river and Amemasu river; and (2) to elucidate the natural attenuation mechanisms Shojin river.

4.2. Sampling and Methods

4.2.1. Study area

Shojin mine was an underground mining site where the activities were active from 1937 to 1958. Iron and sulfur were extracted from 65,000 tons of limonite, 171,000 iron sulfide, and 120,000 elemental sulfur from Shojingawa and Amemasugawa deposits (Watanabe et al., 1996). Shojingawa deposit was classified as the elemental sulfur deposit. Amemasugawa was classified as a sedimentary limonite deposit (Watanabe et al., 1997). The deposits are located in the epithermal base, and precious metals deposit associated with Neogene igneous activity on the Kameda peninsula (Igarashi, 1976).

The mining area was closed several decades ago, but the AMD seepage remains leaking from the waste dam to Shojin and Amemasu river. GHS constructed a geochemical passive-treatment, the open lime channel (OLC) at Shojin river where wastewater meets the surface environment (Fig. IV-1). The construction of OLC successfully elevated the pH of AMD from 2.5 to 3.3 at the effluent of OLC. After 296 days, the pH at the effluent decreased to 2.6 due to the precipitated minerals coated on the limestone surface area. Recently, the OLC method failed to treat the wastewater.

Fig. IV-1. The figure of the open limestone channel at the Shojin wastewater discharge, a). the OLC just after the construction, the photo was taken on 2017/11/14, b) the OLC after 296 days after the construction (2018/09/05).

4.2.2. Samplings and on-site measurement

Shojin mine is in Hokkaido, the northernmost prefecture of Japan, the coldest region with an average temperature of 8 ^{o}C with average annual precipitation of 1150 mm. In winter, the daily snowfall is 5-20 mm water equivalent (Inatsu et al., 2021). The snow starts to melt in mid of April, and the highest temperature is in August. Due to the cold weather in winter and the challenges for water sampling in the study area, the field investigation was only conducted in summer.

Water samples and sediment samples were collected in July 2020 from upstream to downstream in Shojin and Amemasu rivers. The samples were named SR1 to SR9 for Shojin river and AR1 to AR9 in Amemasu river. The wastewater samples from Shojin to Amemasu river represent SW (1-4) and AW (1-3). Amemasu rivers were located in dense forests where the road was inaccessible to collect water samples between AR5 and AR6. The distance from the two sampling points is about 3.5 Km.

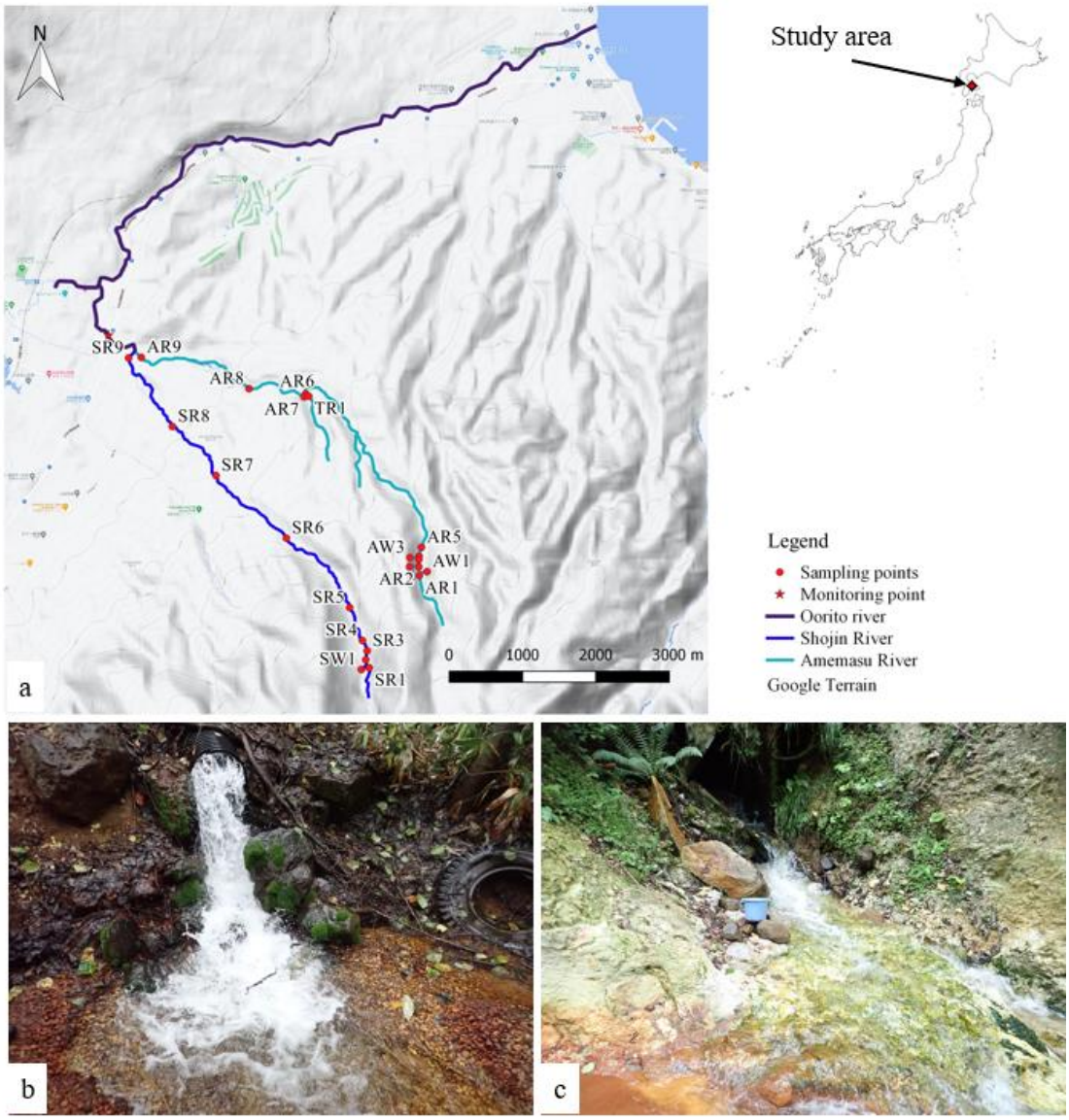

Fig. IV-2. The reconstructed map of the Shojin mine site and the sampling points to the map of Japan, using QGIS version 2.18.24. b) The wastewater flowing from waste dam to Shojin river, c) The wastewater flowing from waste dam to Amemasu river.

Electric conductivity (EC), pH, dissolved oxygen (DO), redox potential (ORP), turbidity, alkalinity, and temperature were conducted on-site for each sampling point. Fe^{2+} was measured by an ion-selective pack test (Kyoritsu Chemical Check Lab., Corp). The alkalinity of water samples was determined by titration of 0.16 N HNO_3 to 50 mL of water, filtered with 0.45 µm syringe ultra-membrane filters for sampling points where pH greater than 3.5. Alkalinity as HCO^{3-} was obtained from Grant-function plots (Rounds and Wilde, 2012). The float method (Dobriyal et al., 2017) was implemented to determine the flow rate in the river.

The water was sampled by syringe membrane ultra-filter size 0.20 µm and stored in two 50 mL acid wash polyethylene bottles. One bottle was acidified with a 1% (v/v) ultrapure nitric acid, preserved for cations analysis. The other bottle without acidification was kept for anions analysis. Yellow-brown suspended sediment was collected upstream of Shojin river and downstream of Amemasu river.

4.2.3. Analytical methods

Total major cations such as Na, Ca, Mg, K, Fe, and Al was measured by inductively coupled plasma–atomic emission spectroscopy (ICP–AES; ICPE-9000, Shimadzu) with multi-element standard solution IV Certipur (Merck, Germany). Trace elements such as As, Cd, and Pb contained in the multi-elements standard solution XSTC-331 (SPEX CertiPrep, USA) were analyzed by inductively coupled plasma–mass spectrometry (ICP–MS; iCap Qc, Thermo Scientific). Fe^{3+} was obtained from the subtraction of total Fe to Fe^{2+}. Total anions were determined by Ion chromatography (IC; IC861, Metrohm, Herisau, Switzerland) using Anion Mixture Standard Solution such as Br, F, NO_2, NO_3, PO_4, Cl, and SO_4.

The mineralogy of suspended sediments was determined by X-Ray Diffraction (XRD-Multiflex, Rigaku; Tokyo, Japan) equipped with a Cu Kα X-ray source and used a working voltage of 40 kV at 30 mA with a scanning speed of 6.5° min-1 ranging from 5° to 70°. Suspended sediment's morphology was characterized by optical and scanning electron microscopy, with the working voltage of SEM being 15 kV (SEM-EDS; JSM-6510LA, JEOL, Tokyo, Japan).

The suspended sediments for chemical composition was digested with 5 M HCl for 2 h at room temperature. The amorphous iron minerals from the suspended sediment samples were extracted with 0.2 M ammonium oxalate at pH 3 for 15 minutes without exposure to UV light. The aqueous solutions were immediately filtered with 0.20 µm membrane filters preserved for ICP-AES, ICP-MS, and IC.

Specific surface areas of the bulk sediment were determined by N_2 adsorption by the Brunauer-Emmett-Teller method (BET; NOVAtouchTM), the exact condition in Chapter III.

4.2.4. Geochemical modeling

Chemical species activities, water-type classifications, and total dissolve solid (TDS) concentration were calculated using GWB geochemist's spreadsheet (GSS) module in the Geochemist's Workbench (GWB) professional package version 15.0. Elemental speciation and stability of iron minerals determined by Act2 module of GWB.

4.3. Results

4.3.1. Characteristics and chemistry of water samples

Shojin river water characteristics

On-site measurement during field sampling and detailed water data results are listed in Supplementary data. The pH of Shojin river water changes from neutral to acidic conditions (pH: 6.88 – 3.09) with EC ranges from 6.6 to 63.6 ms/s, ORP of 308 mv to 585 mv, but DO almost constant with the concentration of 10 mg/L. The upstream turbidity is 0.35 NTU (SR1), and the downstream turbidity is1.68 NTU (SR8).

The wastewater from SW1 pH was 2.6 flowed in the limestone channel (Fig IV-1b), yet the pH at SW2 remained 2.6. SW3 had a slightly higher pH of 3.3, but it provided a minimal contribution to SW4 (pH: 2.7). SW4 later flowed into Shojin river. The average EC of 127 ms/s, ORP ~ 600 mv, turbidity of 0.34 NTU, and DO of 9.31 mg/L. The dominant major cations in wastewater (SW1-SW4) were Ca (6.24 mg/L) and anions SO_4 (1.9 g/L).

The major cations concentration of Shojin background river water SR1 were Ca is about (4.15 mg/L), Mg (1.2 mg/L), and the major anions were HCO_3 (16 mg/L), Cl (6 mg/L), and SO_4 (14.5 mg/L). The Shojin river water SR1 was a Ca-SO_4 water type as it contained SO_4 concentrations of about 50% of total major anions. Commonly, natural river water is dominated by Ca-HCO_3 (Singh and Kumar, 2015). However, the geology of the study area of the mine site contains gypsum or other sulfide minerals, probably affecting the Shojin river water. After SW4 flows to Shojin river, the pH drastically dropped to 3.09 (SR2), and the pH remained constant until SR4 and slightly increased at SR5 (3.15) but decreased to 3.07 at SR6. From SR7 to SR9, pH increased from 3.12 to 3.43.

Trace elements such as Fe, As, Cd, and Pd concentration from wastewater (SW4) were 38.7 mg/L, 83.55 mg/L, 1.3 mg/L, and 25.9 mg/L, respectively. After mixing with the background river (SR4), the trace metals concentration decreased to 14 mg/L, 28.79 µg/L, 0.58 µg/L, and 10.19 µg/L. Cd and Pb decreased about 4 times the wastewater, then slightly increased at SR6 0.82 µg/L and 16.48 µg/L respectively, probably due to the wastewater leaking at the mid-stream again decreasing from SR7. On the other hand, the trend of Fe and As was different from Cd and Pb. Fe and As steadily decreased toward downstream until SR9. Before Shojin and Amemasu river junction, all the As, Cd, and Pb were naturally remediated to less than WHO guidelines. This phenomenon indicates that natural attenuation is successfully treated the Shojin river to less than WHO guidelines.

Amemasu river water characteristics

Amemasu river's pH changed from neutral to acidic conditions (pH: 7.1 – 2.8) with EC ranging from 8.4 to 93 ms/s, ORP of 244 to 564 mv, but DO was almost constant with the concentration of 9.04 mg/L (average value for surface water) except at AT1 (11 mg/L). The upstream (AR1) turbidity was 1.2 NTU and increased about four times after AR7 (5.1 NTU).

The wastewater of AW1, AW2, and AW3 flowed to Amemasu river with a flowrate of 0.06 m^3/min, 0.02 m^3/min, and 5.13 m^3/min, respectively. The average pH of wastewater was 2.8 with EC of 90.6 ms/s, ORP of 600 mv, turbidity of 0.56 NTU, and DO of 5.31 mg/L. Ca (15.8 mg/L) and SO_4 (1.8 g/L) were dominant major-ions.

The average concentration of major cations was Ca (6.4 mg/L), Mg (1.2 mg/L), and the major anions were HCO_3 (12 mg/L), Cl (6 mg/L), and SO_4 (18 mg/L) before contamination. The Amemasu river background water, AR1, and AR3 were Ca-SO_4 water types as they contained SO_4 concentrations of about 50% of total major anions. Water types in the river at sampling points came from AR4 to AR9 shifted from Ca-SO_4 type to H-SO_4 water type after the AR3 mixed with AW3 due to its low pH and high concentration of SO_4.

Amemasu river background river's pH decreased from 7.1 to 5.5 at AR3 after the input of AW1 and AW2. Fig. IV-3b indicates the changing pH from AR4 to AR9 after AW3 contaminated the river water. The pH of Amemasu river at AR4 and AR5 decreases from 5.5 to 2.9. After flowing downstream AR6, there was neutral water

(AT1) input from Amemasu tributaries before AR6 to AR8, which led to pH increased to ~3.1 and 3.3 at AR9 (Fig.IV-3b). A tributary AT1, not affected by AMD, also slightly contains sulfate with major anions but falls into Ca-HCO_3 water type.

The trace elements concentration in wastewater of Amemasu river were Fe (32.6 mg/L), As (251 µg/L), Cd (14.64 µg/L), and Pd (75.85 µg/L), the same as Shojin river. The sources of Fe species from those areas were dominant Fe^{3+} (27.6 mg/L), probably due to the catalyzes of iron-oxidizing bacteria in low acidic conditions (Laroche et al., 2018). The contamination of trace elements started from AR4 toward downstream (Fig. IV-3b&d). The trace metals in the river. Fe, As, Cd, and Pb at AR4 and AR5 were slightly less than AW3 with an average concentration of 25 mg/L, 197 µg/L, 12 µg/L, and 60 µg/L, respectively. The concentration of toxic elements kept flowing downstream, yet drastically decreased at AR6 with a concentration of 15 mg/L, 67 µg/L, 6 µg/L, and 34 µg/L, respectively. From AR7, Fe and As significantly decreased downstream, while Cd and Pb remain almost stable from AR7 to AR9, as shown in Fig. IV-3d. Before merging with Shojin river, only As concentration in Amemasu river decreased to 7 µg/L, which was less than WHO guideline while Cd and Pb remained higher than the environmental regulation limit. The toxic elements of Amemasu river are partially remediated, but it is insufficient to reach the environmental regulation limit.

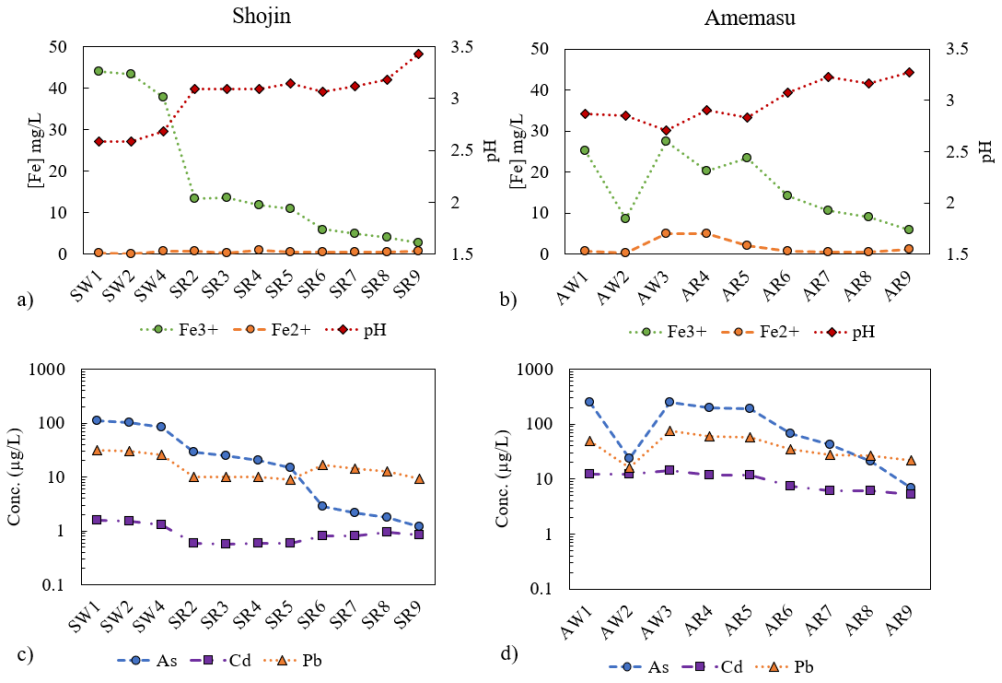

Fig. IV-3. (a). $Fe^{2+,}$ $Fe^{3+,}$ and pH trends across sampling points in Shojin river; (b). $Fe^{2+,}$ Fe^{3+} and pH trends across the sampling points Amemasu river; (c) As, Cd, and Pb trends across Shojin river; (d) As, Cd, and Pb trends across sampling points in Amemasu river. The x-axes of (c) and (d) are on a logarithmic scale.

4.3.2. Sediment mineralogy

The XRD pattern of precipitated sediment is shown in Fig. IV-4a. The XRD shows the schwertmannite formed in the Shojin river as the assigned peak is consistent with the natural schwertmannite peak in previous studies (Acero et al., 2006; Bigham et al., 1990b). The SEM image (Fig. IV-4b) shows the schwertmannite morphology accumulated as spherical structures with needle-like fibrous structures at the outer part. This structure could provide a large specific surface area for metal adsorption or surface complexation (Zhang et al., 2018). The specific surface area of the bulk sediment contained schwertmannite about 50% to 85%, ranging from 53-63 m^2/g (Table IV-1&2).

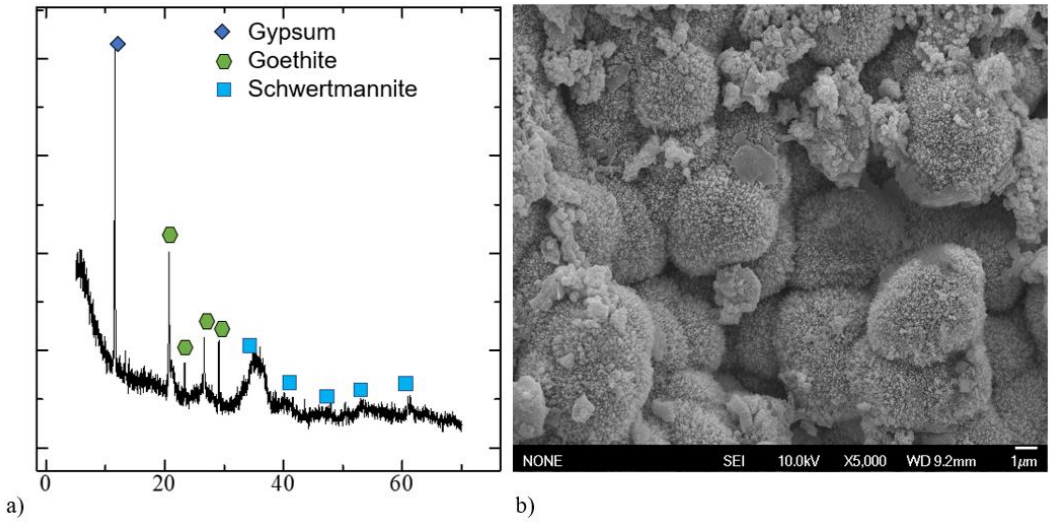

Fig. IV-4. a) The XRD pattern of precipitated minerals in the tributary in the Shojin river. b) The SEM image of the precipitated sediment from Shojin river.

Table IV-1. The result of yellow-brown precipitated sediment collected from the Shojin and Amemasu river that 5 M of HCl dissolved.

Site	**Fe**	**As**	**Cd**	**Pb**
	mg/g	mg/g	mg/g	mg/g
Shojin S1	312	0.06	0	0
Amemasu S1	223	5.97	0	0.22
Amemasu S2	461	2.62	0	0.04

Table IV-2. The yellow-brown precipitated sediment collected from the Shojin and Amemasu river was dissolved by ammonium oxalate at pH 3.

Site	**Fe**	**As**	**Cd**	**Pb**
	mg/g	mg/g	mg/g	mg/g

Shojin S1	272	0.04	0	0
Amemasu S1	186	3.33	0	0.15
Amemasu S2	234	1.73	0	0.03

4.4. Discussion

4.4.1. The impact of background river water mixes with AMD

The mixing of Shojin river with AMD

Dilution of the contaminated wastewater by the background river has a significant role in natural attenuation, enabling neutral water to dilute or neutralize the acid mine drainage (Balistrieri et al., 2007; Ito et al., 2017). Similarly, AMD discharges to natural rivers undergoing the dilution process in this study. The background river of Shojin river accounts for the decreasing Cd and Pb concentration with a ratio of about 1:4 (wastewater: background river). The effect of the dilution of the background was determined the ratio of species concentration of toxic elements (As, Pb, Cd) of each sampling point over the wastewater (SW1) was plotted against the ratio of SO_4 concentration of each sampling point over the concentration of wastewater (SW1) (Berger et al., 2000). The mixing line represents the decreasing of concentration species by dilution. The value of the sampling point falling below the mixing line represents the species concentration removed by coprecipitation and adsorption mechanisms. The value of the species above the mixing line indicates the contaminant is added. In Shojin river, the arsenic concentration of sampling points SR2 to SR4 falls below the mixing line, meaning that other processes removed it rather than dilution (Fig. IV-5a). Cd and Pb are slightly above the mixing line for sampling SR2 to SR4 (Fig. IV-5c&e). The trace metal behavior from sampling points SR6 to SR9 shows the abnormality. Arsenic is located near the mixing line (Fig. IV-5a), but Cd and Pb were about the mixing line (Fig. IV-5c&e), indicating an unidentified wastewater added the contaminant to Shojin river. The concentration of Cd and Pb in Shojin river decreased only due to dilution. Moreover, the background water of Shojin river diluted the total H^+ ions of drainage water, which resulted in the average pH in Shojin river being about 3.1 from SR2 to SR9.

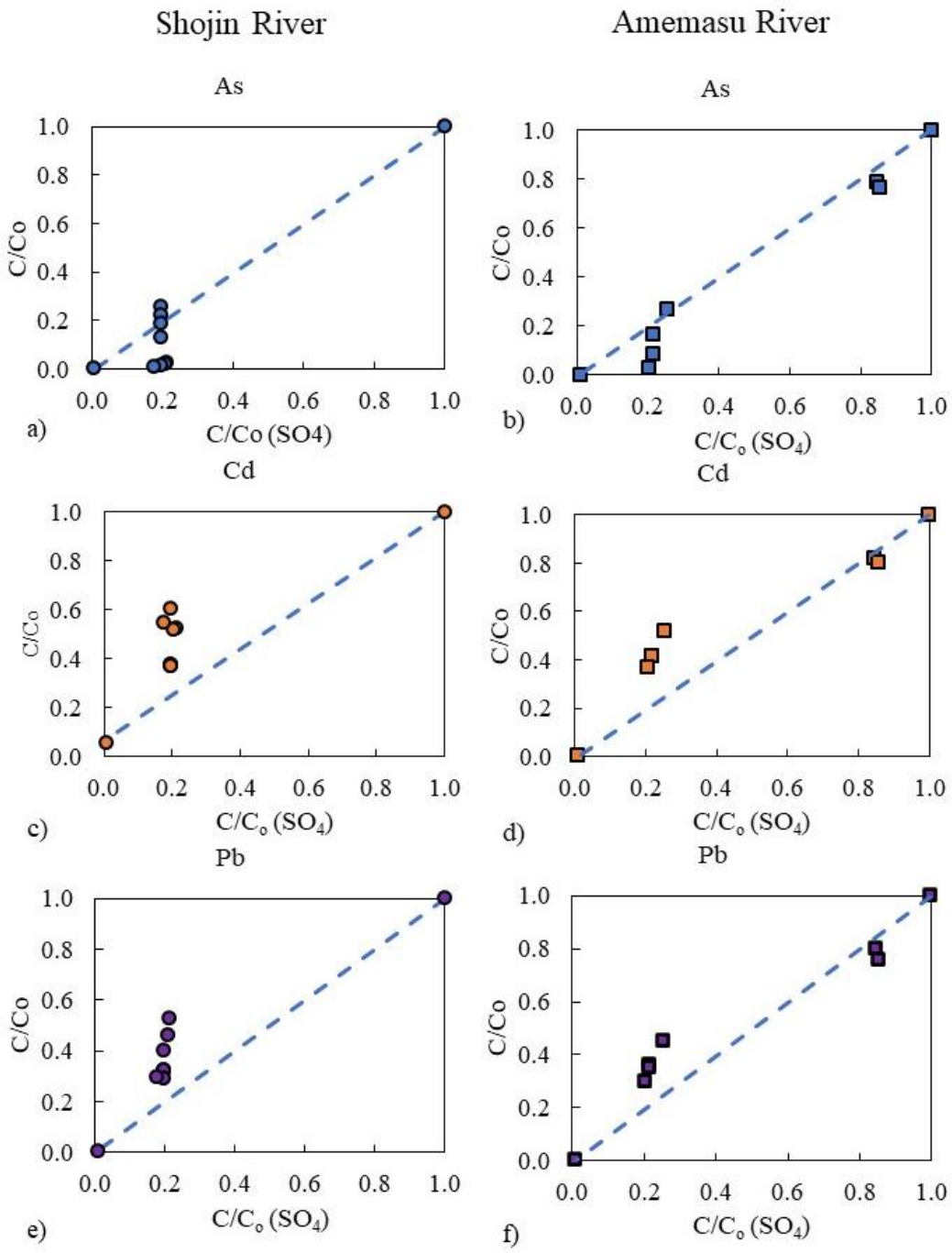

Fig. IV-5. The concentration ratios of the toxic elements As, Cd, and Pb in Shojin and Amemasu river were plotted against concentration ratios of SO_4 concentration (a) As concentration ratios against SO_4 ratios, Shojin river, (b) As concentration ratios against SO_4 ratios, Amemasu river (c) Cd concentration ratios against SO_4 ratios, Shojin river (d) Cd concentration ratios against SO_4 ratios, Amemasu river. (e) Pb concentration ratios against SO_4 ratios, Shojin river (f) Pb concentration ratios against SO_4 ratios, Amemasu river. The dashed line represents the concentration that would result from the mixing of wastewater and background river water. Concentration below the dashed line indicates the removal of the element from the solution by other factors (precipitation or adsorption). Concentration above the dashed line suggests adding the element to the solution by other sources. The concentration along the mixing line represents dilution.

Fe concentration significantly decreased from 38 mg/L (SW4) to 14 mg/L (SR2), indicating schwertmannite precipitation after mixing wastewater with natural river water. At the mixing point, the pH of the river was 3.01, where it was highly suitable

for schwertmannite formation conditions (Zhang et al., 2018). Schwertmannite coated the Shojin river bedrock from SR2 toward downstream, which probably acted as the adsorbent for As removal from Shojin river.

The mixing Amemasu river with AMD

The same methods were applied to Amemasu river to determine the effect of dilution background river water. At the upstream of Amemasu river (AR4&AR5), As, Cd and Pb decreased due to the dilution as those elements fall along the mixing line (Fig. IV-5b, d, f). At the mid-stream from AR6, As concentration falls below the mixing line (Fig. IV-5b) suggested that As was removed by co-precipitation or adsorption. On the other hand, Cd and Pb are slightly above the mixing line (Fig. IV-5d&f) due to the extra dilution from the Amemasu river tributary in between AR5 to AR6 based on the satellite image. Although, there are no accessible roads to reach the tributary. The mixing of Amemasu river plays significant mechanisms, as seen in Shojin river, since it dilutes the concentration of Cd, Pb, and H^+. Though, at the upstream (AR4 and AR5), the dilution ratio is insufficient to decrease Cd and Pd to less than WHO guideline nor pH to above 3. At the mid-stream, where neutral water was added from its tributaries, the pH of the Amemasu river raised to 3.1, and As, Cd, and Pb concentration decreased. Schwertmannite was also found after AR6, which probably promotes the reduction of As concentration in the river water.

At the Mondulkiri mine site, rainwater plays a significant role in natural attenuation, while the background river is essential at Shojin mine. In a temperate climate zone, the highest rainfall is in Summer and snowfall in winter. The long winter periods in Hokkaido accumulate a large amount of snowpack, which might increase runoff during snow melting (Katsuyama et al., 2020) in mid-April. This study is limited to summer; however, it is worth noticing that increasing neutral water input sources would benefit natural attenuation in the rivers.

4.4.2. The relationship of Schwertmannite and trace elements the rivers

Arsenic has a high affinity to absorb and coprecipitate with schwertmannite (Fukushi et al., 2003) since schwertmannite has a high specific surface area as well as a positive surface charge under acidic conditions (Khamphila et al., 2017; Park et al., 2021). Fe and As had a similar reduction trend in Shojin river and Amemasu river. It

indicated that As adsorbed and coprecipitated with schwertmannite in the Shojin river after SR2; and Amemasu river after AR6. In contrast, Cd and Pb provided different trends to As.

This section conducted selective extraction of the bulk suspended sediments to clarify trace metals incorporation with schwertmannite. The released Fe concentration from the selective extraction represents the schwertmannite in the bulk sediment (Table IV-1&2). Up to 80% of schwertmannite was released from the bulk sediment. Arsenic is the dominant element incorporated with schwertmannite. Cd was not detected from the samples, while Pb was slightly released from the extracted solution. Cd does not adsorb to any Fe minerals in acidic conditions as their surfaces are positively charged (Yang et al., 2019). Pb is slightly different from Cd, as it adsorbs onto schwertmannite or iron hydroxide at a more neutral condition pH > 5.5 (Baleeiro et al., 2018). Cd and Pb do not coprecipitate with Fe^{3+} minerals since Cd and Pb have the larger ionic radius and different coordination numbers from Fe^{3+} (Borsari, 2014; Diebold and Hagen, 1998; Hosseini et al., 2012). Thus, schwertmannite formation removed As from the contaminated rivers, but it does not account for Cd and Pb scavenges.

4.4.3. Formation of Schwertmannite

Schwertmannite is a metastable ferric iron mineral formed under biotic or abiotic conditions in a pH range of 2.5–4.5 (Bigham et al., 1990). Its formation requires Fe^{3+} as a source of Fe for mineral precipitation. Whereas, Fe^{2+} is released from the sources in most of AMD. Fe species was dominant by Fe^{3+} in this study, favoring the hydrolysis process of schwertmannite. Schwertmannite plays a major role in metals and metalloid removal in AMD (Paikaray, 2020; Shi et al., 2021). Its formation acts as an absorbent material in the AMD solution (Fukushi et al., 2003a). The pH of Shojin and Amemasu rivers are within the schwertmannite formation stability field (2.5-4.5); however, pH alone is insufficient to determine schwertmannite occurrence. Schwertmannite formation depends on activities of Fe^{3+}, pH, and activities of SO_4 (Bigham et al., 1996) under the chemical formula; $Fe_8O_8(OH)_x(SO4)_{y(s)}$ (where y = 8-22x, and $1 \leq x \leq 1.75$) and reaction (1) (Sánchez-España et al., 2011).

$$Fe_8O_8(OH)_{5.2}(SO_4)_{1.4} + 21.2H^+ = 8Fe^{3+} + 1.4SO_4^{2-} + 13.2H_2O \quad \text{(VI-1)}$$

The geochemical model was conducted to determine the occurrence of schwertmannite in both rivers, using the thermodynamics database from Sánchez-España et al. (2011) with the log equilibrium constant (log K) 18.8. The filed data, activities of Fe^{3+} were used to plot against pH (Fig. IV.6) to determine the pH that enables schwertmannite precipitation. The model revealed that schwertmannite could form in Shojin river from SR2 to SR5. However, Fe^{3+} concentrations from SR6 to SR8 were not high enough for schwertmannite formation. The Fe^{3+} precipitated as schwertmannite until its minimum concentration at SR5. Yet at SR9, schwertmannite could form again after pH was increased to 3.4.

In contrast, at Amemasu river, the pH at AR4 and AR5 were too low to allow schwertmannite precipitation. The activities of Fe^{3+} were almost the constant for each sampling point. Yet, the model shows that the schwertmannite only forms from AR6 to AR9 when pH increases about 3.1. Schwertmannite is the essential absorbent material for the Amemasu river; thus, it is necessary to maintain the river's pH the enable schwertmannite from the upstream. The optimum pH for schwertmannite precipitation for AR4 and AR5 is 3.2 (Fig. IV-6).

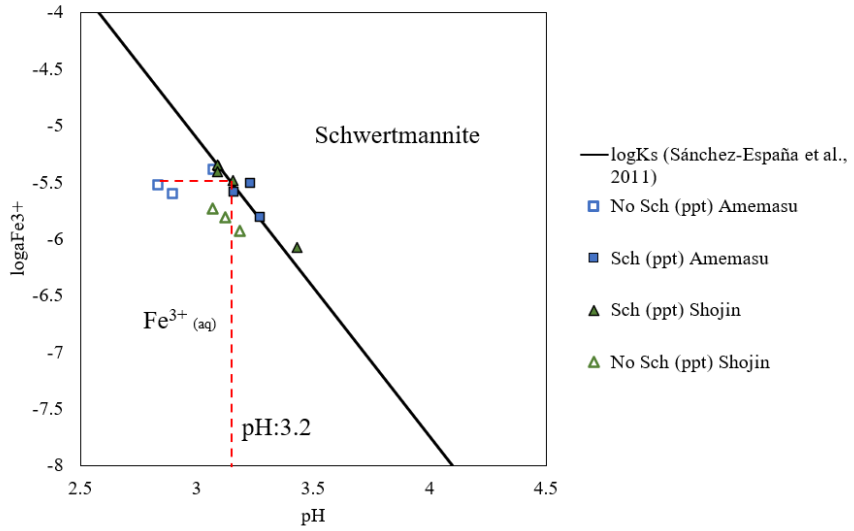

Fig. IV-6. The stability of schwertmannite with different log (equilibrium constant) values with log aSO42- = 10-2.3 and field data from the Shojin and Amemasu rivers. Reference data are from Sánchez-España et al. (2011) (solid line). The dashed line is the extended aFe^{3+} to meet the schwertmannite solubility field to determine the optimum pH that enables schwertmannite to precipitate using the $logK_{sch}$ 18.8 form Sánchez-España et al. (2011).

4.5. Summary

Generation of AMD from the abandoned Shojin mine is an issue similar to other abandoned mine sites worldwide. Shojin mine contamination contaminates As, Cd, and

Pb to Shojin and Amemasu river, through seepage from the waste dams. This study highlighted significant geochemical characteristics of the two rivers that are in the same geological setting and climate condition:

- The same toxic elements contaminate Shojin and Amemasu rivers. Even though, after drainage water into contact with the natural environment, Shojin river successfully self-remediated to less than WHO regulation limit. Nevertheless, the water quality of Amemasu river remains above the WHO regulation limit. Amemasu river required human assistance for the water treatment.
- Natural attenuation in Shojin river is due mainly to the dilution of Shojin background rivers to the drainage water, maintaining the pH above 3 where schwertmannite precipitate. The dilution causes a decrease in Cd and Pb concentration, while Arsenic concentration in Shojin river is scavenged by schwertmannite. The dominant concentration of Fe^{3+} promotes the formation of schwertmannite in the study area.
- The dilution of Amemasu river background is insufficient to dilute the drainage water that flows to the river upstream. The extra input water from Amemasu tributaries at the mid-stream enhances the schwertmannite precipitation and As removal, although it is still inadequate for Cd and Pb.
- The geochemical differences between Shojin and Amemasu rivers are governed by the degree of dilution of the background rivers.

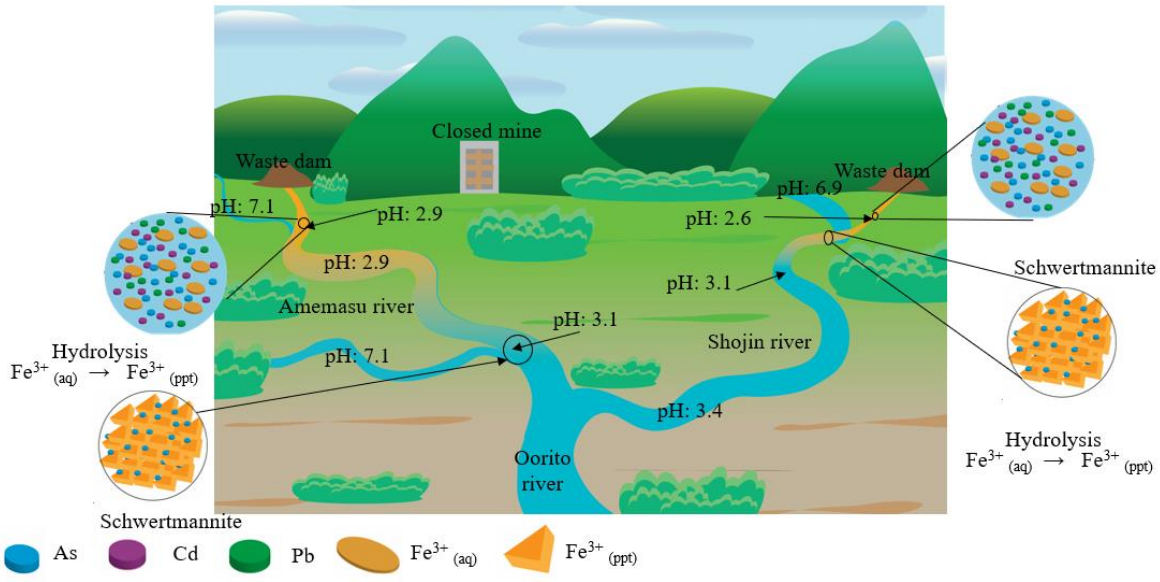

Fig. IV-7. The graphical summery of the Shojin mine site.

4.6. Supplementary data

Table IV-3. Amemasu river data

Site	pH	ORP	EC	Turb.	DO	HCO_3^-	Na	Ca	K	Al	Fe	Fe^{2+}	Fe^{3+}	As	Pb	Cd	Cl	SO_4
		mv	ms/s	NTU	mg/L	mg/L				mg/L				µg/L			mg/L	
AW1	2.87	569.3	80.50	0.33	4.13	-	5.02	15.80	1.98	11.13	26.10	0.8	25.3	254.69	49.74	12.53	4.79	1576
AW2	2.85	564.7	87.90	0.31	4.74	-	5.41	14.14	1.1	11.17	8.74	0.2	8.54	23.91	16.06	12.37	5.65	1343
AW3	2.71	7.05	103.4	0.56	7.05	-	5.12	15.08	1.28	15.11	32.56	5	27.56	251.05	75.85	14.64	5.02	1852
AR1	7.09	310.	8.43	1.43	9.17	12.3	4.32	6.38	0.58	-	-	0	-	0.25	0.14	0.09	6.08	18.75
AR2	6.69	244.7	8.56	2.85	9.24	12.3	4.4	5.53	0.64	-	-	0	-	0.47	0.27	0.27	5.99	22.4
AR3	5.49	519.7	9.70	4.77	8.53	6.4	5.57	7.07	0.65	-	-	0	-	0.4	0.79	1.06	5.92	40.6
AR4	2.90	519.3	93.13	1.23	9.35	-	4.93	12.48	1.12	10.87	25.19	5	20.19	197.74	60.36	12.0	5.14	1565
AR5	2.83	523.3	82.80	1.34	9.80	-	5.09	13.57	1.27	12.38	25.48	2	23.48	192.34	57.20	11.76	4.81	1585
AR6	3.07	563.7	58.20	2.46	6.63	-	5.25	11.08	1.11	9.02	14.98	0.8	14.18	67.3	34.29	7.59	5.54	470.9
AR7	3.23	551.7	45.83	4.92	9.55	-	5.40	10.40	1.09	6.82	11.19	0.5	10.69	41.84	27.43	6.07	5.91	402.3
AR8	316	547.7	48.43	5.14	9.49	-	5.43	10.96	1	7.06	9.49	0.5	8.99	21.30	26.46	6.04	5.59	402.5
AR9	3.27	519.7	43.10	4.57	9.57	-	5.84	11.78	1.26	6.14	7.06	1.2	5.86	7.04	22.28	5.36	8.01	381.6
AT1	7.07	335	11.22	4.99	14.67	30.7	5.97	7.86	1.83	-	-	0	-	1.4	0.17	0.09	9.57	11.82

Table IV-4. Shojin River Data

Site	pH	ORP	EC	Turb.	DO	HCO_3^-	Na	Ca	K	Al	Fe	Fe^{2+}	Fe^{3+}	As	Pb	Cd	Cl	SO_4
		mv	ms/s	NTU	mg/L	mg/L				mg/L				µg/L				mg/L
SW1	2.59	606.3	129.5	0.18	7.79	9.1	4.8	6.24	1.9	10.5	44.2	0.2	44.0	110.9	31.3	1.6	4.1	1937
SW2	2.59	616.3	127.3	0.63	8.22	-	4.6	7.06	2.2	10.5	43.5	0.1	43.4	103.6	30.6	1.5	3.9	1923
SW3	3.3	506.7	36.23	0.34	10.6	-	4.4	5.63	1.2	4.61	6.36	2	3.4	7.19	0.6	0.2	3.9	338
SW4	2.68	588.	114.8	0.43	10.3	-	4.5	8.1	1.4	9.82	38.7	0.8	37.9	83.55	25.9	1.3	5.03	1958
SR1	6.88	308.3	6.61	0.35	9.9	-	4.4	4.15	1.5	-	-	-	-	0.17	0.17	0.1	6.1	14.5
SR2	3.09	561	48.67	0.99	10.2	-	4.5	5.67	1.5	3.14	14.1	0.8	13.3	28.79	10.2	0.6	6.0	382
SR3	3.09	585	49.83	1.46	10.3	-	4.6	5.93	1.6	3.62	13.7	0.2	13.5	24.90	10.0	0.6	5.9	382
SR4	3.09	558.3	50.23	1.46	10.3	-	4.6	6.28	1.6	4.38	12.8	1	11.8	20.71	10.2	0.6	5.1	378
SR5	3.15	559.7	50.67	0.86	10.1	-	4.7	6.83	1.5	4.98	11.5	0.5	11	14.7	9.09	0.6	4.8	379
SR6	3.07	545	63.63	0.91	10	-	5.5	10.7	1.8	8.21	6.42	0.5	5.92	2.83	16.5	0.8	5.5	414
SR7	3.12	529.3	55.47	1.1	9.9	-	5.7	10.7	1.9	8.09	5.40	0.5	4.9	2.2	14.5	0.8	5.9	401
SR8	3.18	522.7	51.10	1.68	10.2	-	5.9	11.1	1.9	8.43	4.43	0.5	3.93	1.8	12.5	0.9	8.01	383
SR9	3.43	495.7	41.67	0.59	9.47	-	6.3	12.0	1.9	7.01	3.48	0.8	2.68	1.2	9.36	0.9	9.57	340

Table IV-5. Oorito River data

Site	pH	ORP	EC	Turb.	DO	HCO_3^-	Na	Ca	K	Al	Fe	Fe^{2+}	Fe^{3+}	As	Pb	Cd	Cl	SO_4
		mv	ms/s	NTU	mg/L	mg/L				mg/L					µg/L			mg/L
OR1	3.32	500	41.27	1.80	9.48	-	6.84	12.32	2.66	6.70	4.78	-	4.78	2.99	14.2	2.74	7.1	325.33
OR2	4.55	350	30.13	6.21	9.55	1.3	14.25	22.11	2.90	2.95	0.55	-	0.55	0.34	5.39	1.56	11.04	205.72
OR3	5.70	154.67	29.93	11.07	9.91	0.1	15.14	26.56	30.9	0	0.04	-	0.04	1.13	0.77	0.98	10.66	114.38
OR4	7.07	105.33	27.83	17.33	9.68	12.3	15.25	24.43	3.13	0	0	-	0	1.11	0.27	0.76	11.69	94.61

V. Iron dynamics and geochemical interactions of hazardous elements with schwertmannite in AMD

5.1. Introduction

Dissolved iron is ubiquity in AMD systems, including Mondulkiri mine and Shojin Mine. The critical role in Fe minerals in natural attenuation is highly advantageous to passive treatment implementation (Skousen and Ziemkiewicz, 2005). The case studies of this research pointed out the critical roles of schwertmannite in natural attenuation. Schwertmannite is the primary mineral from Fe^{3+} in AMD (Feng et al., 2021), but Fe^{2+} iron is abundant in most AMD. Fe^{2+} commonly dissolves from pyrite (Fe_2S), arsenopyrite (FeAsS), or chalcopyrite ($CuFeS_2$) in the ore minerals and waste rocks (Neil et al., 2014; Taylor et al., 2005). As described in Chapter II, the dissolved ferrous iron can oxidize to ferric iron under biotic and abiotic conditions (Auld et al., 2013; Stumm and Lee, 1961). At Mondulkiri mine, Fe^{2+} released from the wastewater and sulfide minerals dissolution. After wastewater flows into the tributary, Fe^{2+} oxidizes to Fe^{3+} with the assistance of iron-oxidizing bacteria. However, at Shojin mine, Fe^{3+} is dominant over Fe^{2+}, released from the AMD seepage. Thus, Fe^{2+} oxidation can be neglected in Shojin mine site. Fe^{3+} in both study areas have gone under the hydrolysis process, forming the ferric iron minerals; schwertmannite. The significant roles of schwertmannite in natural attenuation at the Mondulkiri and Shojin mine motivate the detailed understanding of iron dynamics in both study areas.

This chapter will give the various approaches to understanding the iron dynamics of schwertmannite formation by using field data from the case studies mentioned in Chapters III and IV. The iron dynamics include ferrous iron to ferric iron, ferric iron to ferric minerals, and ferric interactions with toxic elements in AMD. Chapter III described the involvement of iron-oxidizing bacteria in the Mondulkiri mine site that facilitates schwertmannite formation. Thus, this section will discuss the ferrous oxidation rate under biotic conditions. The fourth-order rate law of Pesic et al. (1989) is likely applicable to only a single bacterial species (Garcia-Rios et al., 2020). It is unsuitable for determining Fe^{2+} oxidation rates at the mine site where various bacteria species have mixtures. In natural conditions, the Fe^{2+} oxidation rate constants are varied based on environmental conditions and site specifics. The later study of Larson et al.

(2014) suggests that the Fe^{2+} field oxidation rate ($R_{Fe2+,\ field}$) can be better described by equation (V-1) and field rate constant equation (V-2). Thus, the determination of Fe^{2+} oxidation rate and rate constant is necessary to construct the Fe^{2+} oxidation rate modeling for future AMD treatment implication of Mondulkiri mine.

$$R_{Fe2+,\ field} = -d[Fe^{2+}]/dt = ([Fe^{2+}_{,\ inflow}] - [Fe^{2+}_{,\ outflow}])/t \quad \text{(V-1)}$$

$$k_{Fe2+,\ field} = -(\ln[Fe^{2+}_{,\ outflow}] - \ln[Fe^{2+}_{,\ inflow}])/t \quad \text{(V-2)}$$

where $[Fe^{2+}_{,\ inflow}]$ is the dissolved Fe^{2+} concentration in the initial inflow; $[Fe^{2+}_{,\ outflow}]$ is dissolved Fe^{2+} concentration in the outflow; t is travel time of Fe^{2+} from initial inflow to outflow; and $k_{Fe2+,\ field}$ is a rate constant for oxidation Fe^{2+} in the field.

Precipitation of schwertmannite can be written as shown in reaction (ii) following Bigham et al. (1996). Schwertmannite precipitation is Fe^{3+} and pH-dependent where SO_4^{2-} concentration is between 500 mg/L to 2000 mg/L in AMD, commonly higher than Fe^{3+}(Chen and Jiang, 2012). Asta et al. (2010) simplified the schwertmannite precipitation model rate from pH 2.7–3.5 as follows:

$$8Fe^{3+}_{(aq)} + ySO_4^{2-}{}_{(aq)} + (24\text{-}2y+x)/2H_2O \rightarrow Fe_8O_8(OH)_x(SO4)_{y(s)} + (24\text{-}2y)H^+_{(aq)}$$

(Reaction V-1)

$$R_{sch}=k_{sch}[Fe^{3+}][H^+]^{-1} \quad \text{(V-3)}$$

where R_{sch} is precipitation rate of schwertmannite ($mol.L^{-1}.s^{-1}$). $[Fe^{3+}]$ and $[H^+]$ concentration are in $mol.L^{-1}$, k_{sch} is the rate constant for schwertmannite precipitation in $mol.L^{-1}.s^{-1}$.

Schwertmannite rate constant found in Asta et al. (2010), using Fe^{3+} field data measurement to calibrate with Fe^{3+} modeling given a rate constant result range from 3.16×10^{-9} to 10^{-8} $mol.L^{-1}.s^{-1}$. A considerable variation in the rate constant provides a significant uncertainty in determining the schwertmannite precipitation rate. Therefore, obtaining the rate constant for the schwertmannite precipitation rate is crucial for the study areas.

The field investigation suggests schwertmannite is responsible for As removal in acidic conditions when pH is above 3. Schwertmannite was reported as a significant mineral to remove other metal(loid)s in AMD (Paikaray, 2020; Regenspurg and Peiffer, 2005), even though Ni, Cd, and Pb are not incorporated with schwertmannite of the study areas. It is necessary to clarify the toxic elements that interact with

schwertmannite and its removal mechanisms. Therefore, the objectives of this chapter are (1) to determine Fe^{2+} oxidation rate and rate constant in the biotic system using Fe^{2+} field data measurement from Mondulkiri mine site, (2) to estimate the Fe^{3+} rate constant and precipitation rate of drainage water from the study areas in acidic condition (pH 3.1 to 3.5), (3) to evaluate the rate-limiting of Fe^{2+} oxidation rate and Fe^{3+} precipitation rate that may control the natural attenuation process at Mondulkiri mine site, (4) to understand the adsorption of toxic elements such as As, Ni, Cd, and Pb on schwertmannite in the study area, (5) and to determine the optimum pH for AMD treatment implication for the study areas.

5.2. Materials and Methods

5.2.1. Schwertmannite constant rate experiment

The drainage water in the dry season of the Mondulkiri mine and drainage water of Amemasu river were used to investigate the precipitation rate of schwertmannite within pH; 3.1, 3.3, 3.4, and 3.5. The 0.1N HNO_3 and 0.1N NaOH were used for pH adjustment during the experiment. The experiment was conducted for 24 h until the Fe^{3+} concentration was stable. The aqueous solution was collected from 0 h to 24 h, filtered by 0.20 µm syringe membrane filters, acidified by 1% HNO_3 ultra-pure acid preserved for chemical elements analysis. Rate constant k_{sch} was obtained from the regression line of schwertmannite precipitation rates against proton following equation V-3.

5.2.2. Trace elements adsorption experiment

The batch adsorption method is commonly used for surface complexation model validation. However, this method was carefully conducted in the laboratory without field investigation data validation. It is uncertain for the engineer to apply in the natural environment. Therefore, the titration drainage water is used to validate the batch adsorption experiment in the laboratory from the previous studies. The mine sites' drainage water was used to conduct the adsorption edges experiment for surface complexation modeling. The drainage water pH was titrated between 3 to 11 by 0.1N NaOH and adjusted pH by 0.1N of HNO_3. The solutions were kept for 24 hours. The solutions were later filtered with a 0.20 µm ultra-membrane filter and acidified with 1%

HNO3 preserved for chemical elements analysis. The toxic elements such as As, Ni, Cd, and Pb were analyzed using the method mentioned in chapter III.

5.2.3. Geochemical modeling

Geochemist's Workbench (GWB) professional package version 15.0 was used for geochemical modeling, including Fe^{2+} oxidation rate, Fe^{3+} precipitation rate, and a surface complexation model. Surface complexation modeling was undertaken to predict adsorption behaviors of target toxic elements using a generalized double-layer surface complexation model by Dzombak and Morel. (1990) in the GWB React module. The surface complexation modeling engaged with the ferrihydrite sorbing-surface database due to the similarity of schwertmannite and ferrihydrite's surface properties (Khamphila et al., 2017; Otero Fariña et al., 2015). The predictive models were fitted with the adsorption experiment for model validations.

5.3. Results and discussion

5.3.1. Ferrous oxidation rate in Mondulkiri mine

Ferrous oxidation rate and oxidation rate constant were calculated after Larson et al. (2014) using field data at the Mondulkiri mine site. In the rainy season, Eq. (V-1) yields a Fe^{2+} oxidation rate beyond T2 to T7, where pH averages 3.6, the oxidation rate is 2.96×10^{-8} mol. L^{-1} s^{-1}, with rate constant $k_{Fe2+,\ field}$ 0.0001 s^{-1}. In the dry season (T2 to T7), 1.49×10^{-7} mol. L^{-1} s^{-1}; $k_{Fe2+,\ field}$ 0.0004 s^{-1}at pH 2.8 is about two orders of magnitude lower than the rate determined by Larson et al. (2014). The Fe^{2+} oxidation rate in the drainage is less than that found by Larson et al. (2014), probably because the Fe^{2+} concentration is also an order of magnitude lower. The oxidation field rate constant is not uniform in each field site due to pH-dependent and concentration of iron-oxidizing bacteria. Fe2+ oxidation rates in the Mondulkiri mine were re-estimated using a geochemical model with various rate constants based on pH conditions (Fig. V-1). The rapid oxidation at T1 at pH 2.9 might take ~ 2.5 to 8 hours to oxidize 50% of Fe^{2+} to Fe^{3+} while this process beyond T2, the oxidation Fe^{2+} to Fe^{3+} takes about 8 hours Fig. V-1. At pH range 2.2–4.5, the lower the pH, the higher the Fe^{2+} oxidation rate (Larson et al., 2014; Pesic et al., 1989).

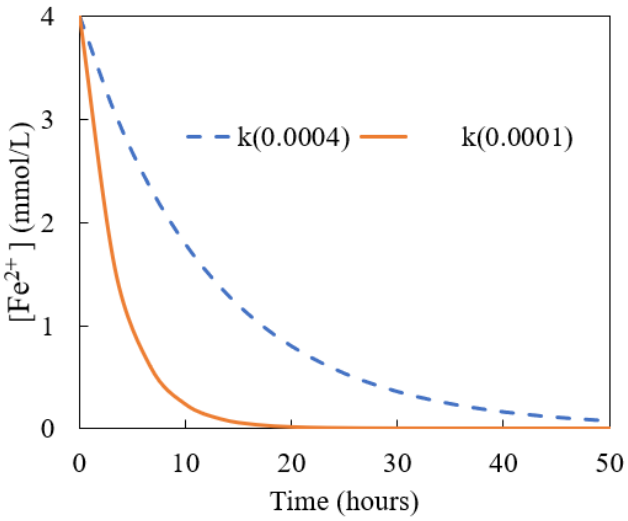

Fig. V-1. The ferrous iron oxidation rate of various rate constants (k) in relation to time.

Table V-1. Fe^{2+} oxidation rate in biotic condition following oxidation field rate formula by Larson et al. (2014)

pH	Fe^{2+} rate ($mol.L^{-1}.s^{-1}$)	$k_{Fe2+,}$(min^{-1})	Study area
2.7	6.63×10^{-8}	0.009	This study
3.5	1.48×10^{-8}	0.006	This study
4.04	1.43×10^{-6}	0.038	Appalachian Coal Basin
2.89	8.13×10^{-6}	0.066	Appalachian Coal Basin
3.13	13.1×10^{-7}	0.003	Iberian Pyrite Belt
2.36	2.44×10^{-7}	0.028	Iberian Pyrite Belt

5.3.2. Precipitation rate of ferric of iron

Experimental results for schwertmannite precipitation rate show decreased Fe^{3+} concerning time for various pH within 24 hours. This experiment assumes that the loss of Fe^{3+} from the solution represents schwertmannite precipitation (section 5.2.2). Fe^{3+} drastically decreases during the first 5 hours yet becomes almost stable after 24 hours (Fig. V.2a). Fe^{3+} precipitation at pH relatively slower than pH 3.4 and 3.5 as it took about 4 hours to 50% of Fe^{3+} while it took only 30 minutes for pH 3.4 and 3.5. The rate constant was taken from the regression line of schwertmannite precipitation rates obtained from experiment data against protons concentration, yielding a rate constant, k_{sch} of 2.84×10^{-9} mol. $L^{-1}.s^{-1}$ (Fig.V.2b). It is slightly less than the minimum rate constant Asta et al. (2010) reported. The precipitation calculated from this study rate

constants is shown in the yellow line in Fig. V-2b. The obtained rate constant was later used in the geochemical model to estimate the precipitation rate of schwertmannite in both study areas.

5.3.3. Fe^{2+} and Fe^{3+} dynamics

Chapter III suggested that the optimum pH for schwertmannite to dominate Fe^{3+} in the system is more significant than 3.1. Within this pH, the oxidation rate from ferrous iron to ferric iron is 2.68×10^{-7} mol. L^{-1} s^{-1}. The schwertmannite precipitation rate would be 1.48×10^{-8} mol. L^{-1} s^{-1}. With the catalysis of iron-oxidizing bacteria, the ferrous iron oxidation rate is approximately ten times faster than the precipitation rate.

Nevertheless, the limited calculation of ferrous oxidation rate and its rate constant in the study area could be affected by the rapid oxidation of ferrous ions in the field during the measurement. The ferrous iron oxidation rate in the field was possibly faster than the calculated value. The flow rate of the tributary was ~0.05 $m^3.s^{-1}$ yielding ~ 6 hours of resident time from T2 to T3. The residence time is sufficient for the formation of schwertmannite in the tributary. It is worth noting that ferrous iron oxidation and schwertmannite formation occurred in the field within a short period, enabling As attenuation in the rainy season (Mondulkiri mine). Fe^{3+} is the rate-limiting control the formation of schwertmannite in Mondulkiri mine. In addition, at the mine site where Fe^{3+} species dominate, for example, Shojin mine, Fe^{2+} (≈ 1/6 of Fe^{3+}) oxidation rate can be neglected. Fe^{3+} at Shojin mine quickly precipitated as schwertmannite while pH increased to 3.2 with the precipitation rate of $R_{sch} = 3.82 \times 10^{-6}$ mol. L^{-1} s^{-1}.

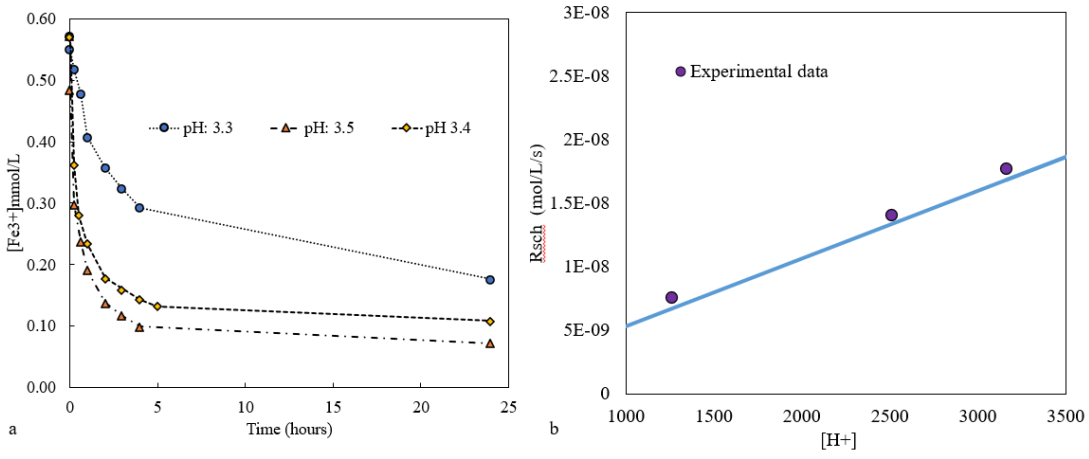

Fig. V-2. (a) The experimental data of ferric iron precipitation in relation to time for various pH. (b) The fitting model of precipitation rate (points) to the model precipitation rate (solid line) concerning to proton $[H^+]$.

5.3.4. Adsorption of trace element on schwertmannite

The toxic elements in both study areas are As, Se, Cu, Cd, Pb, and Ni. However, the Se adsorption mechanism is not discussed in detail as the surface complexation model. Se adsorption behavior on schwertmannite is unpredictable (Khamphila et al., 2017). A different Se removal method will be mentioned in Chapter VI. Cu will not be discussed in the surface complexation either as its concentration is less than WHO guidelines after releasing to the environment. Hence, this system's surface complexation discusses As, Cd, Pb, and Ni adsorption onto schwertmannite.

As adsorption

The effect of pH on surface complexation models has previously included the generalized double-layer (GDL), triple-layer (TLM), charge distribution (CD), and extended triple-layer (ETLM) models with individual-specific criteria based on the behaviors of elements on adsorbent surface structures. Arsenic binds strongly to ≡FeOH on the surface; therefore, the GDL model for As (Dzombak and Morel, 1990) is more appropriate than the other surface complexation models (Otero Fariña et al., 2015). Arsenic adsorption schwertmannite's predictive model and model validation are shown in Fig.V-5a. From pH 3-9, up to 99% of As absorbed onto schwertmannite (Fig. V-5a). The experimental data by titration method can validate As absorption behaviors similar to the batch adsorption experiment conducted by Khamphila et al. (2017).

Ni adsorption and co-precipitation

Ni removal mechanisms for the aqueous solution are coprecipitation and adsorption (Buerge-Weirich et al., 2002; Sarmiento et al., 2018). The coordination number of Ni is similar to Fe^{3+}, which enables Ni to co-precipitate with iron as nickel ferrite and Ni-layer double hydroxide with Fe^{3+} (Kuai et al., 2019). In the selective extraction data, a tiny amount of Ni existed in schwertmannite as the tributary was acidic, yet the removal mechanisms were not identified. Ni can be incorporated with iron hydroxide by adsorbing onto the external surface as monodentate or bidentate complexes (Barrow et al., 2012; Shi et al., 2021). The surface complexation model was conducted to understand the adsorption mechanism of Ni onto schwertmannite (Fig. V-5b). It shows the adsorption Ni behaviors on schwertmannite using GDL predictive model fitted with the experimental data. The predictive model is not well-fitted with the experimental data at the acidic (pH:3-4.5) condition. This miss-fitting is probably

due to the effect of coprecipitation with schwertmannite from pH 3-3.5. At pH 6, the Ni adsorption edge starts to fit with the adsorption model, which indicates the adsorption mechanisms occur. Ni adsorption capacity is about 99% to schwertmannite when pH increases to ~7.5, similar to the Ni adsorption found in Boujelben et al. (2009). This result suggests that the coprecipitation involves a titration experiment to remove Ni, but it does not have the crucial mechanisms in acidic conditions. Ni does not absorb onto iron hydroxide surface at pH below 5 (Buerge-Weirich et al., 2002). Hence, the model can predict Ni adsorption behaviors at pH > 6.

Cd adsorption

Fig.V-3c shows the adsorption Cd behaviors on schwertmannite using GDL predictive model fitting with experimental data. Cd adsorption fraction increases when pH is rising. In acidic conditions, Cd does not show any significant adsorption onto schwertmannite. The adsorption edge occurs at pH 5.5-8.5 (Fig V-3c), where the Cd adsorption behaviors drastically change 0 to also most 99% at 8.5, a similar trend found in Du et al. (2018). The charge distribution (CD) model is suggested for Cd adsorption prediction (Liang et al., 2018). Still, the experimental data here shows that the GDL model can also provide accurate Cd adoption behaviors onto schwertmannite.

Pb adsorption

Fig.V-3d demonstrates Pb adsorption behaviors on schwertmannite using GDL predictive model fitting with experimental data. Pb has a higher capacity to adsorb onto schwertmannite than Cd and Ni. The adsorption edge of Pb onto schwertmannite starts at pH 3.2 to 5 from 0 to 99%, as reported in Barrow et al. (2012). The absorption of Pb slightly occurs in acidic conditions, even though Pb and schwertmannite surface charge is positive. The experimental data is well fitted with the predictive model. Thus, this model can represent the Pb behaviors in the drainage water.

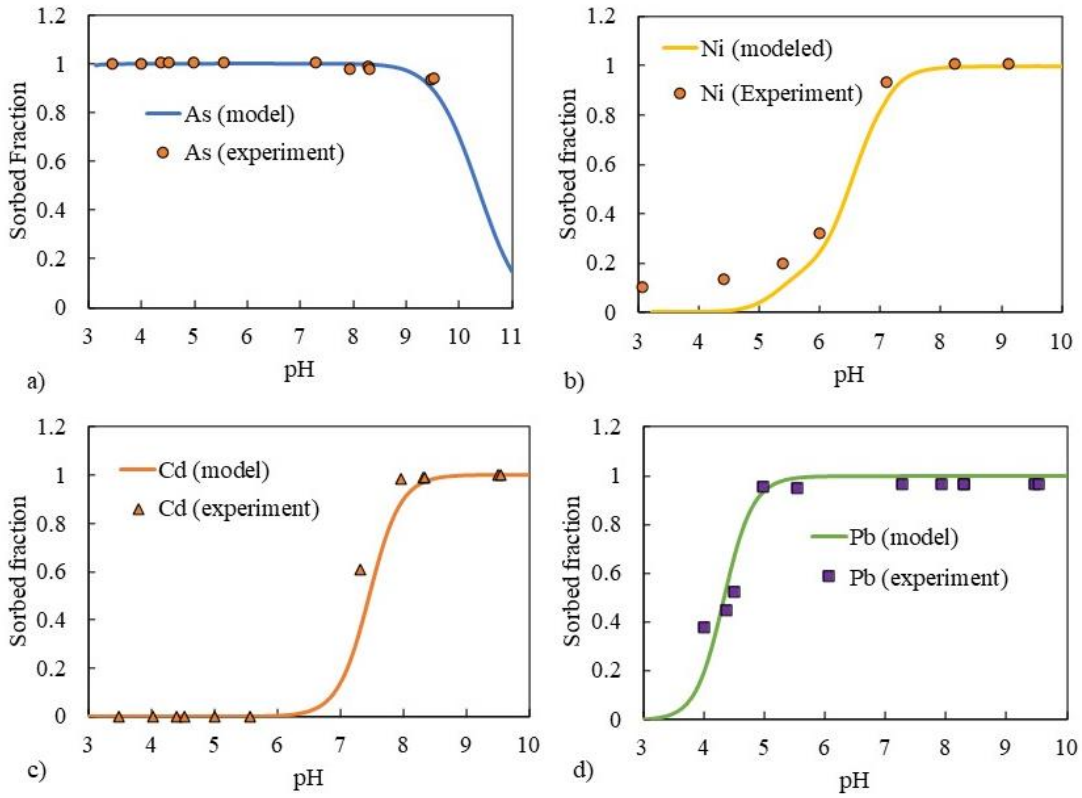

Fig. V-3. The predictive adsorption model of As, Ni, Cd, and Pb on g L^{-1} of schwertmannite. a) The predictive adsorption model fitting with As experimental data. b) The adsorption predictive model fitting with Ni experimental data. c) The predictive adsorption model fitting with Cd experimental data. d) The predictive adsorption model fitting with Pb experimental data.

5.3.5. pH optimization for removal of trace elements

Arsenic and Ni removal by adsorption mechanism at Mondulkiri mine

The predictive model of As adsorption was used to apply to the actual tributary water data. The As concentration measured from sampling point T5 was used as model input to determine the pH that maintains As concentration below the WHO drinking water guidelines. The model shows that at pH less than 7.6, As can be successfully removed by schwertmannite (Fig. V-4a). Similarly, the predictive model of Ni adsorption was applied to Ni concentration of T5 in the dry season. The adsorption of Ni onto schwertmannite to less than WHO regulation limit when pH increases to greater 6.4 (Fig. V4b). To remove As and Ni from the drainage using adsorption mechanism, increasing pH 6.4 to 7.6 can remove As and Ni from the Mondulkiri mine.

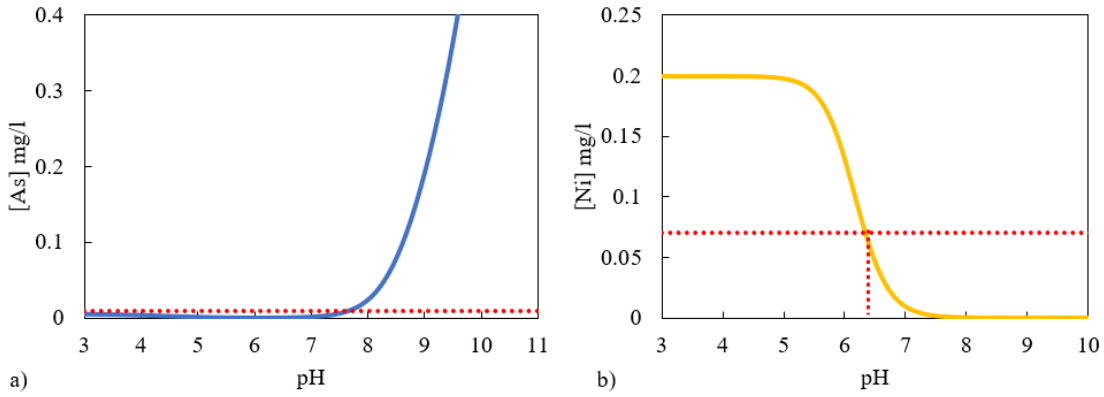

Fig. V-4. a) The predictive As the concentration of Mondulkiri mine concerning pH. b) The predictive Ni concentration of Mondulkiri mine concerning pH. The red line is the WHO regulation limit for drinking water.

Arsenic, Cd, and Pb removal in Shojin mine

In Shojin mine site, Shojin river was successfully treated by natural attenuation. Thus, only Amemasu river is discussed in the adsorption mechanism by schwertmannite. The predictive model of As, Pb, and Cd adsorption predictive models were used to apply to the measurement data AW3 concentration of Amemasu river (Fig. V-5). As is a metalloid in acidic conditions, thus the As can be removed from the drainage water at pH < 9.1 to meet the WHO regulation limit, while Cd and Pb require pH > 7.9 and pH > 4.6, respectively.

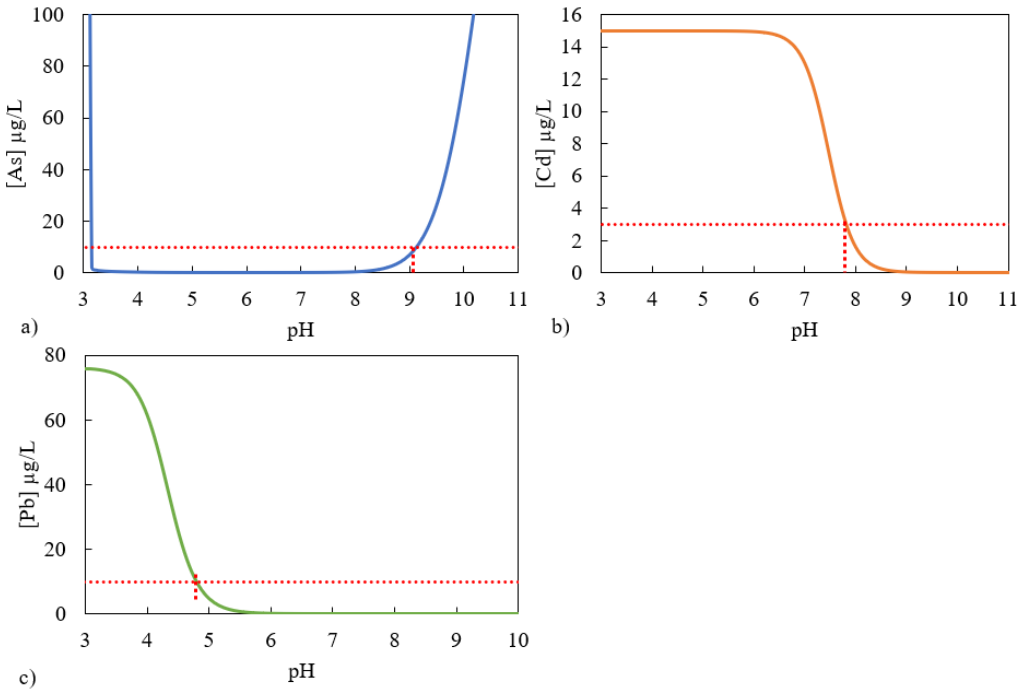

Fig. V-5. a) The predictive As concentration of Amemasu river in relation to pH. b) The predictive Cd concentration of Amemasu river in relation to pH. c) The predictive Pb concentration of Amemasu river in relation to pH. The red line is WHO regulation limit for drinking water.

5.4. Summary

Iron dynamics occurred in the case studies concerning the different sources of iron species. The main characteristic difference in these study areas is; Mondulkiri mine is dominant by Fe^{2+}, while Shojin mine is dominant by Fe^{3+}. The different sources of iron species significantly affect on AMD treatment method. This chapter highlighted the iron dynamic included, oxidation rate Fe^{2+} to Fe^{3+}, Fe^{3+} precipitation rate, and the interaction of toxic elements with schwertmannite as below:

- In the Fe^{2+} dominant system, iron-oxidizing bacteria catalyze the Fe^{2+} oxidation rate. The Fe^{2+} field oxidation can estimate the oxidation rate and rate constant in the field data measurement. The oxidation rate constant can be used to reconstruct the Fe^{2+} oxidation rate model to estimate the duration and amount of Fe^{2+} oxidize to Fe^{3+} in Mondulkiri mine site.
- In the Fe^{3+} dominant system, the Fe^{3+} precipitation rate can be estimated without concerning the Fe^{2+} oxidation rate. Fe^{3+} precipitation rate and rate constant from both study areas using the same methods. The rate constant was used to reconstruct the precipitation rate model to estimate the Fe^{3+} rate in various pH conditions.
- Yet, it is worth mentioning Fe^{3+} is a rate-limiting factor of Fe^{2+} oxidation rate and Fe^{3+} precipitation rate. Thus, the passive treatment implementation depends on Fe^{3+} precipitation rate and schwertmannite formation.
- Surface complexation models of toxic elements (As, Ni, Cd, and Pb) onto schwertmannite show that only As can be removed by schwertmannite in acidic conditions. In contrast, Cd, Pb, and Ni require neutral to alkaline conditions to adsorb onto schwertmannite. The adsorption capacity onto schwertmannite is As>> Pb>Ni>Cd. The surface complexation model using the GDL model is suitable to predict the optimum pH for heavy metals removal. The optimum pH for Mondulkiri mine for As and Ni removal is 7.6, while in Amemasu river is 7.9 to remove As, Cd, and Pb.

VI. Geochemical modeling of the mixing and the neutralization processes of acid mine drainage at Mondulkiri mine site

6.1. Introduction

Natural attenuation at the Mondulkiri mine in the rainy season successfully remediates the tributary water to meet the environmental regulation. On the other hand, the tributary in the dry season is still concerned about the aquatic lives and human health in the surrounding area. Thus, it requires human assistants to maintain the tributary condition as it is the rainy season by using the advantage of natural process. The natural attenuation mechanisms revealed that the mixing of neutral water allowed schwertmannite precipitation, enhancing As removal while dilution reduces Se, Cu, and Ni concentration. The tributary pH is controlled by rainwater water in the rainy season. Commonly, the pH control or neutralization process is implemented in AMD treatment by using a chemical reagent such as; calcium hydroxide, limestone, and other alkaline materials to control the pH of AMD (Huang and Yang, 2021).

In contrast, the pH of the tributary of Mondulkiri mine controls by mixing of neutral water. The lessons learned from the natural attenuation at Mondulkiri point out that an application of neutral water dilution can apply to passive treatment for the dry season. This chapter will describe the possibility of passive treatment implementation by geochemical modeling to elucidate geochemical characteristics in the contaminated area while diluting by rainwater at Mondulkiri mine site, Cambodia. This chapter aims (1) to simulate the natural attenuation mechanisms that occur in the drainage in the rainy season, (2) to evaluate the pH control of the study by mixing AMD with neutral water and adding alkaline material to AMD, (3) to determine the suitable passive treatment methods for the study area.

6.2. Material and Methods

Geochemical modeling has been well developed and popular for geochemists during the last few decades. It is a valuable tool to predict the contamination of the behaviors in the aqueous environment (Camden-Smith et al., 2015). Computer codes such as PHREEQC, ChemEQL, HYDROGEOCHEM, Visual MINTEQ, and Geochemist's Workbench, for example, perform only mathematical framework and

computational tasks without reference to particular to chemical systems. These computer codes give identical answers, yet the differences are convergence and handling capacity. In addition, thermodynamics databases accompany the computer codes are not hard-wired, enabling users to edit the reaction in the database without affecting codes functions (Zhu et al., 2002). Recently, geochemical modeling has been used to investigate the mechanism of water-rock interactions in aquatics systems (Kirk Nordstrom, 2020). The geochemical models are able to address the quantitative data minerals precipitation/dissolution, sorption, gas exchange, ionic strength effects, thermal effects, and transport (Bethke, 2008; Murakami et al., 2020). The improvement of the modern computer plays an essential role in facilitating geochemists' research works.

6.2.1. Mixing model

A React module of Geochemist's workbench (ver. 15.0) professional packages simulated neutral water and drainage water mixing in the field. The input parameters were obtained from the chemical data analysis from Chapter 3. The default thermodynamics database of GWB is used in this modeling. Two React data sets were set up to represent fluid 1 (T2 in the dry season) and fluid 2 (I1 in the rainy season) (Table VI-1). The two data sets were mixed using the "pick-up" function. The Cl^- concentration was used as a tracer in model validation because it was not affected by minerals precipitated in the tributary. The sensitivities of mixing model was acquired by utilizing various mixing solutions; M1, M2, and M3 (listed in Table VI-1). Alkaline materials such as limestone (M1), wooden ash (M2), and portlandite (M3) were added to increase the HCO_3 concentration in the neutral water. The water parameters of fluid 1 remain the same; only fluid 2 parameters, HCO_3, Ca, and pH was, changed in the simulations.

6.2.2. Acid neutralization model

Another neutralization model was obtained by React module (GWB) using a direct chemical reaction of drainage water. Limestone is chosen as an alkaline material for the neutralization processes. Calcite was added, the pH is increasing (reaction VI-1) due to the limestone dissolution reaction and produces more CO_2, which might be degassed via reaction (VI-2) (Berger et al., 2000).

$$CaCO_3 + 2H^+ \rightarrow Ca^{2+} + H_2O + CO_2\ (aq) \qquad (VI\text{-}1)$$

$$CaCO_3 + H^+ \rightarrow Ca^{2+} + HCO_3^- \qquad (VI\text{-}2)$$

Table VI-1. The input data of mixing model by React module. (CB: Charge balance)

Basic species	Fluid 1 (T2)	Fluid 2 (I1)	M1	M2	M3	Units
Ca	616	132	350	400	10000	mg/L
Na	1550	20.7	23	20.7	10	mg/L
K	18.1	1.86	2	1.86	1.8	mg/L
HCO3	-	6	600	750	5	mg/L
Mg	151	41.7	7.7	8.7	11.6	
Cl	34	6.64	6.64	6.64	6.64	mg/L
SO_4	CB	CB	CB	CB	CB	-
pH	2.79	6.67	7.7	8.7	11	-
Fe	147	10^{-6}	10^{-6}	10^{-6}	10^{-6}	mg/L
Mn	35	10^{-6}	10^{-6}	10^{-6}	10^{-6}	mg/L
Ni	0.1	10^{-6}	10^{-6}	10^{-6}	10^{-6}	mg/L
Cu	0.6	10^{-6}	10^{-6}	10^{-6}	10^{-6}	mg/L
As	6.1	10^{-6}	10^{-6}	10^{-6}	10^{-6}	mg/L
Se	0.4	10^{-6}	10^{-6}	10^{-6}	10^{-6}	mg/L
e-	650	300	300	300	300	mV

6.3. Results and Discussion

6.3.1. Mixing of neutral water into the drainage water

Dilution has direct and indirect impacts on natural attenuation during the rainy season. A mixing model was developed to describe the immediate effect of mixing neutral and tributary water during the rainy season. The Cl^- concentration at I1 was 6.5 mg/L or approximately 20% of the dry-season concentration at T2 (~34 mg/L). This dilution ratio provided a pH of 3.44.

The mixing model results for tributary water at T2 and neutral water from I1 from the React module fitted with field data are shown in Fig. VI-1a. The correlation between

Cl's modeled and measured data and the mixing ratio values was strong ($R^2 = 0.99$) (Fig. VI-1a). The pH in the tributary slowly increased with an increase in I1 volume (Fig. VI-1.b), indicating a low buffering capacity for mixing during the rainy season. The HCO_3^- concentration in I1 was too low to buffer the pH of the tributary. Though, the neutral water (I1) in this study increased the pH in the tributary to greater than 3.1, which facilitated schwertmannite precipitation. The ratio from the model of tributary water (T1) to neutral water (I1) is 0.16(T1)/0.84(I1), indicating that 1 L of tributary water needs 5.25 L of neutral water to get pH 3.44 to meet the condition as it was in the rainy season (T2). A large volume of neutral water, more than five times that of the tributary water, was added during the rainy season to increase the pH and reduce the concentrations of As, Ni, Se, and Cu during the rainy season. Fig VI-2 shows the effect of dilution on the toxic elements. The As concentration in the tributary is too high to dilute to less than the WHO regulation limit; however, it effectively dilutes the Ni, Se, and Cu if the dilution ratio is more significant than 0.35(T1)/0.75 (I1). The neutral water could not dilute As to less than the WHO limit, yet the increase in pH to 3.44 let schwertmannite precipitate; thus, it scavenged As.

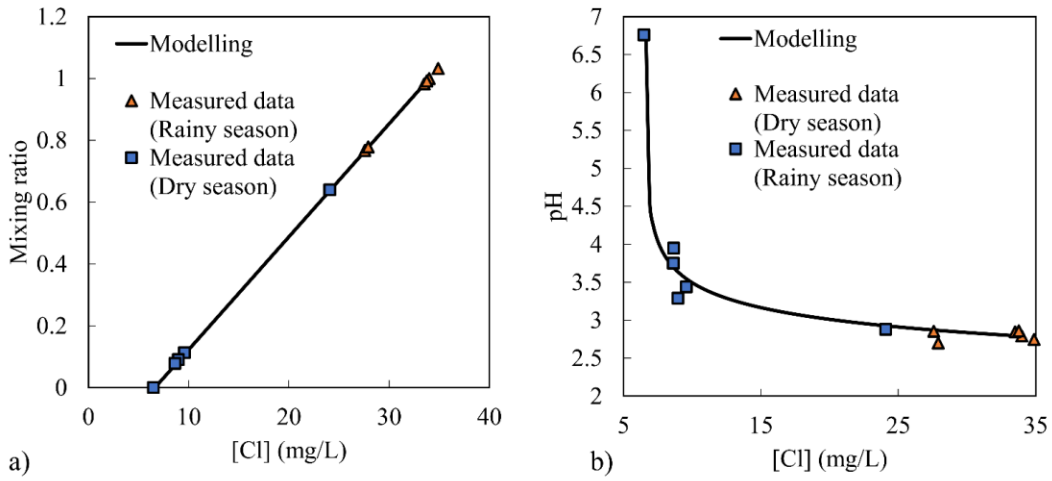

Fig. VI-1. a) The mixing of drainage and neutral water, mixing ratio against plotting Cl– concentration obtained from React module, and the measurement data in the rainy season and dry season (b) pH against Cl– concentration obtained from React module and the measurement data in the rainy season and dry season.

A mixing model with different buffering capacity solutions is conducted to evaluate the neutral effect on drainage water. The impact of buffering capacity of various fluids while adding alkaline materials to neural water (Fig.VI-3). M1 is the fluid added by crushed limestone, and M2 is the fluid added to wooded ash powder. Those two fluids

have similar alkalinity as HCO_3. As a result, M1 and M2 provided almost similar mixing ratios at pH below 3.5, but M2 could raise the mixing ratio slightly higher than M1 after pH increases. M3 is the neutral water, was added by portlandite powder. The M3 pH was elevated to 11.6. Thus, it can potentially improve the mixing ratio of the drainage water quickly.

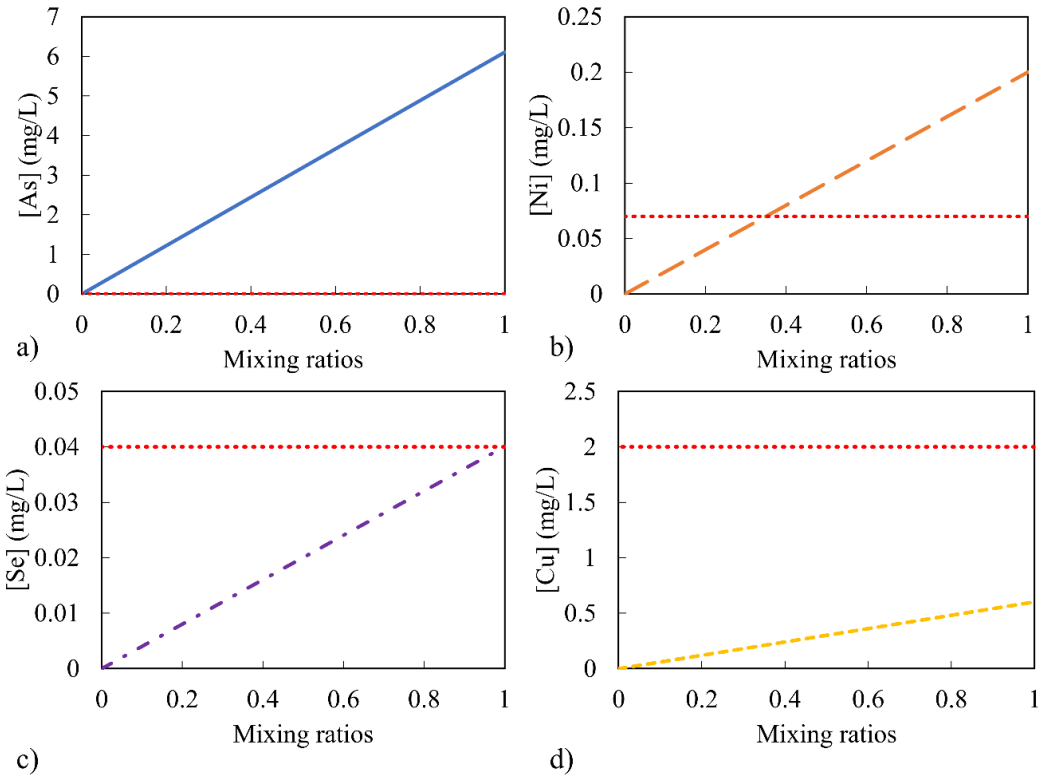

Fig. VI-2. The mixing model shows the predictive concentration of toxic elements concerning the mixing ratio by the mixing model. The red dot line is the WHO environmental regulation limit. (a) As concentration, (b) Ni concentration, (c) Se concentration, and (d) Cu concentration.

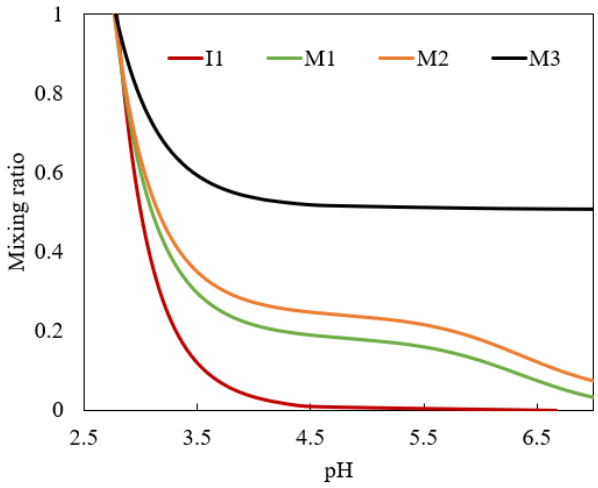

Fig. VI-3. The mixing of drainage and neutral water and various fluids (M1, M2, and M3), the mixing ratio is plotted against pH.

6.3.2. Acid neutralization

The React model simulated the drainage water of the tributary (T1) in the rainy season with initial pH 2.88, 256 mg/L Fe, 32 mg/L Al, 0.11 mg/L Ni, 15 mg/L As, and 4.7 g/L SO_4. Fe^{2+} is dominant from the drainage discharge, although because of the quick oxidation in the tributary, this simulation assumes that total Fe is Fe^{3+}. Calcite was used in the model to represent limestone (VI-2). The reaction was constrained to natural atmospheric conditions. The buffering plateaus occurred at three different pH 2.7-3.4, 4.4, and 6.8. The buffering at 3.4 requires 0.4 g/L as $CaCO_3$, while at pH 4.4 and 6.8 needs 0.6 g/L as $CaCO_3$ and 1g/L as $CaCO_3$, respectively. The buffering at pH below 4.4 is probably due to the hydrolysis and strong acid (H_2SO_4) (Kirk Nordstrom, 2020). It enables minerals formation such as jarosite (H), schwertmannite, and scorodite (Fig. VI-4b). The acidity of T2 (dry season) is about 0.6 g/L as $CaCO_3$, while the total acidity of the drainage water is 0.7 g/L as $CaCO_3$ (88%). The buffering pH 4.4 exhibits ferrihydrite, aluminum hydroxides, diaspore, and nickel ferrite ($NiFe_2O_4$). Once the buffering is finished, the pH reaches equilibrium at 6.8.

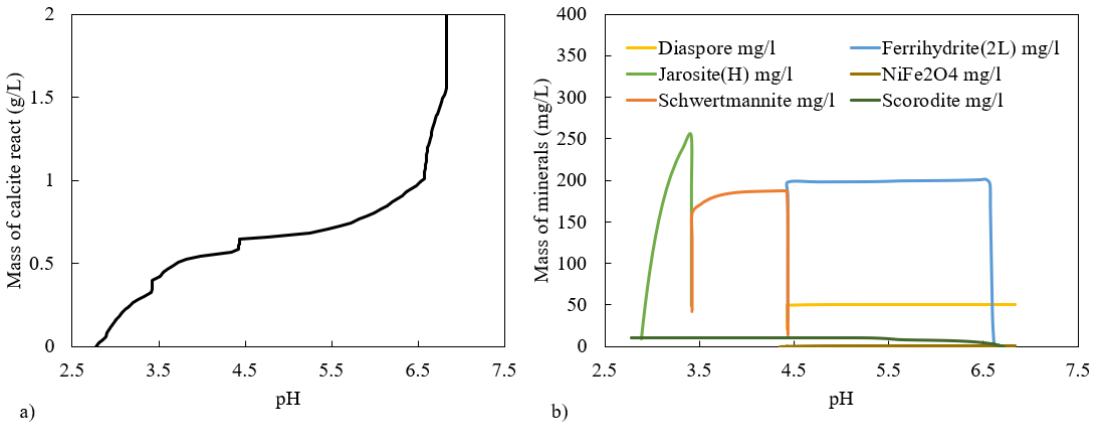

Fig. VI-4. (a) The titration simulation of tributary (T1) with 20 mmol of Calcite by using React module of GWB. (b). The minerals formed during the titration of drainage water.

6.3.3. Implication for passive treatment

Water quality in the dry season requires human intervention to treat As, Ni, and Se concentrations. Cu contaminant from the source was 3.59 mg/L; however, it can be neglected (Cu:0.63 mg/L) for the treatment in the tributary because it is below the WHO drinking water guideline. To remove As from the tributary during the dry season, the formation of schwertmannite was required. The presence of iron-oxidizing bacteria in

tributaries, a biological process, quickly catalyzes ferrous oxidation; thus, only the pH is a crucial factor controlling the formation of schwertmannite and the adsorption of As Ni (geochemical process). The optimum pH suggested in section 3.4.3 enables schwertmannite to precipitate and suitable for As removal (Section 5.3.4). The adsorption model suggested that Ni can be removed from the tributary if pH is increased to 6.6 (section 5.3.5). The removal of Se by schwertmannite is quite complex as Se species in this study is probably Se^{6+}. The Se^{6+} incorporation with schwertmannite is unpredictable; thus other methods should be considered, such as dilution, coprecipitation, or selenate reduction to elemental selenium (Stefaniak et al., 2018; Tokunaga and Takahashi, 2017)

The field investigation and modeling is shown in this research is essential to increase the pH to the suggested target. Open lime channels (OLC) are traditional passive treatment methods (Skousen and Ziemkiewicz, 2005) and are commonly used to treat AMD using limestone to increase the pH of AMD. This method is easily clogged and coated by precipitated minerals when AMD contains high Fe and Al concentrations (Ziemkiewicz et al., 1997). OLC can be applied as a passive treatment method in the study area; however, it is necessary to maintain a pH of less than 3.5 to slow down the clogging of limestone. Within the pH range, only As was removed from the tributary. However, to reduce the concentration of Ni and Se, dilution from neutral water, a physical process must be considered. Natural attenuation mechanisms indicate that the mixing of tributary and neutral water is essential in raising the pH of the tributary and in lowering the concentrations of Ni, Se, and Cu during the rainy season. In this study, simple mixing of neutral water and AMD in section 6.3.2 required diluting the tributary water 1 L over 1.86 L over neutral water to get pH 3.1. This ratio was also suitable to dilute Ni and Se (Supplementary data S10) to less than 0.07 mg/l and 0.04 mg/l, respectively (WHO drinking water guidelines). To maintain neutral water to meet the required dilution seems limited, the combination of increasing pH by alkaline materials and dilution (section 6.3.1) should be applied to a passive treatment method. Limestone leach beds (LLBs) are a geochemical passive-treatment method that includes dilution using limestone to increase the buffering capacity of freshwater or metal-free water before mixing with AMD (Skousen et al., 2017). It is possible to avoid the clogging of limestone. Though, the heavy metal concentrations in I1 remained too high to apply the LLB method. A neutral water source is necessary for implementing this method.

Therefore, an artificial pond or pumping groundwater to feed upstream of the tributary should be considered. Applying LLB in neutral water is also challenging because the dissolution rate of limestone is relatively low. Like alternative treatment methods, anoxic limestone drains (ALDs), a semi-close system of buried limestone (Skousen et al., 2019), can improve the limestone dissolution rate when CO_2 partial pressure increases. The neutral feeding water should flow through buried limestone (ALD) to improve the buffering capacity before mixing with the tributary. ALD has been reported as a low-cost passive treatment method with a long-term life span of approximately 18 years without maintenance (Skousen et al., 2019). Thus, ALD and dilution methods might be the most sustainable treatment methods for artisanal mining, similar to this study area.

6.4. Summary

This chapter highlighted the crucial tools of geochemical models that facilitate passive treatment's implication. The mixing model reflects the vital role of mixing neutral water for passive treatment. When dilution is insufficient to buffer the precipitation of the mineral, additives of alkaline materials can be implemented. The mixing model with a high alkalinity concentration could buffer the pH in systems that enable schwertmannite precipitation in the rainy season. These methods can optimize the mineral reaction and precipitation better than the calcite reaction model. Calcite quickly reacts with drainage water with high dissolved iron resulting from mixed minerals precipitation, including gypsum. Those minerals will coat the limestones and reduce limestone's dissolution and reaction capacity.

The mixing model of neutral water and AMD in the tributary shows that the mixing of neutral water can be used as a treatment method. The neutral water is able to increase the pH in the tributary that is suitable for schwertmannite to form and dilute other elements (Ni, Se). In addition, the chemical reaction of the model indicates that adding alkaline material such as limestone is applicable for passive treatment. For example, the passive treatment, OLC, can be implemented, even though the life span of limestone is short. The mixing of neutral water and using limestone in AMD treatment is applicable in the Mondulkiri mine site, yet mixing neutral water is more convenient and cost-effective than using limestone.

VII. Geochemical modelling of the process during Mixing and Neutralization of Acid Mine Drainage at Shojin Mine Site

7.1. Introduction

Chapter 4 reveals that the natural attenuation at Shojin river by mixing neutral water allowed the toxic elements to decrease to less than the WHO regulation limit without human assistance. The advantage of background water of Shojin river mixed with wastewater maintains the pH in the contaminated river above 3. Schwertmannite plays a significant role in As removal from the river, while Cd and Pd are decreased by dilution. However, Amemasu river remains contaminated; hence, water treatment is necessary. There is no significant geological setting difference between upstream of Amemasu river to the downstream after mixing with wastewater. The wastewater added from AW1 and AW2 did not contaminate to Amemasu river but slightly influenced the pH of the river. The toxic elements in the Amemasu river from AR4 resulted in the wastewater from AW3. The concentration of As, Cd, and Pb slightly decreased from AW3 to AR4 by dilution only. The background river's low buffering capacity cannot buffer the pH of the river after mixing with wastewater. The dissolve toxic metals remain high. Dilution indirectly affects the natural attenuation mechanisms as it raises the pH of the river then accelerates schwertmannite precipitation. If the mixing process of Amemasu river is well understood, thus, assisted natural attenuation or passive treatment would apply to Amemasu river. The geochemical modeling mentioned in Chapter 6 clearly shows its advantages in geochemical characterization and investigating the contaminated river. Therefore, this chapter will describe the application of geochemical processes responsible for the field investigation data, such as toxic elements and pH trends in Amemasu river. The objectives in this chapter are (1) to evaluate the pH control of the study by mixing AMD with neutral water and using additive alkaline material to AMD, (2) to devise suitable passive treatment methods for the study area for sustainable treatment methods.

7.2. Material and Methods

7.2.1. Mixing experiment

The drainage water and river water mixing experiments were conducted to simulate the process occurring in the study area. The filtered samples with 0.20 µm ultra-membrane filters of AW3 and AR3 without acidified used to mix with ratio range from 10% to 90% (Balistrieri et al., 2007) in the 50 ml polyethylene. The total volume of the mixing solution is 40 ml. The mixing solutions were equilibrated for 24 hours. pH was measured after 24 hours, and aqueous solutions were filtered with 0.20 µm membrane filters preserved for further chemical elements analysis by ICP-AES, ICP-MS, and IC analyzers.

7.2.2. Mixing model

Geochemical modeling in the study area was obtained using Geochemist's Workbench professional package with the same database mentioned in Chapter 6. The wastewater of AW3 and AR3 from the analytical measurement in Chapter 4 were used to represent the simulation of the study area. The model procedures were set up as described in Chapter 6. The input parameters are listed in Table VII-1. The model is validated with the experimental data.

Table VII-1. The input data of mixing model by React module. (CB: Charge balance)

Basic species	Fluid 1 (AW3)	Fluid 2 (AR3)	Units
Ca	15.1	5.61	mg/L
Na	1000	120.0	mg/L
Cl	CB	CB	mg/L
HCO_3	-	6.4	
SO_4	1800	40.6	-
pH	2.79	5.61	-
Fe	27.1	$10e^{-12}$	mg/L
Al	10.9	$10e^{-12}$	mg/L
Pb	67.68	$10e^{-12}$	µg/L
Cd	9.54	$10e^{-12}$	µg/L

As	180	$10e^{-12}$	µg/L
e-	650	600	mV

7.2.3. Acid neutralization by limestone

Limestone is commonly used in acid neutralization for decades in AMD treatment because it is safe to handle and low cost (Skousen et al., 2019). To elucidate the reaction of limestone in with drainage water (AW3), calcite is used for the reaction model for acid neutralization as described in section 6.2.2.

7.3. Results and Discussion

7.3.1. Mixing of neutral water and wastewater in Amemasu rivers

The experiment and the simulation of Amemasu background river mixing with the wastewater seepage is shown in Fig. VII-1a. The mixing experiment is fitted to the predictive model to validate the mixing model. Pb was used as the conservative element as it was not influenced by coprecipitation of adsorption, as described in Chapter 4. The predictive model of Pb fitted very well with the experiment data (Fig. VII-1a). The correlation between the modeled and measured data of Pb given the substantial degree of goodness of $R^2 = 0.99$. The dilution of AR3 to AW3 increased the pH (Fig. VII-1b) and the significant toxic elements behaviors (Fig. VII-2). Fe concentrations fall below the mixing line, indicating that iron precipitation took place after 70% of AW3 mix with AR3 at pH of about 3. Arsenic has a similar trend to Fe. It falls below the mixing line after mixing 70% of AW3 to AR3 due to coprecipitation and adsorption with schwertmannite. Cd and Pd follow the mixing line without showing any coprecipitation or adsorption.

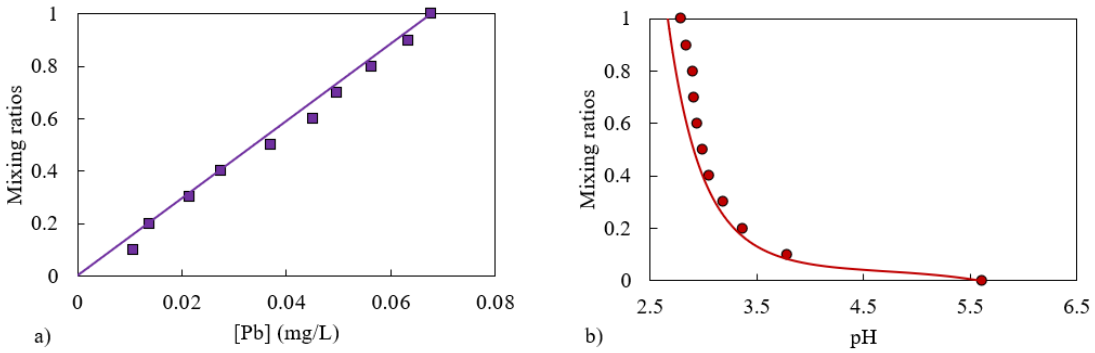

Fig. VII-1. The mixing of drainage water (AW3) and background river water of Amemasu river (AR3), (a) Mixing ratio against Pb concentration obtained React module, and the experimental data. (b) the mixing ratio against plotting pH obtained from React module, and the experimental data.

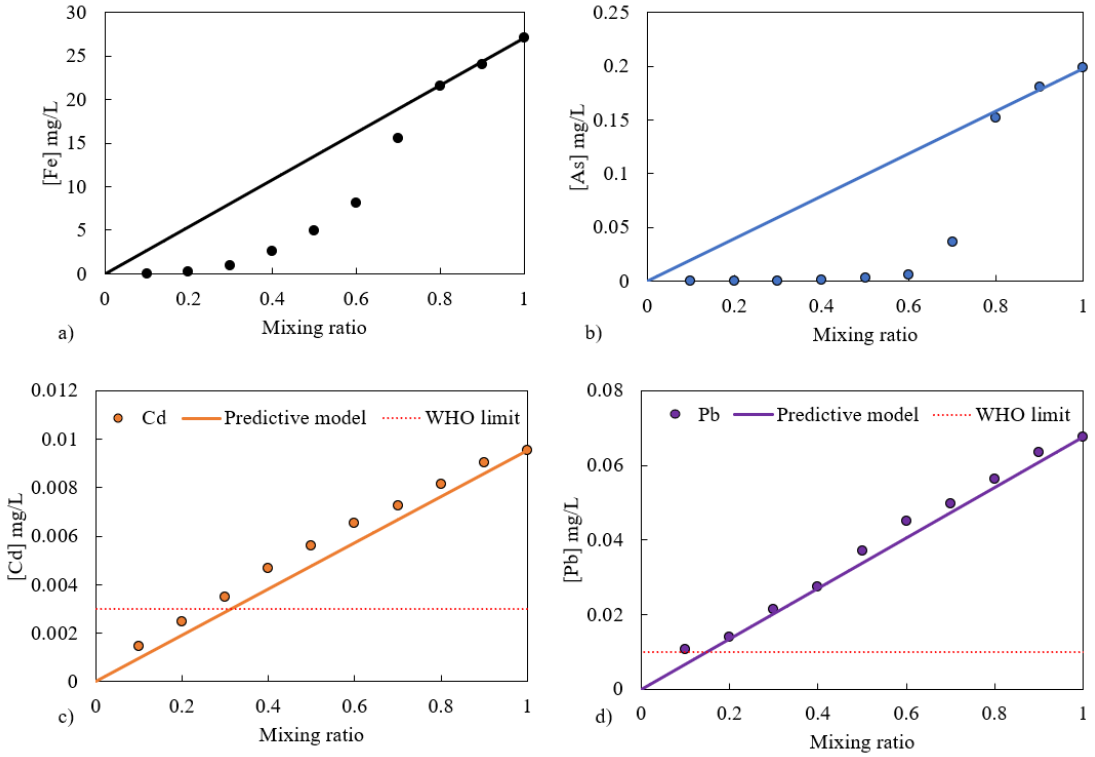

Fig. VII-2. The predictive concentration of toxic elements in relation to mixing ratio by the mixing model, fitting with the experimental data. (a) Fe concentration, (b) As concentration, (c) Cd concentration, and (d) Pb concentration.

7.3.2. Acid neutralization by Limestone

The chemical reaction model simulates the drainage water of Amemasu river with initial pH 2.76, 26 mg/L Fe, 32 mg/L, 0.20 mg/L As, 14 µg/L, 68 4.7 µg/L Pb and 1.5 g/L SO_4 reacted with limestone. Fe^{3+} is dominant from the AW3; this simulation assumes that total Fe is Fe^{3+}. The reaction was constrained to natural atmospheric conditions similar to section 6.3.2. The titration result is shown in Fig. VII-3. The buffering plateaus took place at 2 different pH 2.8-3.3, 3.8 and 7.1. The occurrence

buffering at pH below 3.8 probably caused by the precipitation of scorodite, the hydrolysis and strong acid (H_2SO_4) (Kirk Nordstrom, 2020) which enable minerals formation such as schwertmannite (Fig. VII-3b). To neutralize this acidity required 0.200 g/L as $CaCO_3$, which is responsible for 92% of total the acidity of the drainage water (0.216 g/L as $CaCO_3$). The buffering at pH 3.8 shows the buffering by ferrihydrite and diaspore. The buffering of the heavy metals finished at 7.1.

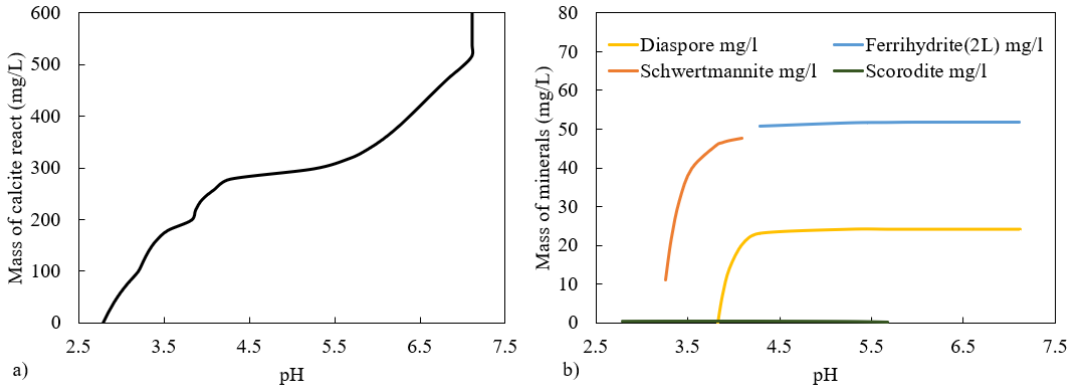

Fig. VII-3. (a) The titration simulation of wastewater (AW3) with 20 mmol of Calcite by using React module of GWB. (b). The minerals formation during the titration.

7.3.3. Implication for passive treatment

The neutral water for Amemasu river dilutes the drainage water (AW3) resulting in an AR4 by mixing ratio of 0.2 (AR3)/0.8 (AW3) given pH 2.9 (Fig. VII-1a). In addition, the mixing model could explain the behavior of trace metals before AR6, where it was not accessible during the field investigation. Fe and As drastically decrease due to the consequences of the dilution from the mid-stream. The field investigation evidence also showed the schwertmannite coated on the stream sediment and boulders in the river until AR9. Schwertmannite successfully adsorbs As to less than WHO guideline before mixing with Shojin river. Yet, the dilution at AR9 is not enough to dilute the Cd and Pb to less than the environmental regulation (Fig. VII-2c&d).

Consequently, more neutral water input to the river is required. The dilution ratios that are necessary to dilute Cd and Pb concentration are 0.7(AR3)/0.3(AW3) and 0.9 (AR3)/0.1 (AW3), respectively (Fig. VII-3c&d). The required dilution ratio is not applicable due to the limitation of neutral water. The diverted river or groundwater pumping is not available in the area.

Passive treatment methods selection flowchart after Skousen et al. (2017), based on Fe^{3+}, Al, Mn, and DO concentrations, even though other factors should be considered. The calcite reaction model reflects that Cd and Pb's coprecipitation did not occur in the system. Therefore, only adsorption mechanisms can be applied to remove Cd and Pb from the drainage water. The surface complexation model suggested that Cd can be removed from the drainage if the pH is 7.9, while Pb only requires pH at 4.6. The Amemasu river drainage water does not need the additive bacteria catalyzer to speed up the oxidation of Fe^{2+} to Fe^{3+}; therefore, the geochemical system of passive treatment is taken into consideration. The chemical reaction of limestone shows the buffering at 3.4 required 0.1 g/L as CaCO3 while at pH 3.8 and 7.1 need 0.2 g/L as $CaCO_3$ and 0.51g/L as $CaCO_3$ respectively. Open limestone channel (OLC) is applicable to the system, but pH elevated by limestone reaction and dissolution could only reach 7.1. Hence, the OLC method will only remove As and Pb, although it seems slightly effective for Cd. Alkaline materials that can raise pH to greater than 8; are magnesite (MgCO3), quicklime (CaO), portlandite ($Ca(OH)_2$), Mg hydroxide ($Mg(OH)_2$), soda ash (Na_2CO_3), or ammonia (NH_3) (Skousen et al., 2019; Taylor et al., 2005). Those materials are much higher cost than limestone.

Moreover, the rapid increase in pH leads to speedy flog or sludge generation, affecting the passive treatment systems (Ziemkiewicz et al., 1997). Another geochemical system that should be considered is the combination of Lime Leach Beds or Steel Slag Leach Beds. This method successfully generated alkalinity of 170-225 mg/L and a pH 8-9.5 at the system's effluent (Skousen et al., 2017). Commonly, other geochemical passive-treatment methods can generate the pH 4.5-6.5 in the system (diversion wells) or other methods targeted for acidic water with low metals concentration (Limestone leach beds). It is not suitable to use passive treatment for Cd removal by using neutral water dilution or increasing pH using limestone. However, dilution by neutral water is probably more appropriate. Thus, the consideration of dilution or using other methods is necessary. Fortunately, Cd concentration of Amemasu river was diluted by Oorito river at the junction with Shojin river and decreased to less than the environmental regulation limit at the monitoring points.

7.4. Summary

This chapter highlighted the roles of dilution and chemical reactions in the Amemasu river by using geochemical modeling for passive treatment. The model indicates that dilution slightly increased the pH at the mid-stream of Amemasu river, where As can be remove from the system by mixing of neutral water. In contrast, mixing of neutral water was insufficient to reduce Cd or Pb concentrations.

The chemical reaction of limestone suggests additive of limestone in Amemasu river can be conducted to remove As and Pb. Yet, it is not suitable for Cd removal from Amemasu river. The passive treatment methods such as OLC, SSLB-LLB, or diverted well are recommend to Amemasu river to treat only As and Pb. Cd removal is remains challenges in the system, but the mixing of neutral water to reduce Cd concentration probably more sustain than using alkaline materials.

VIII. General Conclusion and Implication

8.1. Conclusion

The negative impact of acid mine drainage contaminations has been the primary concern to the aquatic environments during the last few decades. AMD can be generated from active mining, tailing, or abandoned mining sites. Once the dissolution of metals sulfides and acid generation from AMD is exposed to the environment, it is unstoppable. The toxic elements released from AMD generation such As, Ni, Cu, Se, Pb, and Cd highly impact human health and aquatic lives. The historical events are the excellent lesson learned for current water quality challenges, where sustainable AMD treatment methods are necessary. Passive-treatment the sustainable treatment methods are suggested to deal with AMD treatments. Yet, the passive treatments' complications trigger researchers to obtain various case studies as examples for future implications. This research focused on the roles of high dissolved iron concentrations in AMD and the impacts of natural attenuation mechanisms that can be applied to passive treatment. The study areas are in two locations that constrain dissolved iron species concentration and climate conditions.

Using artisanal mine sites and abandoned mine sites as the case studies provides necessary signatures for other mine sites. The concerned problems of AMD generation at Mondulkiri mine site are the tailing discharge and the dissolution of metals sulfides from ore excavated area. Those are the common issues for most of the artisanal mine sites around the world. Shojin mine remains to generate the AMD to the natural environment through the groundwater seepage event if the mine closed for several decades. The lessons learned from these studies are pointed out:

- Seasonal variations in various climate zones, for example, in Cambodia, impact natural attenuation processes in AMD. Rainy and dry seasons are equally six months long in the tropical monsoon climate. Thus, rainwater has a vital role in controlling hydrological factors of the contaminated tributary. In contrast, in the temperate climate, for example, Hokkaido, rainwater in seasonal variations does not significantly impact hydrological characteristics. Still, the snowpack melting might benefit natural attenuation by dilution. In addition, the sources of wild river waters have a crucial role in natural attenuation.

- The physical natural attenuation process of mixing neutral water provides direct and indirect effects to the natural attenuation in both study areas. The neutral water contains low alkalinity concentration and low buffering capacity, but water dilution alone could elevate the drainage water's pH and directly reduce the toxic elements. The increase in pH enables schwertmannite to precipitate in the study areas.
- Natural attenuation mechanisms in both studies were due to the pH control by mixing neutral water where adsorption and coprecipitate of As onto schwertmannite occurred. The toxic element concentrations include Ni, Se, Cu, and Cd dilute by neutral water.

Characterizing the Fe species in the AMD is necessary to determine the iron dynamics, factors controlling attenuation behaviors, and its relationship to the implication of passive treatment. Mondulkiri mine site elaborates the case study of Fe^{2+} dominant while the Shojin mine dominated by Fe^{3+} from drainage sources. The formation of Fe^{3+} minerals in AMD is necessary for scavenging toxic elements thus, understanding the oxidation rate from Fe^{2+} to Fe^{3+} and Fe^{3+} precipitation rate is the crucial steps for AMD treatment likewise:

- Fe^{2+} releases from Mondulkiri mine site are common to most AMD sites worldwide. Yet, the advantage of iron-oxidizing bacteria in the tributary catalyzed the rapid oxidation of Fe^{2+} to Fe^{3+}. The field Fe^{2+} oxidation rate can be estimated using field data measurement. Fe^{2+} oxidation rate constants are not uniform in all the mine sites since it depends on the concentration and the bacteria strains of iron-oxidizing bacteria. Obtaining the field oxidation rate constant can determine the approximated time of Fe^{2+} oxidation. Fe^{2+} oxidation rate can be neglected for the mine site with Fe^{3+} dominant, for example, Shojin mine.
- After oxidation, Fe^{3+} presents in water as dissolved Fe^{3+} unless it meets the suitable environmental conditions to precipitate as ferric minerals. The geochemical model can obtain the schwertmannite formation by using a thermodynamic database after Sánchez-España et al. (2011). The model can bring the optimal pH for schwertmannite formation in natural conditions. The model suggests that pH 3.2 is suitable for schwertmannite precipitation in both study areas.

- The schwertmannite precipitation rate at pH 3 to 3.5 is estimated following the simplify rate law after Asta et al. (2010), assuming Fe^{3+} precipitates as schwertmannite since it is the primary mineral precipitate in the study areas. The precipitation rate constants can be used only to estimate schwertmannite in the other AMD sites within the pH 3 to 3.5.
- Surface complexation model of schwertmannite is used to estimate the adsorption behaviors of toxics elements based on ferrihydrite database. The models successfully describe the adsorption behaviors of As, Cd, and Pb by using the titration method to validate the predictive model. The model is limited to predicting the Ni adsorption because of the effect of the coprecipitation mechanism. However, it is worth noting when pH is greater than 5.

AMD treatment can be accomplished by active or passive treatment, but for the long-term sustainable treatment, passive treatment methods should be implemented for the artisanal and abandoned mines. The natural attenuation mechanisms in this study point out a simple pH control by mixing neutral water from rainwater or background water. This process is applicable for the passive-treatment method, but the availability of neutral water is limited for some study areas, for instance, Amemasu river. In this case, addictive alkaline material is needed for pH control process. The geochemical modeling in this research highlights the as:

- The mixing model of neutral water and drainage corresponds to explain the process occurring in the study areas. The model can estimate the dilution ratios of neutral water to drainage water. The mixing model also elucidates the mechanisms of natural attenuations compared to the field investigation data.
- Limestone is commonly used in acid neutralization as it is an economically safe water treatment material. Thus, a geochemical model of limestone reactions is implemented to estimate the necessary amount of limestone to neutralize the drainage water of the study area.
- Th application of mixing AMD with neutral water commonly neglected in passive treatment design even though it the most straightforward method. There are several challenges of using dilution factors due to the limitation of water supply. For example, the diverted river water flow into the mine site might change the ecological system. In some cases, dilution is effective, especially for

small-scale mines or artisanal mines. Thus, it is necessary to consider the mixing of neutral water as one of the application passive treatment methods

- In the case of dilution of neutral water is not enough, thus the combination of dilution and adding alkaline material should be considered. The geochemical passive treatment method that could be combined with dilution is limestone leach beds (LLBs) or anoxic limestone drain (ALDs).

8.2. Implication

This research conducted on artisanal and abandoned mine studies as the examples for other mine sites for applying the treatment methods. The necessary the research activities can be applied to other study areas for future research constrain to the study area with high dissolve iron. The main activities are divided into field investigations, detail study of iron dynamics, and geochemical models' selection treatment methods.

- Field investigation is implemented for various purposes due to time-consuming, fund, and effort. It is essential to consider the suitable time for water sampling. The differences in the seasonal variation of the tropical monsoon and temperate climate delivered the necessary time for the field investigation. For instance, in AMD treatment, the field investigation should be conducted during the dry season or in summer. On the other hand, field investigation should be conducted in various seasons in the study of natural attenuation.
- The understanding of iron dynamics facilitates passive treatment design. In abiotic conditions, the presence of Fe^{2+} is commonly the main challenge to passive treatment methods. Neurulation process is a common method to increase the pH of AMD to near neutral conditions to enable the Fe^{2+} oxidation. In some cases, engineers add the organic material or iron-oxidizing bacteria to the treatment systems as a catalyzer for Fe^{2+} oxidation. Fortunately, if the iron oxidizing bacteria presents in the mine site, additional iron-oxidizing bacteria are no longer necessary for the system. Fe^{2+} field oxidation rate can be used to distinguish whether there is a presence of iron-oxidizing bacteria without bacteria strain sampling due to the significant difference of Fe^{2+} oxidation rate in abiotic and biotic conditions. The Fe^{3+} precipitation rate constant in this study is suitable for engineers to estimate Fe^{3+} precipitation rate in acidic condition (3-3.5) and imply it the passive treatment system, so they will be able to control

sludge or floc production in the system. The surface complexation (GDL) model of toxic elements (As, Ni, Pb, and Cd) on schwertmannite or iron hydroxide is suitable for determining the optimum pH for treatment implication.

- The implication of the passive treatment in this research is limited to only the study area where dissolved iron is dominant. The benefit of mixing natural water (even low alkalinity) is important to elevate the pH between 3 to 4 for Fe^{3+} minerals to precipitate. The neutral water also directly reduces toxic elements in the system. Thus, engineers should always consider the dilution factor in their design. The chemical reaction model can quantify the required limestone in a closed system, facilitating the passive treatment design.

Passive treatment method selection is complicated due to the site specifics. In contrast, Trumm et al. (2010) develop a quick look at the flowchart to decide on AMD treatment methods between passive and active treatment methods. Following the flowchart, active treatment should be chosen for the tributary at Mondulkiri mine site and Shojin mine. However, the natural attenuation occurred at both study areas indicate that the assisted natural attenuation or passive treatment is probably available. Skousen et al. (2017) passive treatment selection flowchart is used as a guide to applying the passive treatment method. Yet, only Fe^{3+} species are included in his flow chart, where some essential activities are missing. The selection of treatment methods following Trumm et al. (2010) and Skousen et al. (2017) is insufficient for decision-makers to use it for future implications. Therefore, this research modified the passive treatment selection flowchart as shown in Fig. VIII-1 based on the critical understanding of iron dynamics, chemical reaction model, and mixing model. The flowchart from Skousen et al. (2017) is not suitable for Mondulkiri mine and Shojin mine, yet the modification flowchart is ideal for both study areas, as shown in Fig. VIII-2&3. The flowchart modification will universally benefit to another AMD contaminated area for selecting and designing passive treatment methods.

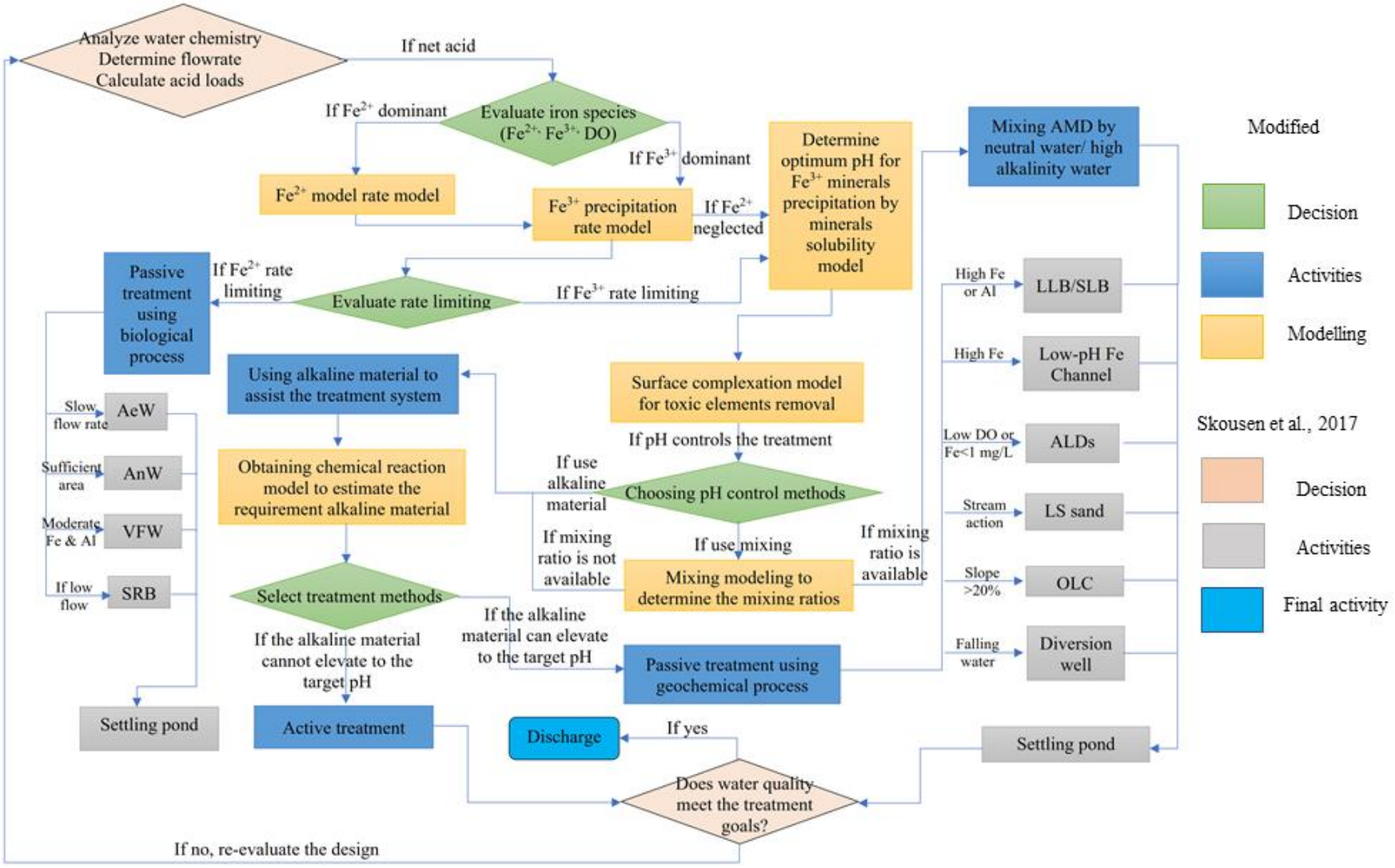

Fig. VIII-1. The flow chart for selecting passive-treatment methods for AMD treatment adapted from Skousen et al. (2017) according to this research.

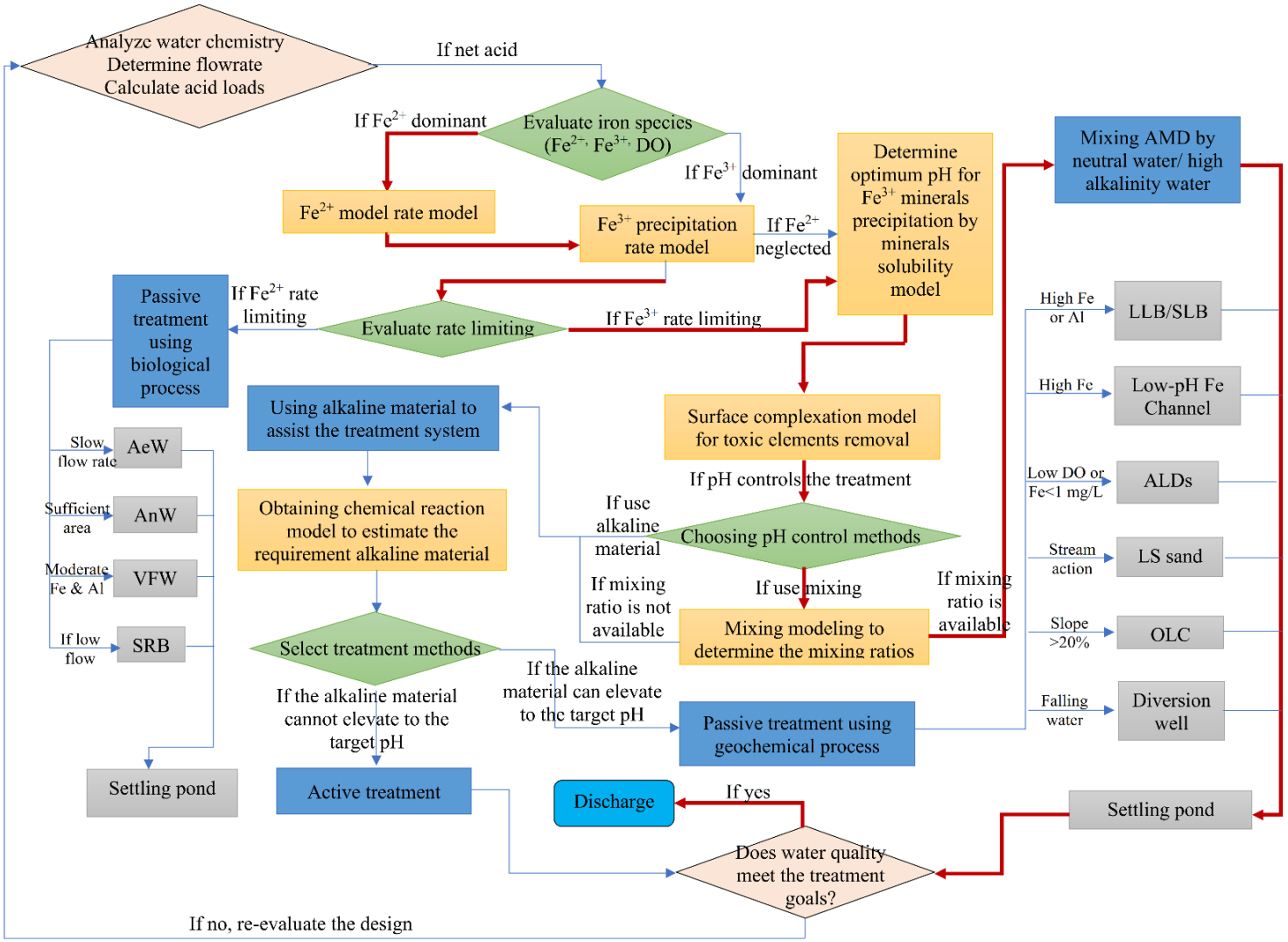

Fig. VIII-2. Selection treatment method for Mondulkiri mine in the dry season site following the modified flowchart. The red arrows represent the flow of selection.

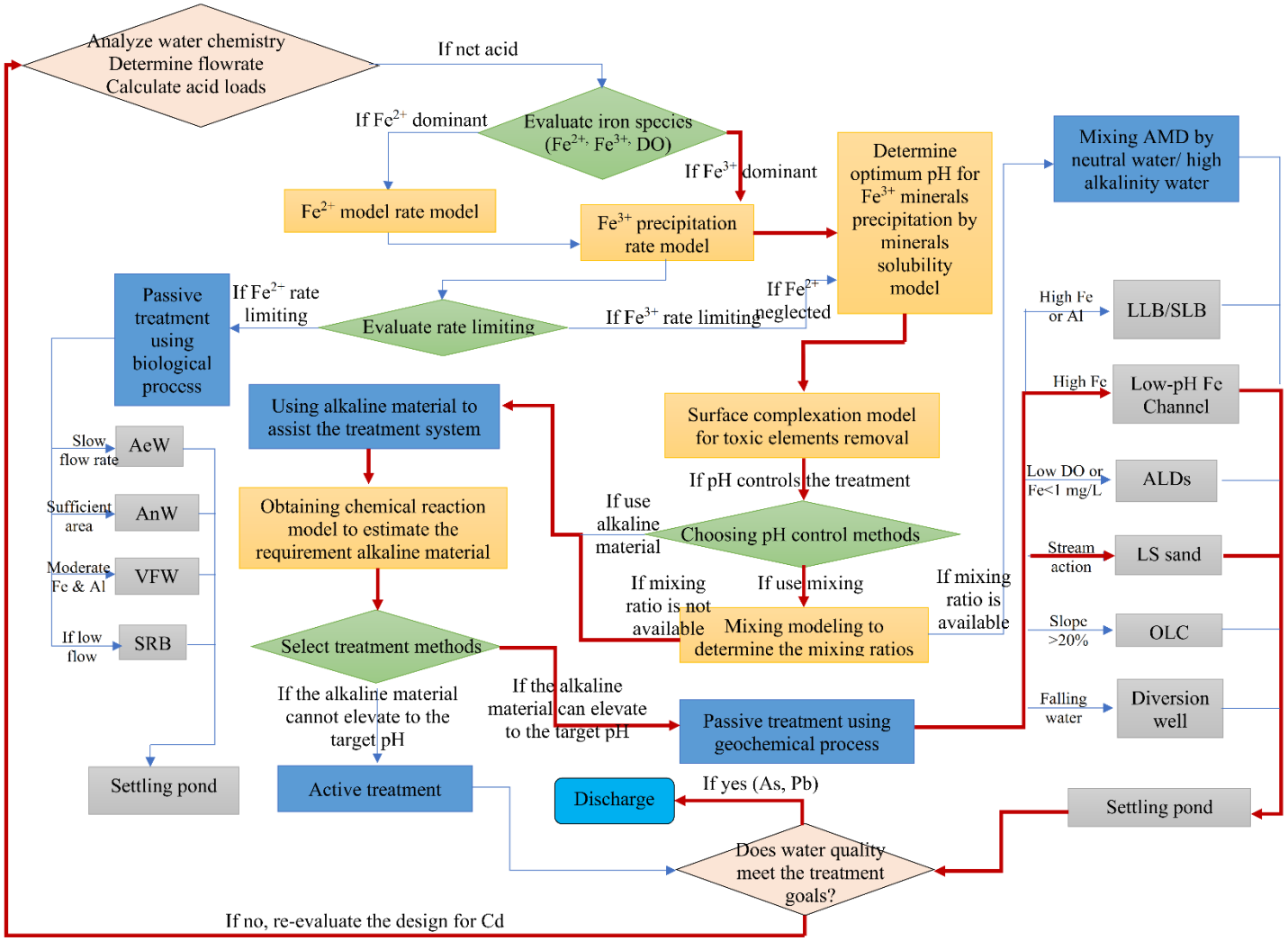

Fig. VIII-3. Selection treatment method for Shojin mine for Amemasu river following the modified flowchart. The red arrows represent the flow of selection.

IX. References

Abreu, M.M., Tavares, M.T., Batista, M.J., 2008. Potential use of Erica andevalensis and Erica australis in phytoremediation of sulphide mine environments: São Domingos, Portugal. Journal of Geochemical Exploration, Trace elements in soils: Baseline levels and imbalance 96, 210–222. https://doi.org/10.1016/j.gexplo.2007.04.007

Acero, P., Ayora, C., Torrentó, C., Nieto, J.-M., 2006. The behavior of trace elements during schwertmannite precipitation and subsequent transformation into goethite and jarosite. Geochimica et Cosmochimica Acta 70, 4130–4139. https://doi.org/10.1016/j.gca.2006.06.1367

Adriano, D.C., Wenzel, W.W., Vangronsveld, J., Bolan, N.S., 2004. Role of assisted natural remediation in environmental cleanup. Geoderma 122, 121–142. https://doi.org/10.1016/j.geoderma.2004.01.003

Appleton, J.D., Williams, T.M., Orbea, H., Carrasco, M., 2000. Fluvial Contamination Associated With Artisanal Gold Mining In The Ponce Enríquez, Portovelo-Zaruma And Nambija Areas, Ecuador 21.

Arnold, D.E., 1991. Diversion wells - a low-cost approach to treatment of acid mine drainage 9.

Auld, R.R., Myre, M., Mykytczuk, N.C.S., Leduc, L.G., Merritt, T.J.S., 2013. Characterization of the microbial acid mine drainage microbial community using culturing and direct sequencing techniques. Journal of Microbiological Methods 93, 108–115. https://doi.org/10.1016/j.mimet.2013.01.023

Baker, B.J., Banfield, J.F., 2003. Microbial communities in acid mine drainage. FEMS Microbiology Ecology 44, 139–152. https://doi.org/10.1016/S0168-6496(03)00028-X

Baleeiro, A., Fiol, S., Otero-Fariña, A., Antelo, J., 2018. Surface chemistry of iron oxides formed by neutralization of acidic mine waters: Removal of trace metals. Applied Geochemistry 89, 129–137. https://doi.org/10.1016/j.apgeochem.2017.12.003

Balistrieri, L.S., Seal, R.R., Piatak, N.M., Paul, B., 2007. Assessing the concentration, speciation, and toxicity of dissolved metals during mixing of acid-mine drainage and ambient river water downstream of the Elizabeth Copper Mine, Vermont, USA. Applied Geochemistry 22, 930–952. https://doi.org/10.1016/j.apgeochem.2007.02.005

Barrow, N.J., Brümmer, G.W., Fischer, L., 2012. Rate of desorption of eight heavy metals from goethite and its implications for understanding the pathways for penetration. European Journal of Soil Science 63, 389–398. https://doi.org/10.1111/j.1365-2389.2012.01450.x

Benjamin, M.M., Leckie, J.O., 1981. Multiple-site adsorption of Cd, Cu, Zn, and Pb on amorphous iron oxyhydroxide. Journal of Colloid and Interface Science 79, 209–221. https://doi.org/10.1016/0021-9797(81)90063-1

Berger, A.C., Bethke, C.M., Krumhansl, J.L., 2000. A process model of natural attenuation in drainage from a historic mining district. Applied Geochemistry 15, 655–666. https://doi.org/10.1016/S0883-2927(99)00074-8

Bethke, C.M., 2008. Geochemical and biogeochemical reaction modeling, Second Edition.

Bigham, J.M., Carlson, L., Murad, E., 1994. Schwertmannite, a new iron oxyhydroxysulphate from Pyhäsalmi, Finland, and other localities. Mineralogical Magazine 58, 641–648. https://doi.org/10.1180/minmag.1994.058.393.14

Bigham, J.M., Schwertmann, U., Carlson, L., Murad', E., 1990a. A poorly crystallized oxyhydroxysulfate of iron formed by bacterial oxidation of Fe(II) in acid mine waters 16.

Bigham, J.M., Schwertmann, U., Carlson, L., Murad', E., 1990b. A poorly crystallized oxyhydroxysulfate of iron formed by bacterial oxidation of Fe(II) in acid mine waters 16.

Bigham, J.M., Schwertmann, U., Traina, S.J., Winland, R.L., Wolf, M., 1996. Schwertmannite and the chemical modeling of iron in acid sulfate waters. Geochimica et Cosmochimica Acta 60, 2111–2121. https://doi.org/10.1016/0016-7037(96)00091-9

Black, C., Ziemkiewicz, P., Skousen, J., 1999. Construction of a limestone leach bed and preliminary water quality results in beaver creek 5.

Blanc, Ph., Lassin, A., Piantone, P., Azaroual, M., Jacquemet, N., Fabbri, A., Gaucher, E.C., 2012. Thermoddem: A geochemical database focused on low temperature water/rock interactions and waste materials. Applied Geochemistry 27, 2107–2116. https://doi.org/10.1016/j.apgeochem.2012.06.002

Borsari, M., 2014. Cadmium: Coordination Chemistry, in: Encyclopedia of Inorganic and Bioinorganic Chemistry. American Cancer Society, pp. 1–16. https://doi.org/10.1002/9781119951438.eibc2261

Boujelben, N., Bouzid, J., Elouear, Z., 2009. Adsorption of nickel and copper onto natural iron oxide-coated sand from aqueous solutions: Study in single and binary systems. Journal of Hazardous Materials 163, 376–382. https://doi.org/10.1016/j.jhazmat.2008.06.128

BRGM, 1973. Geological Map of Cambodia [WWW Document]. Behance. URL https://www.behance.net/gallery/4296207/Geological-Map-of-Cambodia-%28BRGM-1973%29 (accessed 1.11.21).

Buerge-Weirich, D., Hari, R., Xue, H., Behra, P., Sigg, L., 2002. Adsorption of Cu, Cd, and Ni on Goethite in the Presence of Natural Groundwater Ligands. Environ. Sci. Technol. 36, 328–336. https://doi.org/10.1021/es010892i

Camden-Smith, B., Johnson, R.H., Camden-Smith, P., Tutu, H., 2015. Geochemical Modelling of Water Quality and Solutes Transport from Mining Environments, Research and Practices in Water Quality. IntechOpen. https://doi.org/10.5772/59234

Cardenas, E., Tiedje, J.M., 2008. New tools for discovering and characterizing microbial diversity. Current Opinion in Biotechnology, Chemical biotechnology / Pharmaceutical biotechnology 19, 544–549. https://doi.org/10.1016/j.copbio.2008.10.010

Chen, C.-J., Jiang, W.-T., 2012. Influence of waterfall aeration and seasonal temperature variation on the iron and arsenic attenuation rates in an acid mine drainage system. Applied Geochemistry 27, 1966–1978. https://doi.org/10.1016/j.apgeochem.2012.06.003

Chen, M., Lu, G., Guo, C., Yang, C., Wu, J., Huang, W., Yee, N., Dang, Z., 2015. Sulfate migration in a river affected by acid mine drainage from the Dabaoshan mining area, South China. Chemosphere 119, 734–743. https://doi.org/10.1016/j.chemosphere.2014.07.094

Chikanda, F., Otake, T., Koide, A., Ito, A., Sato, T., 2021. The formation of Fe colloids and layered double hydroxides as sequestration agents in the natural remediation of mine drainage. Science of The Total Environment 774, 145183. https://doi.org/10.1016/j.scitotenv.2021.145183

Chikanda, F., Otake, T., Ohtomo, Y., Ito, A., Yokoyama, T.D., Sato, T., 2019. Magmatic-Hydrothermal Processes Associated with Rare Earth Element Enrichment in the Kangankunde Carbonatite Complex, Malawi. Minerals 9, 442. https://doi.org/10.3390/min9070442

Childs, C.W., Inoue, K., Mizota, C., 1998. Natural and anthropogenic schwertmannites from Towada-Hachimantai National Park, Honshu, Japan. Chemical Geology 144, 81–86. https://doi.org/10.1016/S0009-2541(97)00121-6

Cravotta, C.A., Means, B.P., Arthur, W., McKenzie, R.M., Parkhurst, D.L., 2015. AMDTreat 5.0+ with PHREEQC Titration Module to Compute Caustic Chemical Quantity, Effluent Quality, and Sludge Volume. Mine Water and the Environment 34, 136–152. https://doi.org/10.1007/s10230-014-0292-6

Das, S., Jim Hendry, M., Essilfie-Dughan, J., 2013. Adsorption of selenate onto ferrihydrite, goethite, and lepidocrocite under neutral pH conditions. Applied Geochemistry 28, 185–193. https://doi.org/10.1016/j.apgeochem.2012.10.026

Demchak, J., Morrow, T., Skousen, J., 2001. Treatment of acid mine drainage by four vertical flow wetlands in Pennsylvania. Geochemistry: Exploration, Environment, Analysis 1, 71–80. https://doi.org/10.1144/geochem.1.1.71

DeSa, T.C., Brown, J.F., Burgos, W.D., 2010. Laboratory and Field-scale Evaluation of Low-pH Fe(II) Oxidation at Hughes Borehole, Portage, Pennsylvania. Mine Water Environ 29, 239–247. https://doi.org/10.1007/s10230-010-0105-5

Diebold, A., Hagen, K.S., 1998. Iron(II) Polyamine Chemistry: Variation of Spin State and Coordination Number in Solid State and Solution with Iron(II) Tris(2-

pyridylmethyl)amine Complexes. Inorg. Chem. 37, 215–223. https://doi.org/10.1021/ic971105e

Dobriyal, P., Badola, R., Tuboi, C., Hussain, S.A., 2017. A review of methods for monitoring streamflow for sustainable water resource management. Appl Water Sci 7, 2617–2628. https://doi.org/10.1007/s13201-016-0488-y

Du, H., Peacock, C.L., Chen, W., Huang, Q., 2018. Binding of Cd by ferrihydrite organo-mineral composites: Implications for Cd mobility and fate in natural and contaminated environments. Chemosphere 207, 404–412. https://doi.org/10.1016/j.chemosphere.2018.05.092

Dutrizac, J.E., 2008. Factors Affecting the Precipitation of Potassium Jarosite in Sulfate and Chloride Media. Metall and Materi Trans B 39, 771–783. https://doi.org/10.1007/s11663-008-9198-7

Dzombak, D.A., Morel, F.M.M., 1990a. Surface Complexation Modeling: Hydrous Ferric Oxide. John Wiley & Sons.

Dzombak, D.A., Morel, F.M.M., 1990b. Surface complexation modeling: hydrous ferric oxide. Wiley, New York.

Economou-Eliopoulos, M., Eliopoulos, D., 1998. Selenium content of sulfide ores related to ophiolites of Greece. Journal of environmental pathology, toxicology and oncology : official organ of the International Society for Environmental Toxicology and Cancer 17, 199–204.

Egal, M., Casiot, C., Morin, G., Parmentier, M., Bruneel, O., Lebrun, S., Elbaz-Poulichet, F., 2009. Kinetic control on the formation of tooeleite, schwertmannite and jarosite by Acidithiobacillus ferrooxidans strains in an As(III)-rich acid mine water. Chemical Geology 265, 432–441. https://doi.org/10.1016/j.chemgeo.2009.05.008

Emerson, D., Fleming, E.J., McBeth, J.M., 2010. Iron-Oxidizing Bacteria: An Environmental and Genomic Perspective. Annual Review of Microbiology 64, 561–583. https://doi.org/10.1146/annurev.micro.112408.134208

Eppink, F.V., Trumm, D., Weber, P., Olds, W., Pope, J., Cavanagh, J.E., 2020. Economic Performance of Active and Passive AMD Treatment Systems Under

Uncertainty: Case Studies from the Brunner Coal Measures in New Zealand. Mine Water Environ 39, 785–796. https://doi.org/10.1007/s10230-020-00710-w

Favas, P.J.C., Pratas, J., Paul, M.S., Prasad, M.N.V., 2019. Chapter 10 - Remediation of Uranium-Contaminated Sites by Phytoremediation and Natural Attenuation, in: Pandey, V.C., Bauddh, K. (Eds.), Phytomanagement of Polluted Sites. Elsevier, pp. 277–300. https://doi.org/10.1016/B978-0-12-813912-7.00010-7

Feng, K., Wang, X., Zhou, B., Xu, M., Liang, J., Zhou, L., 2021. Hydroxyl, Fe 2+, and Acidithiobacillus ferrooxidans Jointly Determined the Crystal Growth and Morphology of Schwertmannite in a Sulfate-Rich Acidic Environment. ACS Omega 6, 3194–3201. https://doi.org/10.1021/acsomega.0c05606

Fernandez-Martinez, A., Timon, V., Roman-Ross, G., Cuello, G.J., Daniels, J.E., Ayora, C., 2010. The structure of schwertmannite, a nanocrystalline iron oxyhydroxysulfate. American Mineralogist 95, 1312–1322. https://doi.org/10.2138/am.2010.3446

Fitzpatrick, R.W., Mosley, L.M., Raven, M.D., Shand, P., 2017. Schwertmannite formation and properties in acidic drain environments following exposure and oxidation of acid sulfate soils in irrigation areas during extreme drought. Geoderma 308, 235–251. https://doi.org/10.1016/j.geoderma.2017.08.012

Florence, K., Sapsford, D.J., Johnson, D.B., Kay, C.M., Wolkersdorfer, C., 2016. Iron-mineral accretion from acid mine drainage and its application in passive treatment. Environmental Technology 37, 1428–1440. https://doi.org/10.1080/09593330.2015.1118558

Flynn, E.D., Catalano, J.G., 2017. Competitive and Cooperative Effects during Nickel Adsorption to Iron Oxides in the Presence of Oxalate. Environ. Sci. Technol. 51, 9792–9799. https://doi.org/10.1021/acs.est.7b02657

Francisco, P.C.M., Sato, T., Otake, T., Kasama, T., Suzuki, S., Shiwaku, H., Yaita, T., 2018. Mechanisms of Se(IV) Co-precipitation with Ferrihydrite at Acidic and Alkaline Conditions and Its Behavior during Aging. Environ. Sci. Technol. 52, 4817–4826. https://doi.org/10.1021/acs.est.8b00462

Fukushi, K., Sasaki, M., Sato, T., Yanase, N., Amano, H., Ikeda, H., 2003a. A natural attenuation of arsenic in drainage from an abandoned arsenic mine dump. Applied Geochemistry 18, 1267–1278. https://doi.org/10.1016/S0883-2927(03)00011-8

Fukushi, K., Sato, T., 2005. Using a Surface Complexation Model To Predict the Nature and Stability of Nanoparticles. Environmental Science & Technology 39, 1250–1256. https://doi.org/10.1021/es0491984

Fukushi, K., Sato, T., Yanase, N., 2003b. Solid-Solution Reactions in As(V) Sorption by Schwertmannite. Environmental Science & Technology 37, 3581–3586. https://doi.org/10.1021/es026427i

Garcia-Rios, M., De Windt, L., Luquot, L., Casiot, C., 2020. Modeling of microbial kinetics and mass transfer in bioreactors simulating the natural attenuation of arsenic and iron in acid mine drainage. Journal of Hazardous Materials 124133. https://doi.org/10.1016/j.jhazmat.2020.124133

Gazea, B., Adam, K., Kontopoulos, A., 1996. A review of passive system for the treatment of acid mine drainage 20.

Genty, T., Bussière, B., Potvin, R., Benzaazoua, M., Zagury, G.J., 2012. Dissolution of calcitic marble and dolomitic rock in high iron concentrated acid mine drainage: application to anoxic limestone drains. Environ Earth Sci 66, 2387–2401. https://doi.org/10.1007/s12665-011-1464-3

Great Britain, Environment Agency, 2008. Abandoned mines and the water environment. Environment Agency, Bristol.

Grundl, T., Delwiche, J., 1993. Kinetics of ferric oxyhydroxide precipitation. Journal of Contaminant Hydrology 14, 71–87. https://doi.org/10.1016/0169-7722(93)90042-Q

Hengen, T.J., Squillace, M.K., O'Sullivan, A.D., Stone, J.J., 2014. Life cycle assessment analysis of active and passive acid mine drainage treatment technologies. Resources, Conservation and Recycling 86, 160–167. https://doi.org/10.1016/j.resconrec.2014.01.003

Hosseini, S., Marandi, F., Şahin, E., Musevi, S.J., 2012. Synthesis, Crystal Structure and Thermal Properties of Lead(II) Complex with Bathophenanthroline and

Benzoyltrifluoroacetonate Ligands. Journal of Chemistry 2013, e159125. https://doi.org/10.1155/2013/159125

Huang, Z., Yang, T., 2021. Comparative study of acid mine drainage using different neutralization methods. Water Practice and Technology 16, 1026–1035. https://doi.org/10.2166/wpt.2021.039

Hufty, M., n.d. Abandoned Mines: The Scars of the Past [WWW Document]. Global Challenges. URL https://globalchallenges.ch/issue/6/abandoned-mines-the-scars-of-the-past/ (accessed 10.16.21).

Ichikawa, S., Matsumoto, T., Nakamura, T., 2016. X-ray fluorescence determination using glass bead samples and synthetic calibration standards for reliable routine analyses of ancient pottery. Anal. Methods 8, 4452–4465. https://doi.org/10.1039/C6AY01061J

Igarashi, T., 1976. Mineralizan of late Neogene tertiary to quaternary period related to th formation of sulfur, iron-sulphide and limonite ores in Hokkaido Japan.

Inatsu, M., Kawazoe, S., Mori, M., 2021. Trends and projection of heavy snowfall in Hokkaido, Japan as an application of self-organizing map. Journal of Applied Meteorology and Climatology. https://doi.org/10.1175/JAMC-D-21-0085.1

Ito, A., Otake, T., Shin, K.-C., Ariffin, K.S., Yeoh, F.-Y., Sato, T., 2017. Geochemical signatures and processes in a stream contaminated by heavy mineral processing near Ipoh city, Malaysia. Applied Geochemistry 82, 89–101. https://doi.org/10.1016/j.apgeochem.2017.05.007

JOGMEC [WWW Document], n.d. URL http://www.jogmec.go.jp/english/mp_control/mp_control_metal_10_000005.html (accessed 10.16.21).

Johnson, D.B., 2009. Extremophiles: Acidic Environments, in: Encyclopedia of Microbiology. Elsevier, pp. 107–126. https://doi.org/10.1016/B978-012373944-5.00278-9

Katsuyama, Y., Inatsu, M., Shirakawa, T., 2020. Response of snowpack to +2°C global warming in Hokkaido, Japan. J. Glaciol. 66, 83–96. https://doi.org/10.1017/jog.2019.85

Kawano, M., Tomita, K., 2001. Geochemical modeling of bacterially induced mineralization of schwertmannite and jarosite in sulfuric acid spring water. American Mineralogist 86, 1156–1165. https://doi.org/10.2138/am-2001-1005

Kefeni, K.K., Msagati, T.A.M., Mamba, B.B., 2017. Acid mine drainage: Prevention, treatment options, and resource recovery: A review. Journal of Cleaner Production 151, 475–493. https://doi.org/10.1016/j.jclepro.2017.03.082

Khamphila, K., Kodama, R., Sato, T., Otake, T., 2017. Adsorption and Post Adsorption Behavior of Schwertmannite with Various Oxyanions. Journal of Minerals and Materials Characterization and Engineering 05, 90–106. https://doi.org/10.4236/jmmce.2017.52008

Kim, H.-J., Kim, Y., 2020. Schwertmannite transformation to goethite and the related mobility of trace metals in acid mine drainage. Chemosphere 128720. https://doi.org/10.1016/j.chemosphere.2020.128720

Kirk Nordstrom, D., 2020. Geochemical Modeling of Iron and Aluminum Precipitation during Mixing and Neutralization of Acid Mine Drainage. Minerals 10, 547. https://doi.org/10.3390/min10060547

Kitakaze, A., Machida, T., Komatsu, R., 2016. Phase Relations In the Fe–Ni–s System From 875 To 650 °C. Can Mineral 54, 1175–1186. https://doi.org/10.3749/canmin.1500087

Knorr, K.-H., Blodau, C., 2007. Controls on schwertmannite transformation rates and products. Applied Geochemistry 22, 2006–2015. https://doi.org/10.1016/j.apgeochem.2007.04.017

Kruse, N., Hawkins, C., López, D.L., Johnson, K., 2019. Recovery of an Acid Mine Drainage-Impacted Stream Treated by Steel Slag Leach Beds. Mine Water Environ 38, 718–734. https://doi.org/10.1007/s10230-019-00636-y

Kuai, C., Zhang, Y., Wu, D., Sokaras, D., Mu, L., Spence, S., Nordlund, D., Lin, F., Du, X.-W., 2019. Fully Oxidized Ni–Fe Layered Double Hydroxide with 100% Exposed Active Sites for Catalyzing Oxygen Evolution Reaction. ACS Catal. 9, 6027–6032. https://doi.org/10.1021/acscatal.9b01935

Kumpulainen, S., Carlson, L., Räisänen, M.-L., 2007. Seasonal variations of ochreous precipitates in mine effluents in Finland. Applied Geochemistry 22, 760–777. https://doi.org/10.1016/j.apgeochem.2006.12.016

Laroche, E., Casiot, C., Fernandez-Rojo, L., Desoeuvre, A., Tardy, V., Bruneel, O., Battaglia-Brunet, F., Joulian, C., Héry, M., 2018. Dynamics of Bacterial Communities Mediating the Treatment of an As-Rich Acid Mine Drainage in a Field Pilot. Frontiers in Microbiology 9. https://doi.org/10.3389/fmicb.2018.03169

Larson, L.N., Sánchez-España, J., Kaley, B., Sheng, Y., Bibby, K., Burgos, W.D., 2014. Thermodynamic Controls on the Kinetics of Microbial Low-pH Fe(II) Oxidation. Environmental Science & Technology 48, 9246–9254. https://doi.org/10.1021/es501322d

Liang, Y., Tian, L., Lu, Y., Peng, L., Wang, P., Lin, J., Cheng, T., Dang, Z., Shi, Z., 2018. Kinetics of Cd(II) adsorption and desorption on ferrihydrite: experiments and modeling. Environ. Sci.: Processes Impacts 20, 934–942. https://doi.org/10.1039/C8EM00068A

Marouane, B., Klug, M., As, K.S., Engel, J., Reichel, S., Janneck, E., Peiffer, S., 2021. The potential of granulated schwertmannite adsorbents to remove oxyanions (SeO32−, SeO42−, MoO42−, PO43−, Sb(OH)6−) from contaminated water. Journal of Geochemical Exploration 223, 106708. https://doi.org/10.1016/j.gexplo.2020.106708

McCauley, C.A., O'Sullivan, A.D., Weber, P.A., Trumm, D., 2008. Development of Passive Treatment Systems for Treating Acid Mine Drainage at Stockton Mine. New Zealand 11.

McNeal, J.M., Balistrieri, L.S., 1989. Geochemistry and Occurrence of Selenium: An Overview, in: Selenium in Agriculture and the Environment. John Wiley & Sons, Ltd, pp. 1–13. https://doi.org/10.2136/sssaspecpub23.c1

Menendez, R., Clayton, J.L., Zurbuch, P.E., Rauch, H.W., Renton, J.J., 2000. Sand-Sized Limestone Treatment of Streams Impacted by Acid Mine Drainage 18.

Meng, X., Zhang, C., Zhuang, J., Zheng, G., Zhou, L., 2020. Assessment of schwertmannite, jarosite and goethite as adsorbents for efficient adsorption of

phenanthrene in water and the regeneration of spent adsorbents by heterogeneous fenton-like reaction. Chemosphere 244, 125523. https://doi.org/10.1016/j.chemosphere.2019.125523

Moncur, M.C., Ptacek, C.J., Blowes, D.W., Jambor, J.L., 2006. Spatial variations in water composition at a northern Canadian lake impacted by mine drainage. Applied Geochemistry 21, 1799–1817. https://doi.org/10.1016/j.apgeochem.2006.06.016

Moon, E.M., Peacock, C.L., 2012. Adsorption of Cu(II) to ferrihydrite and ferrihydrite–bacteria composites: Importance of the carboxyl group for Cu mobility in natural environments. Geochimica et Cosmochimica Acta 92, 203–219. https://doi.org/10.1016/j.gca.2012.06.012

Murakami, S., Kitamura, T., Suzuki, J., Sato, R., Aoi, T., Fujii, M., Matsugo, H., Kamiki, H., Ishida, H., Takenaka-Uema, A., Shimojima, M., Horimoto, T., 2020. Detection and Characterization of Bat Sarbecovirus Phylogenetically Related to SARS-CoV-2, Japan. Emerging Infectious Diseases 26, 3025–3029. https://doi.org/10.3201/eid2612.203386

Naidu, G., Ryu, S., Thiruvenkatachari, R., Choi, Y., Jeong, S., Vigneswaran, S., 2019. A critical review on remediation, reuse, and resource recovery from acid mine drainage. Environmental Pollution 247, 1110–1124. https://doi.org/10.1016/j.envpol.2019.01.085

Ncube-Phiri, S., Ncube, A., Mucherera, B., Ncube, M., 2015. Artisanal small-scale mining: Potential ecological disaster in Mzingwane District, Zimbabwe. Jàmbá: Journal of Disaster Risk Studies 7, 11 pages. https://doi.org/10.4102/jamba.v7i1.158

Neculita, C.-M., Zagury, G.J., Bussière, B., 2007. Passive Treatment of Acid Mine Drainage in Bioreactors using Sulfate-Reducing Bacteria: Critical Review and Research Needs. J. Environ. Qual. 36, 1–16. https://doi.org/10.2134/jeq2006.0066

Neil, C.W., Yang, Y.J., Schupp, D., Jun, Y.-S., 2014. Water Chemistry Impacts on Arsenic Mobilization from Arsenopyrite Dissolution and Secondary Mineral

Precipitation: Implications for Managed Aquifer Recharge. Environ. Sci. Technol. 48, 4395–4405. https://doi.org/10.1021/es405119q

Nieto, J.M., Sarmiento, A.M., Canovas, C.R., Olias, M., Ayora, C., 2013. Acid mine drainage in the Iberian Pyrite Belt: 1. Hydrochemical characteristics and pollutant load of the Tinto and Odiel rivers. Environ Sci Pollut Res 20, 7509–7519. https://doi.org/10.1007/s11356-013-1634-9

Nordstrom, D.K., Alpers, C.N., Ptacek, C.J., Blowes, D.W., 2000. Negative pH and Extremely Acidic Mine Waters from Iron Mountain, California. Environ. Sci. Technol. 34, 254–258. https://doi.org/10.1021/es990646v

Okvau Gold Project [WWW Document], 2015. . Mining Technology | Mining News and Views Updated Daily. URL https://www.mining-technology.com/projects/okvau-gold-project/ (accessed 9.4.20).

Otero Fariña, A., Gago, R., Antelo, J., Fiol, S., Arce, F., 2015. Surface Complexation Modelling of Arsenic and Copper Immobilization by Iron Oxide Precipitates Derived from Acid Mine Drainage. BSGM 67, 493–508. https://doi.org/10.18268/BSGM2015v67n3a12

Paikaray, S., 2020. Environmental Stability of Schwertmannite: A Review. Mine Water Environ. https://doi.org/10.1007/s10230-020-00734-2

Paikaray, S., Göttlicher, J., Peiffer, S., 2012. As(III) retention kinetics, equilibrium and redox stability on biosynthesized schwertmannite and its fate and control on schwertmannite stability on acidic (pH 3.0) aqueous exposure. Chemosphere 86, 557–564. https://doi.org/10.1016/j.chemosphere.2011.07.055

Park, I., Ryota, T., Yuto, T., Tabelin, C.B., Phengsaart, T., Jeon, S., Ito, M., Hiroyoshi, N., 2021. A novel arsenic immobilization strategy via a two-step process: Arsenic concentration from dilute solution using schwertmannite and immobilization in Ca–Fe–AsO4 compounds. Journal of Environmental Management 295, 113052. https://doi.org/10.1016/j.jenvman.2021.113052

Park, J.H., Han, Y.-S., Ahn, J.S., 2016. Comparison of arsenic co-precipitation and adsorption by iron minerals and the mechanism of arsenic natural attenuation in a mine stream. Water Research 106, 295–303. https://doi.org/10.1016/j.watres.2016.10.006

Pesic, B., Oliver, D.J., Wichlacz, P., 1989a. An electrochemical method of measuring the oxidation rate of ferrous to ferric iron with oxygen in the presence of Thiobacillus ferrooxidans. Biotechnology and Bioengineering 33, 428–439. https://doi.org/10.1002/bit.260330408

Pesic, B., Oliver, D.J., Wichlacz, P., 1989b. An electrochemical method of measuring the oxidation rate of ferrous to ferric iron with oxygen in the presence ofThiobacillus ferrooxidans. Biotechnology and Bioengineering 33, 428–439. https://doi.org/10.1002/bit.260330408

Puchtler, H., Meloan, S.N., Spencer, M., 1985. Current chemical concepts of acids and bases and their application to anionic ("acid") and cationic ("basic") dyes. Histochemistry 82, 301–306. https://doi.org/10.1007/BF00494057

Rawlings, D.E., Kusano, T., 1994. Molecular genetics of Thiobacillus ferrooxidans. Microbiol Rev 58, 39–55.

Regenspurg, S., Brand, A., Peiffer, S., 2004. Formation and stability of schwertmannite in acidic mining lakes. Geochimica et Cosmochimica Acta 68, 1185–1197. https://doi.org/10.1016/j.gca.2003.07.015

Regenspurg, S., Peiffer, S., 2005. Arsenate and chromate incorporation in schwertmannite. Applied Geochemistry 20, 1226–1239. https://doi.org/10.1016/j.apgeochem.2004.12.002

Rezaie, B., Anderson, A., 2020. Sustainable resolutions for environmental threat of the acid mine drainage. Science of The Total Environment 717, 137211. https://doi.org/10.1016/j.scitotenv.2020.137211

Rounds, S.A., Wilde, F.D., 2012. Chapter A6. Section 6.6. Alkalinity and acid neutralizing capacity (USGS Numbered Series No. 09-A6.6), Chapter A6. Section 6.6. Alkalinity and acid neutralizing capacity, Techniques of Water-Resources Investigations. U.S. Geological Survey, Reston, VA. https://doi.org/10.3133/twri09A6.6

Rovira, M., Giménez, J., Martínez, M., Martínez-Lladó, X., de Pablo, J., Martí, V., Duro, L., 2008. Sorption of selenium(IV) and selenium(VI) onto natural iron oxides: Goethite and hematite. Journal of Hazardous Materials 150, 279–284. https://doi.org/10.1016/j.jhazmat.2007.04.098

Saeki, K., Kunito, T., 2012. Influence of chloride ions on cadmium adsorptions by oxides, hydroxides, oxyhydroxides, and phyllosilicates. Applied Clay Science 62–63, 58–62. https://doi.org/10.1016/j.clay.2012.04.018

Sánchez-España, J., Yusta, I., Diez-Ercilla, M., 2011. Schwertmannite and hydrobasaluminite: A re-evaluation of their solubility and control on the iron and aluminium concentration in acidic pit lakes. Applied Geochemistry 26, 1752–1774. https://doi.org/10.1016/j.apgeochem.2011.06.020

Sarmiento, A.M., Grande, J.A., Luís, A.T., Dávila, J.M., Fortes, J.C., Santisteban, M., Curiel, J., de la Torre, M.L., da Silva, E.F., 2018. Negative pH values in an open-air radical environment affected by acid mine drainage. Characterization and proposal of a hydrogeochemical model. Science of The Total Environment 644, 1244–1253. https://doi.org/10.1016/j.scitotenv.2018.06.381

Schaider, L.A., Senn, D.B., Estes, E.R., Brabander, D.J., Shine, J.P., 2014. Sources and fates of heavy metals in a mining-impacted stream: Temporal variability and the role of iron oxides. Science of The Total Environment 490, 456–466. https://doi.org/10.1016/j.scitotenv.2014.04.126

Schoepfer, V.A., Burton, E.D., 2021. Schwertmannite: A review of its occurrence, formation, structure, stability and interactions with oxyanions. Earth-Science Reviews 221, 103811. https://doi.org/10.1016/j.earscirev.2021.103811

Schwertmann, U., Bigham, J.M., Murad, E., 1995. The first occurrence of schwertmannite in a natural stream environment. European Journal of Mineralogy 547–552. https://doi.org/10.1127/ejm/7/3/0547

Schwertmann, U., Carlson, L., 2005. The pH-dependent transformation of schwertmannite to goethite at 25°C. Clay Minerals 40, 63–66. https://doi.org/10.1180/0009855054010155

Seervi., V., H.L, Y., S.K, S., A, J., 2017. Overview of Active and Passive Systems for Treating Acid Mine Drainage. IARJSET 4, 131–137. https://doi.org/10.17148/IARJSET.2017.4525

Shi, M., Min, X., Ke, Y., Lin, Z., Yang, Z., Wang, S., Peng, N., Yan, X., Luo, S., Wu, J., Wei, Y., 2021. Recent progress in understanding the mechanism of heavy metals retention by iron (oxyhydr)oxides. Science of the Total Environment 19.

Simmons, J., Ziemkiewicz, P., Courtney Black, D., 2002. Use of Steel Slag Leach Beds for the Treatment of Acid Mine Drainage. Mine Water and the Environment 21, 91–99. https://doi.org/10.1007/s102300200024

Singh, A.K., Kumar, S.R., 2015. Quality assessment of groundwater for drinking and irrigation use in semi-urban area of Tripura, India 13.

Skousen, J., Ziemkiewicz, P., 2005. Performance of 116 Passive Treatment System for Acid Mine Drainage. JASMR 2005, 1100–1133. https://doi.org/10.21000/JASMR05011100

Skousen, J., Zipper, C.E., Rose, A., Ziemkiewicz, P.F., Nairn, R., McDonald, L.M., Kleinmann, R.L., 2017. Review of Passive Systems for Acid Mine Drainage Treatment. Mine Water and the Environment 36, 133–153. https://doi.org/10.1007/s10230-016-0417-1

Skousen, J.G., Ziemkiewicz, P.F., McDonald, L.M., 2019. Acid mine drainage formation, control and treatment: Approaches and strategies. The Extractive Industries and Society 6, 241–249. https://doi.org/10.1016/j.exis.2018.09.008

Song, J., Jia, S.-Y., Ren, H.-T., Wu, S.-H., Han, X., 2015. Application of a high-surface-area schwertmannite in the removal of arsenate and arsenite. Int. J. Environ. Sci. Technol. 12, 1559–1568. https://doi.org/10.1007/s13762-014-0528-9

Speight, J.G., 2020. Natural water remediation: chemistry and technology. Butterworth-Heinemann, Oxford, United Kingdom ; Cambridge, MA, United States.

Stefaniak, J., Dutta, A., Verbinnen, B., Shakya, M., Rene, E.R., 2018. Selenium removal from mining and process wastewater: a systematic review of available technologies. Journal of Water Supply: Research and Technology-Aqua 67, 903–918. https://doi.org/10.2166/aqua.2018.109

Stumm, W., Lee, G.F., 1961. Oxygenation of Ferrous Iron. Industrial & Engineering Chemistry 53, 143–146. https://doi.org/10.1021/ie50614a030

Tarras-Wahlberg, N.H., 2002. Environmental management of small-scale and artisanal mining: the Portovelo-Zaruma goldmining area, southern Ecuador. Journal of Environmental Management 65, 165–179. https://doi.org/10.1006/jema.2002.0542

Taylor, J., Pape, S., Murphy, N., 2005. A Summary of Passive and Active Treatment Technologies for Acid and Metalliferous Drainage (AMD) 49.

Thisani, S.K., Kallon, D.V.V., Byrne, P., 2021. Review of Remediation Solutions for Acid Mine Drainage Using the Modified Hill Framework. Sustainability 13, 8118. https://doi.org/10.3390/su13158118

Tokunaga, K., Takahashi, Y., 2017. Effective Removal of Selenite and Selenate Ions from Aqueous Solution by Barite. Environ. Sci. Technol. 51, 9194–9201. https://doi.org/10.1021/acs.est.7b01219

Tomiyama, S., Igarashi, T., Tabelin, C.B., Tangviroon, P., Ii, H., 2019. Acid mine drainage sources and hydrogeochemistry at the Yatani mine, Yamagata, Japan: A geochemical and isotopic study. Journal of Contaminant Hydrology 225, 103502. https://doi.org/10.1016/j.jconhyd.2019.103502

Trumm, D., 2010. Selection of active and passive treatment systems for AMD—flow charts for New Zealand conditions. New Zealand Journal of Geology and Geophysics 53, 195–210. https://doi.org/10.1080/00288306.2010.500715

Tsujimoto, K., Ohta, T., Aida, K., Tamakawa, K., So Im, M., 2018. Diurnal pattern of rainfall in Cambodia: its regional characteristics and local circulation. Progress in Earth and Planetary Science 5, 39. https://doi.org/10.1186/s40645-018-0192-7

Wang, H., Bigham, J.M., Tuovinen, O.H., 2006. Formation of schwertmannite and its transformation to jarosite in the presence of acidophilic iron-oxidizing microorganisms. Materials Science and Engineering: C 26, 588–592. https://doi.org/10.1016/j.msec.2005.04.009

Wang, S., Mulligan, C.N., 2006. Natural attenuation processes for remediation of arsenic contaminated soils and groundwater. Journal of Hazardous Materials 138, 459–470. https://doi.org/10.1016/j.jhazmat.2006.09.048

Watanabe, Y., Aoki, M., Nakajima, N., 1996. Age and Style of Epithermal Gold Mineralization in the Minamikayabe Area [WWW Document]. URL https://docplayer.net/179583461-Age-and-style-of-epithermal-gold-mineralization-in-the-minamikayabe-area-yasushi-watanabe-masahiro-aoki-and-nobuhisa-nakajima.html (accessed 12.15.21).

Watanabe, Y., Aoki, M., Yamamoto, K., 1997. Geology, Age and Style of the Advanced Argillic Alteration in the Kobui Area, Southwestern Hokkaido, Japan. Resources Geology 47, 263–281.

Watzlaf, G.R., Schroeder, K.T., Kairies, C.L., 2000. Long-term performance of anoxic limestone drains. Mine Water and the Environment 19, 98–110. https://doi.org/10.1007/BF02687258

Webster, J.G., Nordstrom, D.K., Smith, K.S., 1993. Transport and Natural Attenuation of Cu, Zn, As, and Fe in the Acid Mine Drainage of Leviathan and Bryant Creeks, in: Alpers, C.N., Blowes, D.W. (Eds.), Environmental Geochemistry of Sulfide Oxidation, ACS Symposium Series. American Chemical Society, Washington, DC, pp. 244–260. https://doi.org/10.1021/bk-1994-0550.ch017

Webster, J.G., Swedlund, P.J., Webster, K.S., 1998. Trace Metal Adsorption onto an Acid Mine Drainage Iron(III) Oxy Hydroxy Sulfate. Environmental Science & Technology 32, 1361–1368. https://doi.org/10.1021/es9704390

World Health Organization, 2017. Guidelines for drinking-water quality.

Yan, S., Zheng, G., Meng, X., Zhou, L., 2017. Assessment of catalytic activities of selected iron hydroxysulphates biosynthesized using Acidithiobacillus ferrooxidans for the degradation of phenol in heterogeneous Fenton-like reactions. Separation and Purification Technology 185, 83–93. https://doi.org/10.1016/j.seppur.2017.05.008

Yang, R., Tao, J., Huang, Q., Tie, B., Lei, M., Yang, Y., Du, H., 2019. Co-adsorption of Cd(II) and Sb(III) by ferrihydrite: a combined XPS and ITC study. J Soils Sediments 19, 1319–1327. https://doi.org/10.1007/s11368-018-2140-y

Yannopoulos, J.C., 1991. Gold Mill Tailings, in: Yannopoulos, J.C. (Ed.), The Extractive Metallurgy of Gold. Springer US, Boston, MA, pp. 245–256. https://doi.org/10.1007/978-1-4684-8425-0_12

Yu, J.-Y., Heo, B., Choi, I.-K., Cho, J.-P., Chang, H.-W., 1999. Apparent solubilities of schwertmannite and ferrihydrite in natural stream waters polluted by mine drainage. Geochimica et Cosmochimica Acta 63, 3407–3416. https://doi.org/10.1016/S0016-7037(99)00261-6

Zhang, M., Wang, H., 2014. Organic wastes as carbon sources to promote sulfate reducing bacterial activity for biological remediation of acid mine drainage. Minerals Engineering 69, 81–90. https://doi.org/10.1016/j.mineng.2014.07.010

Zhang, Z., Bi, X., Li, X., Zhao, Q., Chen, H., 2018. Schwertmannite: occurrence, properties, synthesis and application in environmental remediation. RSC Adv. 8, 33583–33599. https://doi.org/10.1039/C8RA06025H

Zhou, S., Sato, T., Otake, T., 2018. Dissolved Silica Effects on Adsorption and Co-Precipitation of Sb(III) and Sb(V) with Ferrihydrite. Minerals 8, 101. https://doi.org/10.3390/min8030101

Zhu, C., Anderson, G., Anderson, A.P. in the D. of P.S.G., Burden, D.S., 2002. Environmental Applications of Geochemical Modeling. Cambridge University Press.

Zhu, J., Gan, M., Zhang, D., Hu, Y., Chai, L., 2013. The nature of Schwertmannite and Jarosite mediated by two strains of Acidithiobacillus ferrooxidans with different ferrous oxidation ability. Materials Science and Engineering: C 33, 2679–2685. https://doi.org/10.1016/j.msec.2013.02.026

Ziemkiewicz, P.F., Skousen, J.G., Brant, D.L., Sterner, P.L., Lovett, R.J., 1997. Acid Mine Drainage Treatment with Armored Limestone in Open Limestone Channels 9.

X. Publication and International conferences

List of publication

1. "Seasonal Effects of Natural Attenuation on Drainage Contamination from Artisanal Gold Mining, Cambodia: Implication for Passive Treatment", **Sereyroith Tum,** Tatsuya Matsui, Kanako Toda, Ryosuke Kikuchi, Sitha Kong, Panha Meas, Ear Unsovath, Yoko Ohtomo, Tsubasa Otake and Tsutomu Sato, Journal of Science of the Total Environment, Impact factor: 7.963 (2020)
   DOI: 10.1016/j.scitotenv.2021.150398

International conferences

1. "Geochemical Behaviors of Dissolved Fe, As, Se and Mn from Artisanal and Small-Scale Gold Mine in Cambodia", **Sereyroith Tum,** Tatsuya Matsui, Sitha Kong, Tsubasa Otake and Tsutomu Sato
   11th Regional Conference on Geological and Geo-resources Engineering, October 2019, Quezon City, Philippines
2. "A Natural Attenuation of Heavy Metals in a Stream Contaminated by Acid Mine Drainage from Artisanal Gold Mining in Cambodia", **Sereyroith Tum,** Tatsuya Matsui, Sitha Kong, Tsubasa Otake and Tsutomu Sato
   Virtual Goldschmidt Conference, June 2020
3. A Process Model of Natural Attenuation of Heavy Metals in a Stream Contaminated by Acid Mine Drainage from Artisanal Gold Mining in Cambodia", **Sereyroith Tum,** Tatsuya Matsui, Ryosuke Kikuchi, Sitha Kong, Yoko Ohtomo, Tsubasa Otake and Tsutomu Sato,
   Virtual JpGU - AGU Joint Meeting 2020, July 2020
4. "Geochemical Characterization of Rivers Contaminated by Acid Mine Drainage from an Abandoned Mine in Northern Japan." **Sereyroith Tum,** Tatsuya Matsui, Ryosuke Kikuchi, Yoko Ohtomo, Tsubasa Otake and Tsutomu Sato,
   Virtual JpGU - Meeting 2021, June 2021

5. “Geochemical modeling of a natural remediation of an acid mine drainage from an abandoned mine in northern Japan.” **Sereyroith Tum,** Tatsuya Matsui, Ryosuke Kikuchi, Yoko Ohtomo, Tsubasa Otake and Tsutomu Sato,
   Virtual Goldschmidt Conference, July 2021